Structure, Dynamics and Rheological Behavior of Thermo-responsive Dense Microgel Suspensions

By

RAJENDRA GANPAT JOSHI

Enrolment No: PHYS02200804011

Indira Gandhi Centre for Atomic Research, Kalpakkam, India

A thesis submitted to the Board of Studies in Physical Sciences

In partial fulfillment of requirements

for the Degree of

DOCTOR OF PHILOSOPHY

of

HOMI BHABHA NATIONAL INSTITUTE, MUMBAI

August, 2014

HomiBhabha National Institute

Recommendations of the Viva Voce Committee

As members of the Viva Voce Committee, we certify that we have read the dissertation prepared by Rajendra Ganpat Joshi entitled "Structure, Dynamics and Rheological Behavior of Thermo-responsive Dense Microgel Suspensions" and recommend that it may be accepted as fulfilling the thesis requirement for the award of Degree of Doctor of Philosophy.

Chairman - Dr. G. Amarendra **Date:**

Guide / Convener - Dr B.V.R.Tata **Date:**

External examiner **Date:**

Member 1 - Dr. C.S.Sundar **Date:**

Member 2 - Dr. John Philip **Date:**

Final approval and acceptance of this thesis is contingent upon the candidate's submission of the final copies of the thesis to HBNI.

I/We hereby certify that I/we have read this thesis prepared under my/our direction and recommend that it may be accepted as fulfilling the thesis requirement.

Date:

Place: IGCAR, Kalpakkam **Guide**

CERTIFICATE

I hereby certify that I have read this dissertation prepared under my direction and recommend that it may be accepted as fulfilling the dissertation requirement.

Date: **(Dr. B.V.R.Tata)**

Place: Kalpakkam **Ph. D. Guide**

STATEMENT BY AUTHOR

This dissertation has been submitted in partial fulfillment of requirements for an advanced degree at Homi Bhabha National Institute (HBNI) and is deposited in the Library to be made available to borrowers under rules of the HBNI.

Brief quotations from this dissertation are allowable without special permission, provided that accurate acknowledgement of source is made. Requests for permission for extended quotation from or reproduction of this manuscript in whole or in part may be granted by the Competent Authority of HBNI when in his or her judgment the proposed use of the material is in the interests of scholarship. In all other instances, however, permission must be obtained from the author.

(Rajendra Ganpat Joshi)

DECLARATION

I, hereby declare that the investigation presented in the thesis has been carried out by me. The work is original and has not been submitted earlier as a whole or in part for a degree / diploma at this or any other Institution / University.

(Rajendra Ganpat Joshi)

List of Publications

A. Journal publication

1. “Dynamics in thermo-responsive nanogel crystals undergoing melting”
   R.G. Joshi, B. V. R. Tata and J. Brijitta, J. Chem. Phys. 139, (2013) 124901.

2. “Thermo-responsive Nanogel Dispersions: Dynamics and Phase Behavior”
   B.V.R.Tata, J. Brijitta and **R.G. Joshi,** Int. J. Adv. Eng. Sci. Appl. Math. 5, (2013) 240-249.

3. “Subdiffusive dynamics and two step yielding of dense thermo-responsive microgel glasses”
   R. G. Joshi and B. V. R. Tata (submitted)

4. *“Crystalline arrays of submicron-sized particles through colloidal route”
   B.V.R. Tata, **R.G. Joshi**, D.K. Gupta, J.Brijitta and Baldev Raj,Current Science 103, (2011) 1175-1184.

5. ***“**RHCP and FCC structures in thermo-responsive microgel crystals**”**
   J.Brijitta, B.V.R.Tata, **R.G Joshi** and T. Kaliyappan, J. Chem .Phys, 131, (2009) 074904.

B. Conference Publications

1. “Yielding behavior of dense microgel glasses”
   R.G. Joshi, B.V.R. Tata and D. Karthickeyan, AIP conf. proc. 1512, (2013) 164-165.

2. “Pressure Tuning of Bragg Diffraction in Stimuli Responsive Microgel Crystals”
   R. G. Joshi, B. V. R. Tata and J. Brijitta, AIP conf. proc.1349, (2010) 208-209.

3. “Entanglement Effect on Melting of Photonic Crystals of Thermo-responsive Microgels”
   R. G. Joshi, B. V. R. Tata and J. Brijitta, MRSI IUMRS-ICA, Bangalore, India [16th- 20th Dec. 2013]

4. “Osmotic Deswelling of Nanogel Particles: Comparison of Experiments with Theory”
   R.G.Joshi and B.V.R.Tata, International conference on nanoscience and technology, Hydrabad, India [20th – 23rd Jan. 2012]

5. “Thermo-responsive Nanogel Crystals: Structure, Disorder and Dynamics”
   R. G. Joshi, B.V.R.Tata and J. Brijitta, JSPS-DST Asian Academic Seminar, 2010, SINP, Kolkata, India [29th Nov. – 4th Dec. 2010]

*- Not included in thesis

(Rajendra Ganpat Joshi)

ACKNOWLEDGEMENTS

First of all, I express my deep sense of gratitude to my thesis supervisor, Dr. B. V. R. Tata, Head, LSSS, for his invaluable guidance, support and concern during my Ph.D. He has been a true mentor during this period.

I thank my doctoral committee members Dr. G Amarendra, Dr. C. S. Sundar, Dr. John Philip and Dr. A. K. Arora for their valuable suggestions during Ph.D. I especially thank Dr. C. S. Sundar, for his support and encouragement.

I would like to thank the director IGCAR, Dr. P. R. Vasudeva Rao, director MSG, Shri M. P. Janwadkar and head CMPD, Dr. A. Bharathi for their support.

I thank Mrs. P. V. Rajamani and Dr. Karunakar Mishra for taking immense effort in correcting the thesis.

I thank Dr. T. R. Ravindran, Dr. V. Shivasubramanium and Dr. G. Jaiganesh for going through the thesis and providing valuable suggestions.

I thank Dr. J. Brijitta for helping me in the synthesis of microgels and sample preparation.

I am grateful to my lab mates Mr. Deepak Kumar Gupta, Mr. D. Karthickeyan, Mrs. Soumee Pal for their co-operation and timely help in correcting mistakes in the thesis.

I would like to thank my past lab mates Dr. M. Sivanantham, Dr. K. Saravanakumar, Mr. Santhosh Kumar and Mr. Rajesh Kannan for their co-operation.

I express my heartiest gratitude to all my friends and family members.

(R. G. Joshi)

CONTENTS

Page No.

4.3 Results and Discussion

SYNOPSIS

Poly (N-isopropyl acrylamide) (PNIPAM) microgel particles are thermo-responsive, which show decrease in size with increase in temperature and exhibit volume phase transition (VPT) by undergoing sudden transition from swollen to deswollan state at ~ 34°C. Under suitable conditions, monodisperse PNIPAM microgel particles dispersed in a solvent exhibit structural ordering (gas, liquid, crystal and even glass) similar to that of atomic systems and hence serve as ideal model condensed matter system. Unlike hard sphere colloidal particles, which are rigid and homogeneous in density, PNIPAM microgel particles are soft and inhomogeneous in nature having core-shell structure with densely crosslinked polymer core and a thin shell (20-30 nm) containing dangling polymer chains. The dense core is known to deswell more compared to the shell upon increasing the temperature. The effect of this differential deswelling (swelling) upon increase (decrease) in temperature and dangling polymer chains on the structural ordering, dynamics and flow behavior of dense suspensions has not been investigated. This thesis report the results on above three aspects, in dense PNIPAM microgel suspensions, investigated using static light scattering (SLS), dynamic light scattering (DLS), UV-Vis spectroscopy and rheology.

Use of SLS and DLS techniques for probing dense suspensions of hard spheres for their structural ordering and dynamics is restricted due to multiple scattering effects. In case of PNIPAM microgels, polymer content of the microgel particles in the swollen state is only 2-3% and rest is water making their refractive index closely matched with that of solvent. This index matching allows one to probe dense PNIPAM microgel suspensions for their structural ordering and dynamics, at temperatures below VPT, using SLS and DLS techniques. At temperatures close to and above VPT, PNIPAM microgel suspensions become turbid due to multiple scattering of light. This thesis also reports the results on ordering and dynamics in turbid PNIPAM microgel suspension probed using 3D DLS, which employs cross correlation technique. In hard sphere suspensions, size of the particle is fixed and can be altered only by changing the synthesis conditions. On the other hand, PNIPAM microgel system offers tunability of particle size and hence volume fraction using temperature. The variation of particle size with respect to temperature helps to study the phase behavior of PNIPAM microgel suspensions in more controlled way as compared to that of hard sphere colloidal suspensions.

In addition to PNIPAM microgel particle being thermo-responsive, these particles are known to undergo compression upon application of osmotic pressure, exerted by the addition of non adsorbing polymer to suspensions under dilute condition. In this thesis, we report experimental evidence for compression of PNIPAM microgel particles under osmotic pressure exerted by its own PNIPAM microgel particles due to structural ordering in dense suspensions. PNIPAM microgels are shown to undergo reduction in particle size by observing interparticle separation being smaller than original particle diameter. The interparticle separation was measured by recording the

Bragg diffraction from PNIPAM microgel crystals of different volume fraction using a UV visible spectrometer. In dense suspensions, where interparticle separations are of the order of the particle diameter, the core shell nature of PNIPAM microgel particle is expected to influence the particle dynamics via overlapping and entanglement of dangling polymer chains in the thin sell of neighboring particles. This thesis reports the light scattering results on dynamics in dense PNIPAM microgel crystals close to their melting transition. Analysis of these results reveal that short time dynamics of PNIPAM microgel particles is subdiffusive. In case of the hard sphere colloidal suspensions short time dynamics is always diffusive. The observation of subdiffusive dynamics at short time has been explained in terms of entanglement of dangling polymer chains between neighboring particles. Further, In order to know the influence of dangling polymer chains on the shear flow of dense PNIPAM microgel suspensions, non linear rheological measurements have been carried out on the dense PNIPAM microgel glasses and results are presented in this thesis. Rheological measurements reveal that dense PNIPAM microgel glasses yield in two steps in contrast to one step yielding observed in hard sphere glasses. Though such two step yielding have been reported in attractive glasses, our experiment gives first evidence for two step yielding in a soft sphere repulsive glass. Observed two step yielding behavior is explained in terms of disentanglements and cage breaking mechanisms. Towards above studies, PNIPAM microgel suspensions of various particle sizes have been prepared and investigated using dynamic light scattering (DLS), static light scattering (SLS), UV-Vis spectroscopy techniques for their dynamics and structural ordering and rheometer for their flow and deformation behavior. This thesis is organized in six chapters and contents of each chapter are summarized as follows,

Chapter 1. Introduction

Colloidal suspensions of hard spheres and thermo-responsive microgels are discussed with respect to their stability, interparticle interactions, ordering, dynamics and phase behavior in this chapter. Rheology of viscoelastic materials is described. Flow and deformation behavior of hard and soft sphere colloidal suspensions under linear and nonlinear shear deformation is discussed. The chapter ends with the motivation and investigations taken up for the present thesis work.

Chapter 2. Experimental Methods

Free radical precipitation polymerization, a method used for synthesis of PNIPAM microgel particles is discussed. Detailed procedures for the preparation of PNIPAM microgel crystals and glasses are reported in present thesis. The instrumental details, measurement schemes and methods of analysis underlying these techniques are presented.

Chapter 3. Effect of osmotic pressure on deswelling behavior of microgel particles in dense PNIPAM microgel crystals

PNIPAM microgel particles are known to be thermo-responsive. With increase in temperature, PNIPAM microgels deswell and undergo VPT at ~ 34°C. In present study, it is shown that in addition to the temperature, osmotic pressure also serve as stimulus for PNIPAM microgel particles. PNIPAM microgel particles are shown to undergo compression (deswell) osmotically in the crystalline as well as glassy states of dense PNIPAM microgel suspensions. There are only limited numbers of studies on dilute PNIPAM microgel suspensions showing deswelling of PNIPAM microgel particles under osmotic pressure. This thesis presents detailed studies on dense PNIPAM microgel crystals and glasses showing deswelling under osmotic pressure. Towards this, dense PNIPAM microgel crystals with different volume fractions have been prepared by compressing the suspensions osmotically. Bragg diffraction of these crystals have been recorded using UV-Vis spectrometer. Upon increasing the osmotic pressure (particle concentration), Bragg peak is found to exhibit a blue shift. The Bragg peak has been used to determine the interparticle separation. Beyond a certain osmotic pressure, interparticle separation is found to be smaller than the size of PNIPAM microgel particle under swollen state (measured using DLS on dilute suspension). In dense PNIPAM microgel crystals, the interparticle separation being lesser than the particle size than its swollen the state provides direct evidence for shrinking (deswelling) of PNIPAM microgel particles under osmotic compression in crystalline state. The experimentally observed swelling/ deswelling behavior of the PNIPAM microgel particles with temperature and pressure is understood using Flory-Rehnar (FR) theory. Only qualitative agreement has been observed between theory and experiments. Results reported here suggest the need for improvement of the FR theory for obtaining quantative agreement with the experiments.

Chapter 4. Dynamics across the melting of PNIPAM microgel crystals

Löwen *et al.* have proposed a dynamical criterion for identifying the melting/freezing transition of colloidal crystals/liquids. According to this criterion the ratio of long time diffusion coefficient (D_L) to short time diffusion coefficients (D_S) at freezing/melting transition is 0.1. The D_S and D_L characterizes the diffusive motion of colloidal particle at short time (*i.e.* within the cage formed by neighboring particles) and long time (*i.e.* after the escape from the cage) respectively. This criterion is reported to be universal as applicable to colloidal systems, with different interparticle interactions, exhibiting Brownian motion. However its applicability for PNIPAM microgel crystals/liquids undergoing melting/freezing is unknown.With this as motivation, dynamics across the melting of dense PNIPAM microgel crystals as a function of temperature have been studied using DLS technique. Melting transition of PNIPAM microgel colloidal crystals of two different volume fractions ϕ = 0.49 and 0.79 have been identified. D_S and D_L have been measured across the melting. Results of SLS and DLS measurements are presented in this chapter. In dense PNIPAM microgel crystals undergoing melting, the ratio D_L/D_S is found to be less than 0.1. This deviation is found to be larger in the suspension with higher ϕ. Possible reasons for the observed deviation in D_L/D_S are discussed. Careful studies on the behavior of mean square displacement (MSD) close to the melting transition showed the particle motion to be subdiffusive at short times. The subdiffusive behavior at short times, is understood in terms of the entanglement of the dangling polymer chains between the shells of the neighboring PNIPAM microgel particles and argued to be the reason for the observed deviation (*i.e.* $D_L/D_S < 0.1$). Earlier reports on hard sphere or charged colloidal systems showed short time dynamics close to melting/freezing to be always diffusive. Thus observation of subdiffusive dynamics at short time close to melting transition of PNIPAM microgel crystals is first of its' own kind. Subdiffusive dynamics at short times suggest that dynamical criterion is inapplicable for melting of PNIPAM microgel crystals, since there is no proper scale for long time diffusion.

Chapter 5. Yielding behavior of PNIPAM microgel glasses

Colloidal glasses are viscoelastic in nature and yield under application of external shear. The viscoelastic response of the soft glass is often measured by performing the rheological measurements under application of the oscillatory strain of constant frequency, ω and variable amplitude, γ. The storage modulus (G') and loss modulus (G'') are measured as a function of applied γ. For small γ values, the response is linear *i.e.* G' and G'' are independent of γ. At large γ values response of viscoelastic materials becomes nonlinear i.e. G' and G'' becomes dependent on γ. The point of onset of nonlinearity is defined as yield point. For a typical soft glassy material, upon yielding, G' decreases monotonically whereas G'' exhibits a peak. In purely repulsive colloidal glass of hard spheres or charged colloids, yielding behavior has been well studied and understood to be due to breaking of the cages formed by topological neighbors. PINPAM microgel glasses consist of soft inhomogeneous (core shell) particles where their interparticle interactions in a suspension are complex and unknown. There are no reports on the yielding behavior and dynamics of such core shell soft sphere colloidal system.This chapter discusses the yielding behavior of dense PNIPAM microgel glasses studied using the nonlinear rheology. Dense PNIPAM microgel glasses of two volume fractions ϕ = 0.63 and 0.80 have been prepared and characterized for their glassy behavior using SLS and DLS techniques. The glass transition temperature of PNIPAM microgel suspensions is identified by investigating the dynamics as a function of temperature. For low γ, PNIPAM microgel glasses showed linear response. At large γ, G' showed a monotonic decreases, whereas G'' exhibited two peaks in contrast to a single peak observed in hard sphere glasses. Prior to our observations, two peaks in G'' have been reported in attractive glasses where interparticle interactions are made attractive by introducing the depletion attraction in hard sphere glass via addition of external polymer. In our studies, the interparticle interactions between PNIPAM spheres are soft sphere repulsive. So the observation of two peaks in G'' for dense PNIPAM microgel glasses is novel and is argued to arise from i) first due to disentanglement of dangling polymer chains of neighboring particles and ii) second due to breaking of cages due to the topological neighbors. In addition to two step yielding, mean square displacement at short times showed subdiffusive behavior constituting the direct evidence for entanglement of dangling polymer chains among neighboring particles in dense PNIPAM microgel glasses. The temperature and shear rate dependence of two step yielding is also investigated and results are presented in this chapter.

Chapter 6. Summary

This chapter presents summary and conclusions of investigations carried out using SLS, DLS, UV-Vis techniques and Rheology. Chapter ends with directions for future work. The important findings from these studies are also presented.

1. PNIPAM microgel particles are found to shrink upon osmotic compression of PNIPAM microgel suspension beyond critical osmotic pressure.
2. DLS has been employed to study the dynamics across the melting of dense PNIPAM microgel crystals. Careful analysis of mean square displacement showed for the first time that dynamics of PNIPAM microgel particles, close to melting of the crystals, is subdiffusive at short times. The subdiffusive dynamics at short times is argued to arise due to the entanglement of dangling polymer chains of neighbouring PNIPAM microgel particles.
3. On the contrary to earlier reports on hard sphere or charged colloidal crystals/liquids where short time dynamics close to melting/freezing is found to be always diffusive, our experiments on PNIPAM microgel crystals constitutes first evidence for the particles exhibiting subdiffusive dynamics at short time close to melting transition.
4. Subdiffusive dynamics at short times suggest that dynamical criterion is deviated for melting of PNIPAM microgel crystals, since there is no proper scale for long time diffusion.
5. Our non linear rheological measurements revealed that dense PNIPAM microgel glasses yield in two steps. Though two step yielding have been reported earlier in attractive glass, our observation of two step yielding in PNIPAM microgel glass constitute the first report in purely repulsive colloidal glass of soft spheres.
6. Two step yielding observed in dense PNIPAM microgel glasses is argued to arise due to i) breaking of the entanglements of dangling polymer chains and ii) breaking of topological cages. Short time behavior of mean square displacement is observed to be subdiffusive which constitutes direct evidence for entanglement of dangeling polymer chains among neighboring particles in PNIPAM microgel glasses.

LIST OF FIGURES

List of Tables

List of Symbols

Diameter of colloidal particle : d

Radius of colloidal particle : a

Volume fraction of colloidal suspension : ϕ

Number of colloidal particles in suspension : N

Volume of colloidal suspension : V

Number density of colloidal particles : n_p

Boltzmann constant : k_B

Temperature : T

Number of monovalent charges on colloidal particle : Z

Electronic charge : e

Dielectric constant of the solvent : ε

Inverse Debye-screening length : κ

Salt concentration : C_S

Hamaker constant : A_H

Hydrodynamic diameter of PNIPAM colloidal particle : d_h

Hydrodynamic radius of PNIPAM colloidal particle : a_h

Radius of core of PNIPAM microgel particle : a_c

Shell thickness of PNIPAM microgel particle : ρ

Pair correlation function : $g(r)$

Mass of colloidal particle : M

Time : t

Instantaneous velocity : $V(t)$

Coefficient of friction : ζ

Random force : $F(t)$

Solvent viscosity : η_S

Mean square displacement of colloidal particle : $<\Delta r^2(t)>$

Brownian time : τ_B

Cage rearrangement time : τ_R

Slow or alpha relaxation time of glasses : τ_α

Fast or beta relaxation time of glasses : τ_β

Slow or alpha relaxation frequency of glasses : ω_α

Fast or beta relaxation frequency of glasses : ω_β

Free diffusion coefficient : D_0

Short time diffusion coefficient : D_S

Long time diffusion coefficient : D_L

Index of subdiffusion : α

Viscosity of the suspension : η

Shear rate : $\dot{\gamma}$

Shear stress : σ

Shear strain : γ

Shear modulus : G

Storage modulus : G'

Loss modulus : G''

Instantaneous strain : $\gamma(t)$

Amplitude of oscillatory strain : γ_0

Frequency of strain/stress oscillation : ω

Incident light wave vector : $\overrightarrow{k_\iota}$

Scattered light wave vector : $\overrightarrow{k_s}$

Scattering wave vector : $\vec{q}$

Scattering angle : θ

Refractive index of medium : μ_s

Wave length of incident light : λ

Refractive index of colloidal particle : μ_p

Number of point scattering centers in a colloidal particle : n

Scattering amplitude of point scatterer : f

Electric field scattered from N particles at time t : $E_s(\vec{q},t)$

Origin of coordinate system : O

Position of the center of mass colloidal particle w.r.t. origin : $\vec{R}(t)$

The intensity of scattered light : $<I(q,t)>$

Particle form factor : $P(q)$

Refractive index of colloidal particle relative to medium : μ_r

Intensity of the incident light : I_0

Distance between sample and detector : P

Fluctuating property : $A(t)$

Delay time : τ

Relaxation time of correlation function : τ_c

Normalized intensity auto correlation function : $g^{(2)}(q,t)$

Normalized electric filed correlation function : $g^{(1)}(q,t)$

Coherence factor due to instrument optics : β_c

Dynamic structure factor : $F(q,t)$

Normalized dynamic structure factor : $f(q,t)$

Decay constant : Γ

Non-ergodicity factor : Y

Coherence factor due to multiple scattering : β_m

Coherence factor due to overlap of laser beams : β_{12}

Normalized intensity cross correlation function : $g_{12}^{(2)}(q,t)$

Mean square fluctuation in scattered intensity : σ_I^2

Molar attenuation coefficient : ε

Thickness of sample : z

Angle of cone : Θ

Radius of cone : R_P

Height of the cone from bottom plate : H

Angular speed of the rheometer tool : Ω

Torque : M

Imaginary number : i

Stress amplitude : σ_0

Phase shift between strain and stress : $\delta(\omega)$

Osmotic pressure due to mixing of polymer : Π_{mix}

Polymer volume fraction within microgel particle : Φ

Flory’s polymer-solvent interaction parameter : χ

Osmotic pressure corresponding to the elasticity of the polymer network : Π_{ela}

Volume fraction of polymer within microgel in collapsed state : Φ_0

External osmotic pressure : Π_{ext}

Position of the first peak in $S(q)$: q_m

Average interparticle separation : l

Lattice constant : l_a

CHAPTER 1

INTRODUCTION

Colloidal suspensions are solutions of micron/submicron sized solid particles suspended in a solvent. In a suspension, bare colloidal particles have a tendency to undergo aggregation due to van der Waals attraction between the particles. The aggregation can be prevented and hence suspensions can be made stable, via steric stabilization by adding a thin layer of polymer on particle surface or via charge stabilization by creating the charge on the surface of the colloidal particles. Under suitable conditions, monodisperse colloidal particles dispersed in a solvent exhibit structural ordering (gas, liquid, crystal and even glass) similar to that of atomic systems [1-3], with larger interparticle length scales (100 nm - 10 μm) and slower dynamics (10^{-6} sec -10^{3} sec) giving an easy access to the experiments. Typical values of elastic constants for dense colloidal suspensions (~10^{13} particles per cubic centimeter) are ~10 dyne cm^{-2} in contrast to ~10^{12} dynes cm^{-2} for atomic systems (~10^{23} particles per cubic centimeter) [2, 4]. The latent heat of melting for colloidal crystal of size 1 cm^{3} is of the order of μCal [5-6], but when scaled properly, the molar elastic constants as well as molar latent heat of the colloidal suspensions match closely with that of atomic systems [4, 6]. Thus colloidal suspensions mimic atomic systems, hence serve as model condensed matter system to understand many fundamental phenomena like crystal nucleation and growth [7-11], defects and dynamics in crystals [10, 12-13], glass transition [14-16], shear flows in glasses [17], fragility [18] and dynamical heterogeneity [14-16] in glasses etc. Ordered structures of monodisperse colloids are found to have several high tech applications *viz.*, sensors [19-21], Bragg filters [22], optical switches [23-24], display devices [25] etc. Many of the industrial processes and applications involve shearing of the colloidal suspensions. Upon application of shear stress, colloidal suspensions undergo flow/deformation. Under dilute condition, flow in colloidal suspensions is Newtonian (*i.e.* viscosity, η of the suspension is independent of the applied stress) [26]. On the other hand, dense colloidal suspensions show shear thickening (η increases with applied stress) as well as shear thinning (η decreases with applied stress) [26]. Dense colloidal suspensions behave like viscoelastic solids, which possesses properties in between that of ideal elastic solids and ideal viscous liquids [27]. Upon application of large shear stress, dense colloidal suspensions undergo yielding [27]. Study of yielding and flow behavior (rheology) of colloidal suspensions is important for successful formulation and manipulation of many industrial products such as cosmetics, paints, inks, medicines, food products etc. This chapter gives brief introduction about colloidal suspensions for their interparticle interactions, phase behavior, dynamics and rheology.

1.1 Hard sphere colloidal suspensions

Simplest colloidal system studied for its phase behavior is suspensions of hard sphere particles [1]. Hard sphere particles do not interact with each other and experience steep repulsion on contact with other particle. The interparticle interaction potential for hard sphere colloidal particles of diameter, *d* is written as,

$$\begin{aligned} U(r) &= 0\,;\ if\ r \geq d, \\ &= \infty;\ if\ r < d\,. \end{aligned} \tag{1.1}$$

Colloidal suspensions of sterically stabilized poly methyl methacrylate (PMMA) forms best example of hard sphere suspensions [1, 14]. Figure 1.1 shows the phase diagram of the monodisperse hard sphere colloidal suspensions [1]. The only control parameter available to vary phase behavior of hard sphere colloidal suspensions is volume fraction, ϕ (= $n_p \pi d^3/6$, where $n_p = N/V$ is particle number density, with N being the number of colloidal particles in a suspension of volume, V). Under dilute conditions, the suspension shows disordered (gaseous) phase. Upon increasing the ϕ, suspension exhibits liquid like order. At ϕ = 0.495, the hard sphere colloids start to organize spontaneously into a crystalline phase with fluid-crystal coexistence extending up to ϕ = 0.545, where it shows complete crystallization. The equilibrium crystal structure of hard spheres is found to be a face centered cubic (fcc), which is entropically favored minimum energy configuration [28-30]. Hard sphere suspensions also exhibit hexagonal close packed (hcp) structure or fcc-hcp coexistence due to very small difference ($10^{-3}k_BT$) in the free energies of hcp and fcc structures [28-30]. Here k_B is the Boltzmann constant and T is the temperature. With further increase in ϕ, the colloidal particle dynamics become slower and it undergoes kinetic arrest into a disordered state (glass) by exhibiting glass transition at ϕ = 0.58. At ϕ = 0.64, randomly arranged particles touch each other leading to random close packed (RCP) glassy state in hard sphere suspensions. In fcc as well as in hcp crystals, hard spheres can be packed to maximum of ϕ = 0.74.

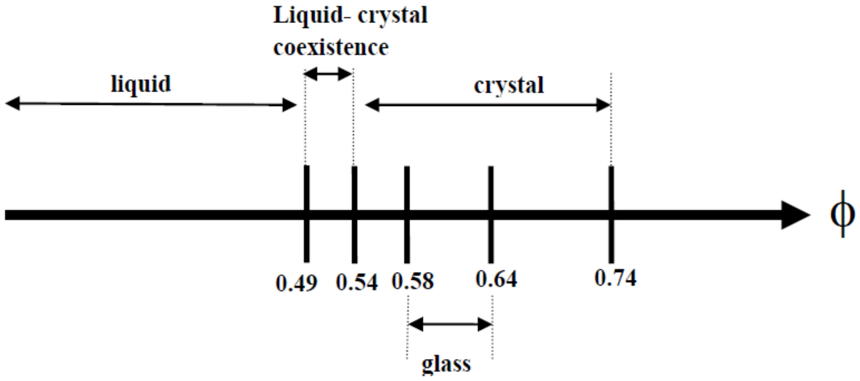

Fig. 1.1 Phase diagram of monodisperse hard sphere colloidal suspensions.

When colloidal particles are polydisperse in size, phase behavior of their suspension has been found to differ from that of the monodisperse particle's case [31]. With increase in polydispersity, the crystallization point has been observed to shift to higher ϕ. Suspensions of colloidal particles having size polydispersity (SPD) up to 11% are only found to exhibit crystalline ordering. Suspensions with SPD larger than 11% have been found to freeze into disordered (glassy) state [31].

1.2 Charge stabilized colloidal suspensions

Another well studied colloidal system is charge stabilized colloidal suspensions. Interparticle interactions in suspensions of charged colloidal particles, with low surface charge, are well described within formulation of Derjaguin–Landau–Verwvey–Overbeek (DLVO) theory [2, 32]. According to the DLVO theory, the net interaction between charged colloidal particles is written as sum of screened coulomb repulsion, $U_R(r)$ and van der Walls attraction, $U_A(r)$.

$$U(r) = U_R(r) + U_A(r). \tag{1.2}$$

Screened coulomb repulsion arises due to screening of the coulomb repulsion between like charged particles by counter-ions and salt ions present within a suspension and is given as,

$$U_R(r) = \frac{e^2}{\varepsilon}\left[\frac{Ze^{\kappa a}}{1+\kappa a}\right]\frac{e^{-\kappa r}}{r}\ , \tag{1.3}$$

where, a is the radius of the particle, Ze is the effective charge on a colloidal particle with Z being number of monovalent charges and e is electronic charge , ε is the dielectric constant of the solvent and κ is the inverse Debye-screening length given by,

$$\kappa^2 = \frac{4\pi e^2}{\varepsilon k_B T}\left(n_p Z + C_s\right), \tag{1.4}$$

with k_B being the Boltzmann constant, T is the temperature, n_pZ are the number of counterions and C_S is the salt concentration. The van der Walls attraction potential is given as,

$$U_A(r) = -\frac{A_H}{6}\left[\frac{2a^2}{r^2-4a^2}+\frac{2a^2}{r^2}+ln\left(\frac{r^2-4a^2}{r^2}\right)\right], \tag{1.5}$$

where A_H is Hamaker constant which sets the scale for attraction.

Thus, the charged colloids offer suspension parameters like particle charge, Z and ionic strength, C_S as control parameters to vary phase behavior along with ϕ. The deionized suspensions of charged colloids exhibit crystalline ordering at ϕ as low as 0.005 due to long ranged coulomb repulsive interactions. Phase diagram of the charge colloidal suspensions [33] is shown in Fig. 1.2. At low ϕ and high C_S, suspensions show liquid like order. Upon reducing the C_S, low ϕ (< 0.2) suspensions crystallize into body centered cubic (bcc) structure. With increase in ϕ, crystal structure of charged colloids is found to change to face centered cubic (fcc) with bcc-fcc coexistence at intermediate ϕ and C_S (shown by shaded region in Fig. 1.2). At higher ϕ, suspensions freeze into glassy state. Glassy state has also been observed in low ϕ suspensions upon pressure quenching [16].

Deionized charged colloidal suspensions have been found to turn inhomogeneous (in the form of gas-solid and gas-liquid coexistence) when the charge density of particle is high [2]. Though the exact mechanism responsible for the occurrence of inhomogeneous phases under certain conditions is unknown, it was interpreted that it arises due to long range attraction between like charged particles mediated by counterions [35-36]. Recent experiments on dilute highly charged colloids have shown direct evidence for existence of attraction between like charged colloidal particles [37]. In the case of charged colloidal particles, charge polydispersity (CPD) alongside the size polydispersity (SPD), plays an important role in structural ordering [38]. In dilute suspensions, where interparticle distances are several times larger than particle diameter, CPD is shown to be dominant. Suspensions with CPD up to 26% exhibits crystalline order in contrast to 11% SPD [31] observed in the case of hard sphere colloidal suspensions [38].

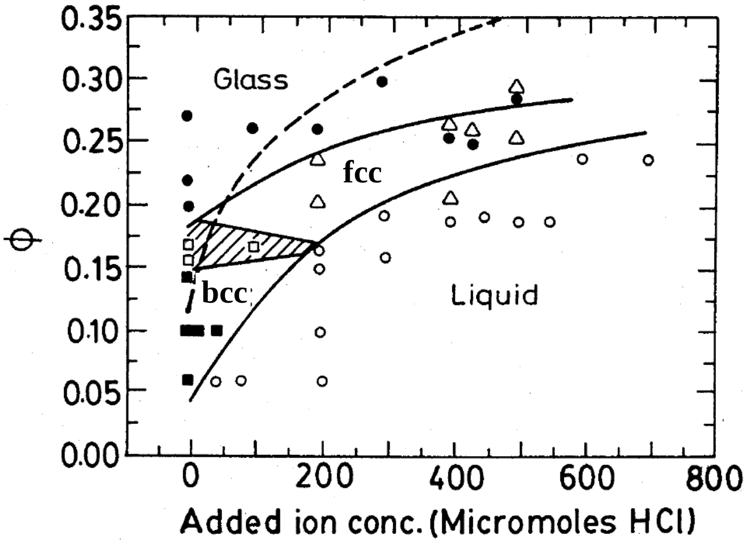

Fig. 1.2 Phase diagram of charged polystyrene colloidal suspensions, (Adapted from Sirota *et al.* [33]). Different phases of the suspensions are shown as, open circles: Liquid, open triangle: fcc, closed square: bcc, open square: bcc-fcc coexistence, closed circles: glass. Continuous lines are obtained from density functional theory [34].

1.3 Stimuli-responsive microgel suspensions

In hard sphere or charge stabilized colloidal suspensions, size of the particle is fixed and can be altered only by changing the synthesis conditions. On the other hand, stimuli-responsive microgels offer tunability of particle size by tuning external stimuli like temperature, pH, ionic strength etc. Microgel particles consist of crosslinked polymer chains network immersed in a solvent. The polymer chains network expand/contract with respect to variation in stimuli, which causes gel particle to swell/deswell and hence increase/decrease in their size. When stimulus is temperature, microgels are known as thermo-responsive microgels. Aqueous suspensions of poly

(N-isopropyl acrylamide) (PNIPAM) microgels is one of the thermo-responsive microgel system [39]. PNIPAM microgels can also be made responsive to pH [40] and to various chemicals [41-42] by proper functionalization. Therefore PNIPAM microgels have found applications in sensing various chemical elements and in solvent extraction. PNIPAM microgels are biocompatible and are used for controlled drug delivery [43].

1.3.1 Thermo-responsive behavior of PNIPAM microgels

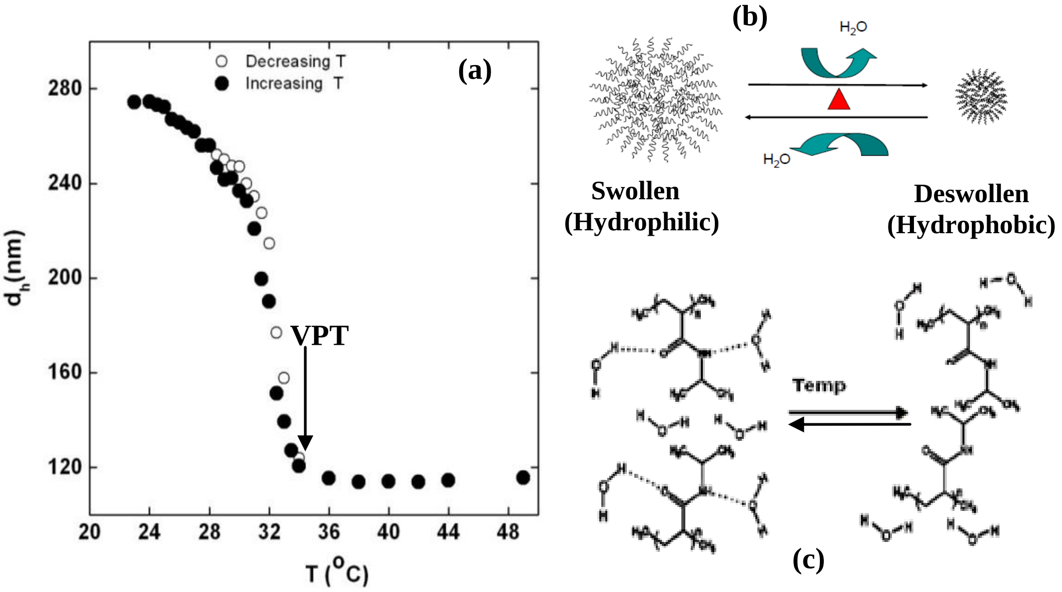

Fig. 1.3 (a) Variation of hydrodynamic diameter, d_h of PNIPAM microgel particles with temperature, (b) Schematics showing transition of PNIPAM microgel from swollen (hydrophilic) to deswollen (hydrophobic) state and vice-versa. (c) Schematic diagram of the chemical structure change occurring across the volume phase transition for the PNIPAM microgel.

PNIPAM microgel particles show decrease in their size (deswell) with increase in temperature and undergo transition from swollen state to collapsed state at T ~ 34°C (shown in Fig. 1.3(a)), which is known as volume phase transition (VPT) [39-44]. The transition from swollen to deswollen state is reversible and is understood to occur due to PNIPAM polymer chains turning from hydrophilic at temperatures below VPT to hydrophobic at temperatures above VPT [45-46], which is depicted schematically in Fig 1.3(b). In swollen state, PNIPAM microgel particle contains ~2-3% polymer and rest water (solvent), whereas in collapsed state (deswollen state) it contains about 60% of polymer and 40% of water [47]. Also below VPT, water molecules are bonded with the PNIPAM chains via hydrogen bonding. Upon VPT, hydrogen bonds break and water expels out contributing to the deswelling of the PNIPAM microgel particles [45-46], which is shown schematically in Fig. 1.3(c).

1.3.2 Internal structure of PNIPAM microgel particles

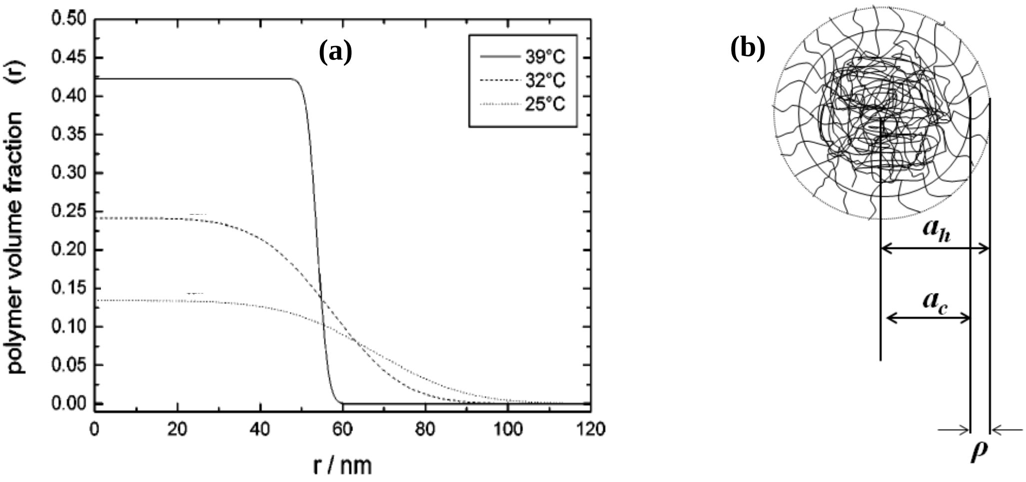

Fig. 1.4 (a) Radial polymer density profiles of PNIPAM microgel particle at various temperatures measured using small angle neutron scattering, (Adapted from Stieger *et al*. [50]), and (b) Schematic showing core-shell structure of PNIPAM microgel particles in swollen state, with core of radius a_c and shell of thickness ρ. $a_h = d_h / 2$, is the hydrodynamic radius.

PNIPAM microgel particles are known to consist of ~2-3% polymer and rest is water (solvent) [47]. The polymer chains are crosslinked together, either via external crosslinking agent or via self crosslinking of polymers [48-49], to form polymer network which spans the volume of the particle. Thus, unlike hard sphere particles, PNIPAM microgel particles are porous, solvent permeable in nature. The internal structure of PNIPAM microgels were investigated using small angle neutron scattering

(SANS) [47, 50]. Radial polymer density profiles determined from SANS curves at temperatures below VPT [50] showed that, the polymer volume fraction at the central part is almost constant and decreases rapidly towards the edge of the particle (Fig. 1.4(a)). These measurements thus suggest that PNIPAM microgel particles have core shell structure with dense core and fuzzy shell. Radius, a_c of the PNIPAM microgel particle measured using SANS has been found to be smaller than the hydrodynamic radius, a_h measured using dynamic light scattering (DLS) [47, 50]. Smaller value of a_c than a_h have been interpreted in terms of the core-shell structure of PNIPAM microgel particles [47, 50], with densely crosslinked core of radius a_c and thin shell of dangling polymer chains with thickness ρ. The core-shell structure of PNIPAM microgel particle is shown schematically in Fig. 1.4(b). Due to low polymer content, the shell does not contribute to the scattered intensity in SANS measurements, whereas, it affects the particle dynamics in a solvent making a_h to be larger than a_c. Difference between a_h and a_c gives the thickness of the shell (*i.e.* $\rho = a_h - a_c$). Typical value of ρ is found to be 20-30 nm [47, 50]. With increase in T, the polymer density in the central part of the microgel has been found to increase considerably, indicating deswelling of the core of the PNIPAM microgel particle. Whereas, thickness of the shell have been found to remain unaffected by temperature [47]. Core size and shell thickness of PNIPAM microgel particles have been found to depend on the crosslinker concentration [49]. With increase in crosslinker concentration, while the total size of PNIPAM microgel (core + shell) decreases, size of the core relative to the thickness of the shell increases [49].

1.3.3 Phase behavior of PNIPAM microgel suspensions

As mentioned earlier, PNIPAM microgel particles in the swollen state contains 97% of water [47], hence its refractive index is not very much different from that of the solvent. Hence, PNIPAM microgel suspensions are free from multiple scattering of light and offer an advantage of probing the dense suspensions for their structural ordering, dynamics and phase behavior using static and dynamic light scattering techniques. At low T, dense suspensions of monodisperse PNIPAM microgel particles exhibit liquid, crystalline and glassy phases [39, 45, 51]. The variation of particle size and hence ϕ with T, allows one to use T as a control parameter to vary the phase behavior of the dense PNIPAM microgel suspensions, which is not possible in the case of hard sphere or charged colloidal suspensions. Upon increasing the temperature, crystals and glasses melt into liquid like order and further exhibit fluid (liquid like) to fluid (gas like) transition [39, 45].

Another important parameter that governs the phase behavior of the PNIPAM microgel suspensions is the soft nature of the microgel particles [52]. PNIPAM microgels are soft particles which can be compressed by application of osmotic pressure [52]. Softness of the particles can be varied by varying the amount of crosslinking agent. Smaller the amount of crosslinking agent, higher is the softness of the microgel particles [18, 39]. The exact nature of interparticle interaction potential that can describe the phase behavior of PNIPAM microgels with respect to temperature and softness is yet unknown. Phase behavior of soft spheres, modeled assuming the soft repulsive interaction potential of the kind, $U(r) = (d/r)^n$ [53, 54], suggested that with increasing the degree of softness ($1/n$), liquid-crystal transition point shifts to higher ϕ and the liquid crystal coexistence region narrows down as compared to that of the hard sphere system. Crystallization of PNIPAM microgel suspensions, at low T, is also found to occur at ϕ much higher than that for hard sphere suspension (ϕ = 0.494) [39, 51], suggesting that the low temperature interactions between PNIPAM microgel particles can be described as soft repulsive type. Wu *et al.* [45] have found that, when temperature of PNIPAM microgel suspension is increased above VPT, interparticle interactions turn to be attractive. Change of interparticle interactions from soft repulsive type at low T to attractive type at high T have been realized via measurement of second virial coefficient [45]. Up to VPT, second virial coefficient is found to be positive, whereas for temperatures above VPT, it is found to turn negative [45]. The change of virial coefficient from positive to negative is explained in terms of the change of polymer content of the microgel particles [45]. At low temperatures, polymer content of microgel particle is 2-3% and rest is water, whereas above VPT it increases to 60% [47]. Therefore, at temperature below VPT van der Walls attraction between microgel particles is negligible and interparticle interactions are repulsive, whereas above VPT van der Walls attraction becomes prominent due to high polymer content of the particle making interparticle interactions to be attractive.

1.3.4 Structure of PNIPAM microgel crystals

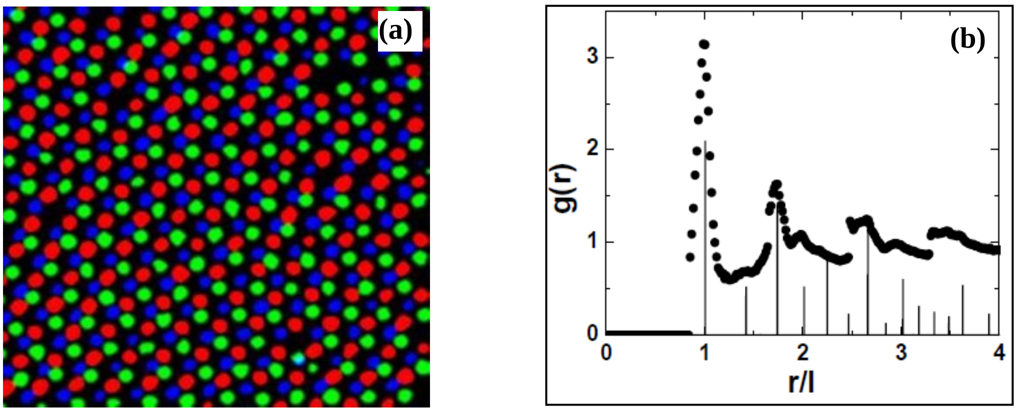

Fig. 1.5. (a) Overlay of confocal images of three successive layers showing ABC stacking in PNIPAM microgel crystal having fcc structure (layer A – red, layer B - green, layer C - blue) (b) Experimental *g(r)* (dark circles) along with simulated *g(r)* (lines) for fcc structure. (Adapted from Brijitta *et al*. [55]).

In our earlier studies, structure of PNIPAM microgel crystals have been investigated, using confocal laser scanning microscopy (CLSM) [55]. CLSM studies by Brijitta *et al.* [55] on PNIPAM microgel crystal of $\phi = 0.44$ have showed that the structure of PNIPAM microgel crystal, which experiences shear in the process of sample handling and transfer of crystal from one container to another, is random hexagonal close packed (RHCP). When crystal with RHCP structure was melted by raising temperature beyond melting point and then cooled slowly, stacking faults got annealed out and equilibrium crystal structure has been found to be fcc [55]. The crystal structure has been determined by obtaining the stacking probability of crystal layers in <111> direction and by comparing the experimentally obtained pair correlation function, *g(r)* to that of the simulated one. Stacking probability have been obtained by overlaying confocal images of three successive crystal layers, which is assigned to be 1 for ABC, BCA and CAB type stacking and zero, otherwise. Overlay of three successive layers showing ABC stacking in fcc PNIPAM microgel crystal is shown in Fig. 1.5(a). Stacking probability for slow cooled PNIPAM microgel crystal is found to be 0.95 [55] and the experimental *g(r)* is found to match with that of the simulated for fcc structure (Fig. 1.5(b)), confirming the crystal structure to be fcc. By taking this study as an input, structures of all the PNIPAM microgel crystals used in the present thesis work are considered to be fcc.

1.4 Dynamics in colloidal suspensions

Colloidal particles suspended in a solvent undergo Brownian motion. Brownian motion of colloidal particles in a suspension is described by Langevin equation of motion and given as,

$$M\frac{dV(t)}{dt} = -\zeta V(t) + F(t). \tag{1.6}$$

Left term in the above equation gives the total force on the Brownian particle with mass M and acceleration $dV(t)/dt$, which is the sum of systematic frictional force ($-\zeta V(t)$) and random force ($F(t)$). Systematic frictional force represents the slowing down tendency of colloidal particle due to more collisions of solvent molecules (on average) on its front side than back side. ζ is called the coefficient of friction and in case of spherical particle it is given as $\zeta = 6\pi\eta_s a$, with η_S being solvent viscosity and a is radius of the sphere. The random force arises from the occasional fluctuations of solvent molecules, in which the particle experiences collisions that accelerates and decelerates it. Thus, random collisions of solvent molecules act as driving motors which drive colloidal particle motion. Solution to eqn. (1.6) gives,

$$V(t) = V(0)exp\left(-\frac{\zeta}{M}t\right) + \int_0^t d\tau\, exp\left(-\frac{\zeta}{M}(t-\tau)\right)F(\tau). \tag{1.7}$$

From Eqn. (1.7), velocity correlation function, averaged over Maxwell velocity distribution, is written as,

$$\langle V(t)V(0)\rangle = \langle V(0)\rangle^2 exp\left(-\frac{\zeta}{M}t\right) = \frac{3k_BT}{M}exp\left(-\frac{\zeta}{M}t\right). \tag{1.8}$$

Second term from Eqn. (1.7) disappears upon averaging, because $<V(0)F(t)> = 0$ as random force is uncorrelated to initial velocity. Mean square displacement (MSD) of the colloidal particle is related to the velocity correlation function as,

$$\langle \Delta r^2(t)\rangle = 2\int_0^t d\tau\ (t-\tau)\langle V(\tau)V(0)\rangle. \tag{1.9}$$

In order to describe the dynamics of colloidal particle, MSD is divided broadly into three time scales namely short time, intermediate time and long time. These time scales are determined on the basis of the Brownian time (τ_B), which is the time required to decouple the colloidal particle dynamics from that of the solvent, and the time, which particle takes to move over its own distance (cage rearrangement time -τ_R). Motion of particle within times $\tau_B << t << \tau_R$ is called short time motion where as motion at

$t >> \tau_R$ is called long time motion. Time scales in the vicinity of τ_R are regarded as intermediate time scales.

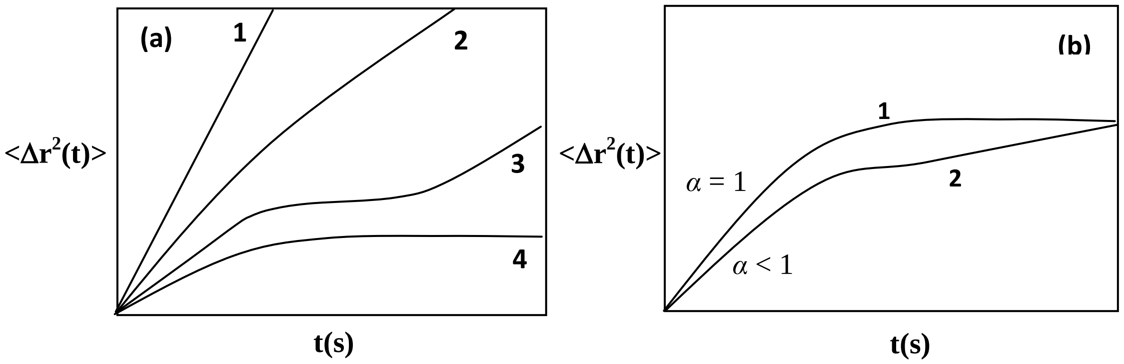

Fig. 1.6 (a) Schematic showing behavior of mean square displacement (MSD) of hard sphere particles as a function of time, t in gaseous state - 1, liquid like state - 2, supercooled liquid state - 3 and crystalline/glassy state - 4, of the suspensions. (b) Schematics showing behavior MSD with t for colloidal particles in repulsive glasses -1 and attractive glasses -2. α values indicate the diffusive (α = 1) and subdiffusive (α < 1) behavior of MSD in repulsive and attractive glasses, respectively at short times.

Mean square displacements (MSD), $<r^2(t)>$ as a function of time, for colloidal particle in suspensions with different particle densities and/or interaction strengths are shown schematically in Fig. 1.6(a). In dilute non interacting suspensions (gaseous state), colloidal particles show free diffusive motion ($<r^2(t)> \propto t$) over all the time scales, which is characterized by single diffusion coefficient, D_0 called as free diffusion coefficient (as shown in Fig. 1.6(a)-1). In the case of moderately dense (liquid like ordered) suspensions, short time diffusion of colloidal particles become slower than D_0, due to hydrodynamic interactions,(*i.e.* interparticle interactions mediated by solvent velocity field) and given as short time diffusion coefficient, D_S [56]. Whereas at longer times, colloidal particles experience direct interparticle interactions alongside with hydrodynamic interactions causing further slowing down of diffusive motion, which is described by long time diffusion coefficient D_L [56]. MSD of colloidal particles in liquid like ordered suspension is depicted schematically in Fig. 1.6(a)-2. Change of diffusion coefficient from D_S to D_L can be seen from change of slope of MSD at intermediate times. In the case of supercooled liquid state, colloidal particles experience a cage from the neighboring particles [14]. At short times, colloidal particles exhibit diffusive motion within the cage, with diffusion coefficient D_S. At intermediate timescales, where the particle experiences cage from surrounding particles, its motion become subdiffusive (*i.e.* $<\Delta r^2(t)> \propto t^{\alpha}$, with $\alpha < 1$). Subdiffusive motion of the colloidal particle is seen as a plateau in MSD at intermediate times in Fig. 1.6(a)-3. At longer time, the particle escapes from the cage due to the dynamic nature of cages and exhibits diffusive motion with diffusion coefficient D_L. When supercooled liquids freeze in the glassy state or normal liquid freeze in to crystalline state, long time diffusion gets ceased out making D_L to be zero, whereas shorter time motion continues to exist (Fig. 1.6(a)-4) [14, 57].

Eckert *et al.* [58] have shown that when attractive interaction is introduced in the hard sphere glasses, via depletion attraction by addition of external polymer, the glass initially melts into a liquid and upon further increase in interaction strength an entirely new glassy state is formed, where particles are bonded together with attractive interactions. This new glassy state is referred as attractive glass. Arrest of the particle motion in the attractive glass occurs due to bonding between the particles as well as due to trapping of particle within the near neighbor cage [58]. MSD’s for repulsive and attractive colloidal glasses are compared in Fig. 1.6(b). In repulsive glass, MSD shows plateau at long times due to arrest of particle dynamics within near neighbour cage, whereas at short time MSD shows diffusive behavior (*i.e.* $<\Delta r^2(t)> \propto t$, as shown in Fig. 1.6(b)-1). On the other hand, in the case of attractive glasses, short time MSD shows subdiffusive behavior (*i.e.* $<\Delta r^2(t)> \propto t^{\alpha}$, with $\alpha < 1$) [59] and reaches saturation limit of the repulsive glass at very long times, as shown in Fig. 1.6(b)-2.

1.5 Yielding behavior of hard sphere colloidal glasses

Colloidal suspensions belong to the class of viscoelastic materials, which possess properties in between that of ideal elastic solids (obeys Hooks' law of elasticity, $\sigma = G\,\gamma$ where σ is a stress, γ is a strain and G is the shear modulus) and ideal viscous liquids (obeys Newton's law of viscosity, $\sigma = \eta\dot{\gamma}$) [27]. The viscoelastic response of the colloidal suspensions is described in terms of storage modulus, G' (which represents the elastic properties of the material) and loss modulus, G'' (which represents the viscous properties of the material). $G' > G''$ indicates that the elastic response of the material is dominant and the material shows solid like behavior. Whereas, $G' < G''$ suggests that the viscous response of the material is dominant and the material shows liquid like behavior. G' and G'' can be measured by deforming the material using oscillatory shear strain, $\gamma(t) = \gamma_0 \exp(i\omega t)$, with a strain amplitude, γ_0 and frequency of oscillation, ω.

Figure 1.7 shows the variation of G' and G'' with applied γ_0, for the hard sphere suspension close to its glass transition, at constant ω. At low γ_0, both the G' and G'' show plateaus, indicating their independence with respect to γ_0. Within this plateau region the deformation of colloidal suspension is linear. Beyond a certain critical γ_0, G' and G'' start varying with γ_0, indicating the yielding of the colloidal glass at large γ_0 [60]. It has been shown that locally, yielding of the hard sphere glasses occur via irreversible rearrangements of colloidal particles (breaking of the near neighbour cages) under applied shear [61, 62]. While yielding, G' shows monotonic decrease with γ_0, whereas G'' shows a peak. The peak in G'' appears at $\gamma_0 \sim 10\%$ where irreversible rearrangements of colloidal particles (breaking of near neighbour cages) takes place [60, 61], suggesting that the peak is associated with the process of cage breaking.

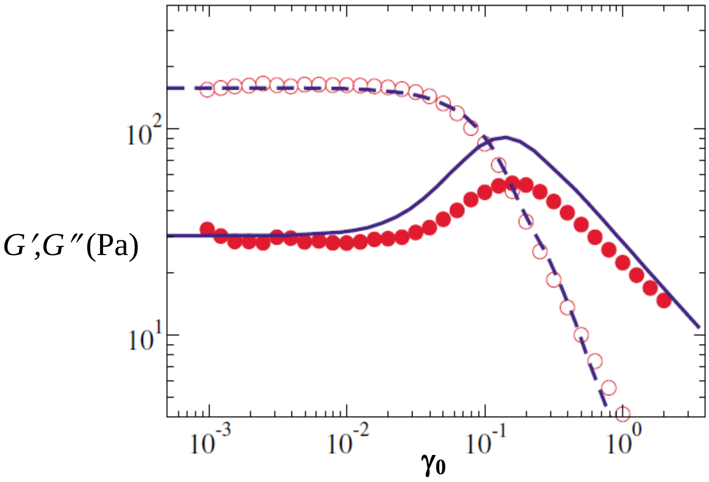

Fig. 1.7 Yielding behavior of dense hard sphere colloidal suspension close to its glass transition (ϕ = 0.57). Symbols are from experimental data. Lines are results from mode coupling theory. G'' - solid symbols & continuous line. G' - open symbols & dotted line. (Adapted from Miyazaki *et al.* [60]).

A peak in G'' is characteristic of soft glassy materials [60-63].According to soft glassy rheology model [63], the peak in G'' arises as the particles experience activated barrier from near neighbor cages during the shear flow. Miyazaki *et al.* [60] have shown that the peak in G'' is generic characteristic of materials having slow relaxation times and can be present even in the absence of activated barriers. It has been shown that the peak in G'' arises due to decrease in the relaxation time of the materials (slow or alpha relaxation time, τ_α in the case of hard sphere glasses) with increase in the rate at which the material is sheared [60, 64]. The apparent relaxation time, τ at given shear rate is written as,

$$\frac{1}{\tau(\dot{\gamma}_0)} = \frac{1}{\tau_\alpha} + K\dot{\gamma}_0{}^{\upsilon}, \qquad (1.10)$$

where ν is an exponent and K is a constant. $\dot{\gamma}_0 = \gamma_0\omega$ gives the shear rate. The peak in

G''occurs at position, where $\dot{\gamma}_0 \sim 1/\tau$.

The relaxation times in the colloidal suspensions can be measured by deforming the material linearly at constant small γ_0 (within the plateau regime) and varying the ω. Behavior of the G' and G'' with ω for linearly deformed colloidal glasses is shown schematically in Fig. 1.8. At very small ω, where suspension can completely relax, $G' < G''$, suggesting a liquid like behavior. As ω increases, G' and G'' both increases and cross each other at ω_α, where the corresponding shear rate $\dot{\gamma}_0 = \gamma_0 \omega_\alpha$ becomes equal to inverse alpha relaxation time ($1/\tau_\alpha$). Beyond the crossover point, $G' > G''$ where G' stays constant and G'' starts decreasing causing a peak. G'' continues to decrease till ω_β, reaches the minimum and then start increasing. At higher ω, both the G' and G'' increase with power law behavior. From the peak and the minimum in G'', alpha and beta relaxation times in the colloidal glasses can be determined.

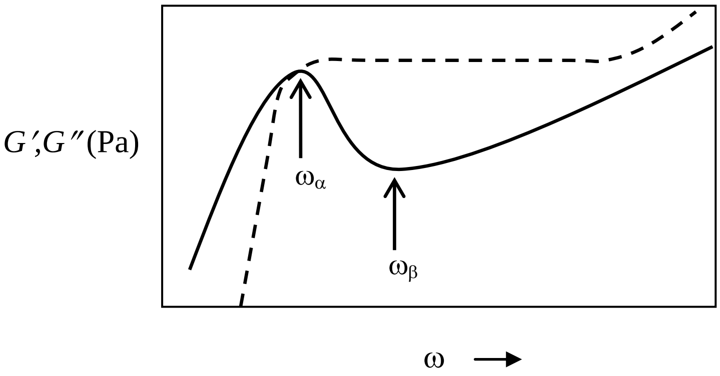

Fig. 1.8 Variation of G' (dotted line) and G'' (continuous line) with ω for hard sphere colloidal glasses measured at small γ_0. Arrows indicate the peak in G''(corresponding to alpha relaxation frequency, ω_α) and the minimum in G'' (corresponding to beta relaxation frequency, ω_β).

When the glasses are deformed with large γ_0, the peak in G'' (shown in Fig. 1.8) shifts to higher ω due to decrease in τ_α with increase in the shear rate ($\gamma_0\omega$) [60, 64], which causes the peak in G'' to arise while yielding of the glasses (shown in Fig. 1.7).

1.6 Yielding behavior of attractive colloidal glasses

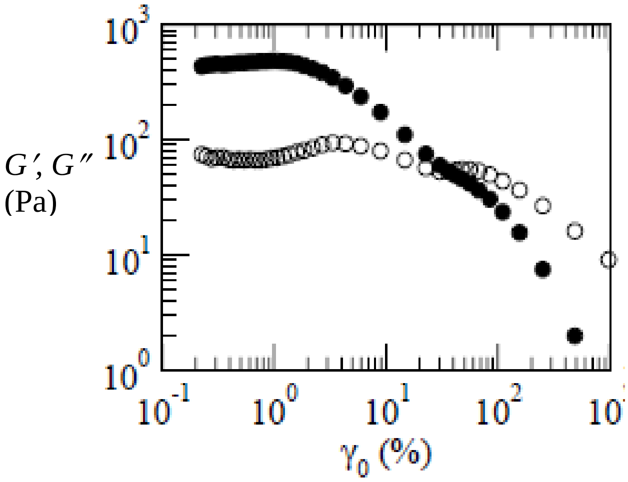

Fig. 1.9 Yielding behavior of attractive glasses. PMMA particles dispersed in cis-decaline at ϕ = 0.6 with added polymer (depletant). (Adapted from Pham *et al.* [65]).

Yielding behavior of the attractive glasses has been found to be distinct from that of the hard sphere glass. While hard sphere glass yields with one peak in G'' (Fig. 1.7), attractive glass is found to yield with two peaks in G'' (Fig. 1.9) [65]. In attractive glasses, in addition to the caging from the neighboring particles, arrest of particle dynamics arises from the interparticle bonding due to attractive interaction. Pham *et al.* [65] have interpreted two peaks in G'' in the yielding of attractive glasses as the one at lower strain arises due to breaking of the interparticle bonds and the second at higher strain arises due to breaking of topological cages formed by neighbouring particles.

1.7 Motivation for the thesis

PNIPAM microgel particles are temperature sensitive, inhomogeneous (core-shell structured) particles having densely crosslinked core and a thin shell (~ 20-30 nm) of dangling polymer chains [47, 50]. PNIPAM microgel particles show decrease in size with increase in temperature and undergo sudden collapse in size at 34°C, called as volume phase transition, VPT. The dense core is known to deswell more compared to the shell upon increasing the temperature [47]. Dense suspensions of PNIPAM microgels exhibit liquid, crystalline and glassy phases similar to the other colloidal or atomic/molecular systems [39, 45, 55]. PNIPAM microgels offer tunability of particle size and hence volume fraction using temperature [39], which helps to study the phase transitions driven by temperature in PNIPAM microgel suspensions. In addition, PNIPAM microgel particles in swollen state contain 2-3% of polymer and rest is water [47], hence are closely matched in the refractive index with the solvent (water). Thus, PNIPAM microgel suspensions are relatively free from multiple scattering of the light and offer the advantage of probing their structural ordering, dynamics and phase behavior using static and dynamic light scattering techniques.

Along with being temperature responsive, PNIPAM microgels are known to be responsive to osmotic pressure and undergo compression upon application of osmotic pressure [52, 66], as their Bulk modulus is of the order of ~ kPa [66]. When the osmotic pressure experienced by PNIPAM microgel particles exceeds their Bulk module value, they are expected to undergo deswelling. Effect of osmotic pressure exerted by the addition of a non-adsorbing polymer to the PNIPAM microgel suspensions under dilute conditions has been studied using DLS [52, 66]. Osmotic pressures of the order of kPa can also be experienced by PNIPAM microgel particles under dens conditions (particle number densities of the order of 10^{12} to 10^{13} cm^{-3}). However effect of osmotic pressure in dense suspension arising from the neighbouring particles has not been investigated. In this thesis we report experimental evidence for compression of PNIPAM microgel particles under osmotic pressure exerted by its own PNIPAM microgel particles due to structural ordering in dense suspensions. Towards this PNIPAM microgel crystals under different osmotic pressures have been prepared and their Bragg diffraction has been recorded using UV-Vis spectrometer. The osmotic compression of PNIPAM microgel particles in dense suspensions have been realized by observing interparticle separation in osmotically compressed PNIPAM microgel crystals being smaller than original microgel diameter.

In dense suspensions, where interparticle separations are of the order of particle diameter, the core-shell structure of the PNIPAM microgel particles is expected to influence their dynamics. DLS studies on dense liquid like ordered suspensions of PNIPAM microgels by Eckert *et al.* [67] have shown that the microgel dynamics is influenced by its core-shell structure. However, the influence of core-shell structure of PNIPAM microgel particles on their dynamics in dense crystalline and glassy state of the suspensions has not been investigated. Towards this the dynamics in dense PNIPAM crystals and glasses across their melting transition have been investigated using DLS technique.

In the study of dynamics across melting of dense PNIPAM microgel crystals, we verify the applicability of dynamical criterion for their melting. Dynamical criterion has been proposed by Löwen *et al.* [68] for identifying the melting/freezing transition of colloidal crystals/liquids. According to this criterion, the ratio of long time diffusion coefficient (D_L) to short time diffusion coefficients (D_S) at freezing/melting transition is reported to be $D_L/D_S \sim 0.1$. This criterion is reported to be universal as it was found to be applicable to colloidal systems, with different interparticle interactions, exhibiting Brownian motion. However, its applicability for PNIPAM microgel crystals/liquids undergoing melting/freezing has not been verified. With this as the motivation, dynamics across the melting of PNIPAM microgel crystals have been studied using DLS technique. It is shown for the first time that at melting/freezing of PNIPAM microgel crystals/liquids the value of D_L/D_S is < 0.1. Further analysis suggested that dynamics of PNIPAM microgel particles at short times close to the melting/freezing transition is subdiffusive, indicating the inapplicability of dynamical criterion for melting of PNIPAM microgel crystals. The subdiffusive dynamics at short times and hence inapplicability of dynamical criterion for melting of dense PNIPAM microgel crystals is argued to arise due to the entanglement of the dangling polymer chains of neighbouring PNIPAM microgel particle,

Motivated by the observation of subdiffusive short time dynamics in dense PNIPAM microgel liquids and crystals, we studied the dynamics in dense PNIPAM microgel glasses and showed that entanglements of the dangling polymer chains also exist in the glassy state by observing the subdiffusive dynamics of PNIPAM microgel particles at short times.

Colloidal glasses are viscoelastic in nature and yield under application of the large shear [27]. The yielding behavior of colloidal glasses has been found to depend on the nature of inetrparticle interactions between colloidal particles [60, 65]. While the hard sphere colloidal glass yield in one step (one peak in G″) [60], attractive colloidal glasses have been found to yield in two steps (two peaks in G″) [65]. In PNIPAM microgel glasses, interparticle interactions are soft repulsive [45] and there exist the entanglements of dangling polymer chains between neighboring particles (evidenced by short time subdiffusive dynamics). With the motivation that how does the soft repulsive glasses of PNIPAM microgel particles with entangled polymer chains will respond to the applied shear, their yielding behavior has been studied by performing non-linear rheological measurements. Rheological measurements have revealed that dense PNIPAM microgel glasses yield in two steps, which has been interpreted to occur due to i) breaking of the entanglements of dangling polymer chains of neighboring particles and ii) breaking of topological cages from neighboring particles.

Towards all the above mentioned studies, nearly monodisperse PNIPAM microgel particles of various sizes have been synthesized. At higher temperatures, where PNIPAM microgel suspension turns turbid due to multiple scattering [69], investigations have been carried out using 3D DLS techniques which uses cross-correlation methods to avoid the multiple scattering effect. The thesis is organized in following way. The details of synthesis and characterization techniques are discussed in Chapter 2. Chapter 3 reports the results on the osmotic compression of the PNIPAM microgel particles in dense suspensions. Studies on dynamics in PNIPAM microgel crystals across melting are presented in Chapter 4. Chapter 5 reports the investigations on dynamics and yielding behavior of dense PNIPAM microgel glasses. Summary and conclusions of investigations that are carried out using SLS, DLS, UV-Vis spectroscopy and Rheology techniques, important findings of the thesis and directions for future work are discussed in Chapter 6.

1.8 Major findings of the thesis

1. PNIPAM microgel crystals of different volume fractions have been prepared and Bragg diffraction from these crystals has been recorded using UV-Vis spectrometer. The interparticle separation in PNIPAM microgel crystals with $\phi > 0.74$, determined from the Bragg peak position, is found to be smaller than the diameter (d_h) of the PNIPAM microgel particles measured under dilute condition.
2. The observation of interparticle separation being lesser than the particle diameter (d_h), in dense ($\phi > 0.74$) PNIPAM microgel crystals, constitute first evidence for deswelling of PNIPAM microgel particles under osmotic compression. PNIPAM microgel particles undergo osmotic compression as osmotic pressure on microgel particles exceeds their Bulk modulus (~ kPa).

3. Flory-Rehner (FR) theory is shown to provide the qualitative understanding for osmotic compression of PNIPAM microgel particles beyond a certain volume fraction.
4. DLS has been employed to study the dynamics across the melting of dense PNIPAM microgel crystals. Careful analysis of mean square displacement showed for the first time that dynamics of PNIPAM microgel particles, close to melting of the crystals, is subdiffusive at short times. The subdiffusive dynamics at short times is argued to arise due to the entanglements of dangling polymer chains of neighbouring PNIPAM microgel particles. Observation of subdiffusive dynamics at short times implies the deviation of the dynamical criterion for melting of PNIPAM microgel crystals.
5. Upon sudden cooling, dense PNIPAM microgel liquids are shown to freeze into a glassy state. The glass transition temperatures of dense PNIPAM microgel liquids have been identified using 3D DLS technique. Non-ergodicity parameter, $f(q,\infty)$ is shown to show discontinuity across glass transition.
6. The dynamics in dense PNIPAM microgel glasses is shown to be subdiffusive at short times, suggesting the existence of the entanglements of the dangling polymer chains between neighbouring PNIPAM microgel particles in the glassy state as well as in the super cooled liquid state (*i.e.* above the glass transition temperature).
7. Non-linear rheological measurements on dense PNIPAM microgel glasses have shown that these glasses yield in two steps by exhibiting two peaks in $G''(\omega, \gamma_0)$. It is the first report of two step yielding in a soft repulsive glass. Earlier reports of the two step yielding are in attractive colloidal glasses.
8. Two step yielding observed in dense PNIPAM microgel glasses is argued to arise i) due to breaking of the entanglements of dangling polymer chains between

neighbouring particles and ii) due to breaking of topological cages formed by neighbouring particles.

References

1. P.N. Pusey and W. van Megen, Nature 320, (1986) 340-342.
2. B.V.R. Tata and S.S. Jena, Solid State Commun. 139, (2006) 562-580.
3. P. S. Mohanty and W. Richtering, J. Phys. Chem. B 112, (2008) 14692-14697.
4. R. S. Crandall and R. Williams, Science 198, (1977) 293-295.
5. R. Williams, R.S. Crandall and P.J. Wojtowicz, Phys. Rev. lett. 37, (1976) 348-351.
6. J. C. Zahorchak, R. Kesavamoorthy, R. D. Coalson and S. A. Asher, J. Chem. Phys. 96, (1992) 6873-6879.
7. Ke-Qin Zhang and X. Y. Liu, Nature 429, (2004) 739-743.
8. U. Gasser, E. R. Weeks, A. Schofield, P. N. Pusey and D. A. Weitz, Science 292, (2001) 258-262.
9. A. Cacciuto, S. Auer and D. Frenkel, Nature 428, (2004) 404-406.
10. P. Schall, I. Cohen, D. A. Weitz and F. Spaepen, Nature 440, (2006) 319-323.
11. J. K. G. Dhont, C. Smits and H. N. W. Lekkerkerker, J. Colloid Interf. Sci.152, (1992) 386-401.
12. Peter Schall, Itai Cohen, David A. Weitz, Frans Spaepen, Science 305, (2004) 1944-1948.
13. H. K. Nagamanasa, S. Gokhale, R. Ganapathy, and A. K. Sood , PNAS, 108, (2011) 11323-11326.
14. W. van Megen and S. M. Underwood , Phys. Rev. E 49, (1994) 4206-4220.
15. E. R. Weeks, J. C. Crocker, A. C. Levitt, A. Schofield, D. A. Weitz, Science 287, (2000) 627-631.
16. B. V. R. Tata, P. S. Mohanty and M. C. Valsakumar, Phys. Rev. Lett. 88, (2002) 018302.
17. P. Schall, D. A. Weitz, F. Spaepen, Science 318, (2007) 1895-1899.
18. J. Mattsson, H. M. Wyss, A. Fernandez-Nieves, K. Miyazaki, Z. Hu, D. R. Reichman and D. A. Weitz, Nature 462, (2009) 83-86.
19. J. H. Holtz and S. A. Asher, Nature 389, (1997) 829-832.

20. C. Geary, I. Zudans, A. Goponenko, S. Asher, S. Weber, Analytical Chemistry 77, (2005) 185-192.

21. J. M. Weissman, H. B. Sunkara, A. S. Tse , and S. A. Asher, Science 274, (1996) 959-960.

22. P. L. Flaugh, S. E. O'Donnell, and S. A. Asher, Appl. Spectrosc. 38, (1984) 847-850.

23. G. Pan, R. Kesavamoorthy, S. A. Asher, Phys. Rev. Lett. 78, (1999) 3860-3863.

24. C. E. Reese, A. V. Mikhonin, M. Kamenjicki, A. Tikhonov and S. A. Asher, J. Am. Chem. Soc. 12 6, (2004) 1493-1496.

25. S. Hyun Kim, S. Yeon Lee, S. Man Yang and Gi-Ra Yi, NPG Asia Mater. 3 , (2011) 25-33.

26. N. J. Wagner and J. F. Brady, Physics Today 62, (2009) 27-32 and references therein.

27. C. W. Macosko, Rheology Principles Measurements and Applications, WILEY-VCH, New York (1994) ; T. A. Mazder, Rheology Handbook, Vincentz Network GmbH & Co, K.G.

28. L. V. Woodcock, Nature, 385 (1997) 141-143.

29. P. G. Bolhuis, D. Frenkel, Siun-Chuon Mau, D. A, Nature 388, (1997) 235-236.

30. P. N. Pusey, W. van Megen, P. Bartlett, B. J. Ackerson, J. G. Rarity, and S. M. Underwood, Phys. Rev. Lett. 63, (1989) 2753-2756.

31. S. I. Henderson, T. C. Mortensen, S. M. Underwood, W. van Megen, Physica A 233, (1996) 102-116.

32. E. J. W. Verwey, J. T. G. Overbeek, Theory of the Stability of Lyophobic Colloids, Elsevier, Amsterdam, 1948.

33. E. B. Sirota. H. D. Ou-Yang, S K. Sinha, P. M. Chaikin, J. D. Axe and Y. Fujii, Phys. Rev. Lett. 62, (1989) 1524-1527.

34. J. Chakraborti, H. R. Krishnamurthy, S. Sengupta and A. K. Sood, Chapter 9 in ordering and phase transitions in charged colloids, edt. A. K. Arora and B. V. Tata, VCH publishers, New York (1996).

35. I. Sogami and N. Ise, J. Chem. Phys. 81, (1984) 6320.

36. K.S. Schmitz, L.B. Bhuiyan, Phys. Rev. E 63, (2001) 011503.

37. B.V.R. Tata , P.S. Mohanty, M.C. Valsakumar, Solid State Communications 147, (2008) 360–365.

38. B. V. R. Tata and A. K. Arora, J. Phys. Condens. Matter 4, (1992) 7699; 7, (1995) 3817-3834.

39. J. Brijitta, B. V. R. Tata and T. Kaliyappan, J. Nanosci. Nanotechnology 9, (2009) 5323-5328.

40. C. D. Jones and L. Andrew Lyon, Macromolecules 33, (2000) 8301-8306.

41. Li-Yi Chen, Chung-Mao Ou, Wei-Yu Chen, Chih-Ching Huang, and Huan-Tsung Chang, Appl. Mater. Interfaces 5, (2013) 4383-4388.

42. Q. Luo, Y. Guan, Y. Zhang, M. Siddiq, Journal of Polymer Science: Part A: Polymer Chemistry 48, (2010) 4120-4127.

43. S. V. Vinogradov, Curr Pharm Des. 12, (2006) 4703-4712.

44. M. Ballauff, Y. Lu, Polymer 48, (2007) 1815-1823.

45. J. Wu, B. Zhou and Z. Hu, Phys. Rev. Lett. 90, (2003) 048304.

46. E. C. Cho, J. Lee, and K. Cho, Macromolecules 36, (2003) 9929-9934.

47. B. R. Saunders, Langmuir 20, (2004) 3925-3932.

48. J. Gao and B. J. Frisken, Langmuir 19, (2003) 5217-5222.

49. I. Varga, T. Gilányi, R. Mészáros, G. Filipcsei and M. Zrínyi, J. Phys. Chem. B 105, (2001) 9071-9076.

50. M. Stieger, W. Richtering, J.S. Pedersen, and P. Lindner, J. Chem. Phys. 120, (2004) 6197-6206.

51. H. Senff and W. Richtering, J. chem.. phys. 111, (1999) 1705-1711.

52. A. Fernández-Nieves, A. Fernández-Barbero, B. Vincent and F. J. de las Nieves, J. Chem. Phys. 119, (2003) 10383-10388.

53. W. G. Hoover, S. G. Gray and K. W. Johnson, J. Chem. Phys. 55, (1971) 1128.

54. R. Agrawal and D. A. Kofke, Mol. Phys. 85, (1995) 23-42.

55. J. Brijitta, B. V. R. Tata, R. G. Joshi and T. Kaliyappan, J. Chem. Phys. 131, (2009) 074904.

56. M. Medina-Noyola, Phys. Rev. Lett. 60, (1988) 2705-2708.

57. A. van Blaaderen, J. Peetermans, G. Mat-et and J. K. G. Dhont, J. Chem. Phys. 96, (1992) 4591-4603.

58. T. Eckert and E. Bartsch, Phys. Rev. Lett. 89, (2002) 125701.

59. E. Zaccarellia and W.C. K. Poon, PNAS , (2009).

60. K. Miyazaki, H. M. Wyss, D. A. Weitz, and D. R. Reichman, Europhys. Lett. 75, (2006) 915-921.

61. G. Petekidis, A. Moussaïd and P. N. Pusey, Phys. Rev. E 66, (2002) 051402.

62. P. Sollich, Phys. Rev. E 58, (1998) 738-759.

63. P. Sollich, F. Lequeux, P. Hébraud, and M. E. Cates, Phys. Rev. Lett. **78**, (1997) 2020-2023.

64. H. M. Wyss, K. Miyazaki, J. Mattsson, Z. Hu, D. R. Reichman and D. A. Weitz, Phys. Rev. Lett. 98, (2007) 238303.

65. K. N. Pham, G. Petekidis, D. Vlassopoulos, S. U. Egelhaaf, P. N. Pusey and W. C. K. Poon Europhys. Lett. 75, (2006) 624-630.

66. B. Sierra-Martín, Y. Laporte, A. B. South, L. A. Lyon and A. Fernández-Nieves, Phys. Rev. E 84, (2011) 011406.

67. T. Eckert and W. Richtering, J.Chem. Phys. 129, (2008) 124902.

68. H. Löwen, T. Palberg, and R. Simon, Phys. Rev. Lett. 70, (1993) 1557-1560.

69. F. Grüner and W. Lehmann, J. Phys. A: Math. Gen. 13, (1980) 2155-2170.

CHAPTER 2

EXPERIMENTAL TECHNIQUES AND SYNTHESIS METHOD

This chapter deals with experimental techniques used for characterization of structural ordering, dynamics and rheological behavior of colloidal suspensions. The instrumental details, measurement schemes and methods of analysis underlying the used techniques, *i.e.* static light scattering (SLS), dynamic light scattering (DLS), cross-correlation light scattering, UV visible spectroscopy and Rheology, are presented. Detailed method for synthesis of PNIPAM microgels and procedures for preparation of dense PNIPAM microgel crystals and glasses are discussed.

2.1 Light Scattering techniques

In colloidal suspensions, length scale of interest ranges from ~ 100 nm to several microns and time scale ranges from ~ 10^{-6}sec to ~ 10^{3}sec, hence static light scattering (SLS) and dynamic light scattering (DLS) are the appropriate techniques to study their structural ordering and dynamics, respectively [1-2]. Basic principles of operation, instrumental details and analysis methods of SLS and DLS techniques used for characterization of structural ordering and dynamics in transperent, turbid and non-ergodic colloidal suspensions are discussed below.

2.1.1 Static light scattering

Static light scattering consider elastic scattering of the light, in which scattered photon undergo only a change in momentum without a change in energy. The change in momentum of the photon is given as,

$$\hbar\vec{q} = \hbar\vec{k}_i - \hbar\vec{k}_s\,, \tag{2.1}$$

where $\hbar = h/2\pi$ and h is Plank's constant. $\overrightarrow{k_\iota}$ is wave vector of incident light, $\overrightarrow{k_s}$ is wave vector of scattered light and $\vec{q}$ is called as scattering wave vector. Ray diagram for elastic scattering of light is shown in Fig. 2.1(a). For elastic scattering process $|\vec{k_i}| = |\vec{k_s}|$, giving rise to the amplitude of scattering wave vector as, $q = (4\pi\mu_s/\lambda)\ sin(\theta/2)$. Here θ is scattering angle, μ_s is solvent refractive index and λ is wavelength of incident light.

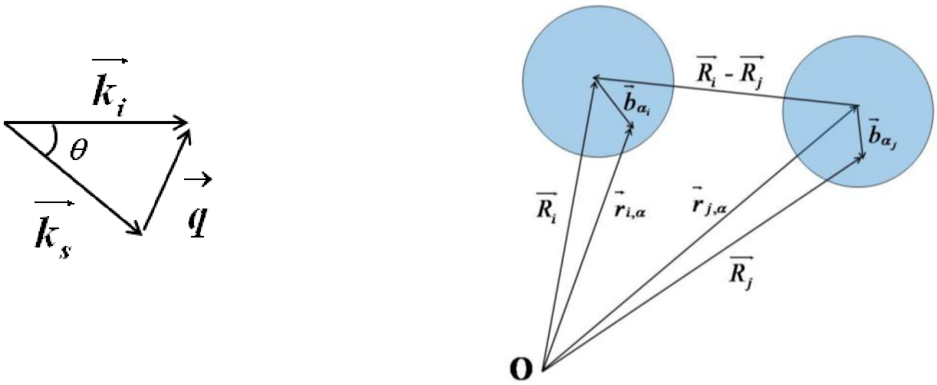

(a) **(b)**

Fig. 2.1 (a) Ray diagram of elastic scattering of light, (b) Two spheres having center of mass at $\vec{R_i}$ and $\vec{R_j}$ with respect to origin, O and separated by $\vec{R_i} - \vec{R_j}$. $\vec{r}_{i,\alpha}$ and $\vec{b}_{\alpha_i}$ are the distances of the α^{th} scatterer from O and center of the i^{th} sphere, respectively.

Let us consider a suspension of N rigid monodisperse colloidal particles of refractive index μ_p and radius a dispersed in medium. Let each colloidal particle consists of n point scattering centers of individual scattering amplitude f. The scattered electric field, $E_s(\vec{q},t)$ from N colloidal particles present in scattering volume, V_s at any time t is given by,

$$E_s(\vec{q},t) \propto \sum_{i=1}^{N}\sum_{\alpha_i}^{n} f\ exp\left[i\vec{q}.\vec{r}_{i,\alpha}(t)\right], \tag{2.2}$$

where $\vec{r}_{i,\alpha}(t)$ is the distance of the α^{th} point scatterer of i^{th} sphere with respect an arbitrary origin, O and is given as,

$$\vec{r}_{i,\alpha}(t) = \vec{R}_i(t) + \vec{b}_{\alpha_i}(t). \tag{2.3}$$

here, $\vec{R}_i(t)$ is the distance of center of mass of colloidal sphere with respect to origin and $\vec{b}_{\alpha_i}(t)$ is the distance of scatterer from the center of sphere, which is shown in Fig. 2.1(b). The time averaged intensity, *<I(q)>* of scattered light is given by

$$\langle I(q)\rangle = \langle |E_s(\vec{q})|^2\rangle \propto f^2 \langle \sum_{i,j,\alpha_i,\beta_j} exp\left[i\vec{q}.\left(\vec{r}_{i,\alpha} - \vec{r}_{j,\beta}\right)\right]\rangle. \tag{2.4}$$

Eq. (2.4) can be rewritten as

$$\langle I(q)\rangle \propto f^2 \langle \sum_{i,j,\alpha_i,\beta_j} ex\,p\left[i\vec{q}.\left(\vec{R}_i - \vec{R}_j\right)\right].exp\left[i\vec{q}.\left(\vec{b}_{\alpha_i} - \vec{b}_{\beta_j}\right)\right]\rangle. \tag{2.5}$$

When interparticle averages are independent of intra-particle averages, average scattered intensity from non interacting suspensions is given as,

$$\langle I(q)\rangle_0 \propto f^2 \langle \sum_{\alpha_i,\beta_j} exp\left[i\vec{q}.\left(\vec{b}_{\alpha_i} - \vec{b}_{\beta_j}\right)\right]\rangle \propto \; f^2\, P(q). \tag{2.6}$$

P(q) is called as particle form factor or intra-particle structure factor. In case of spherical particles *P(q)* is given as [3],

$$P(q) = \left\{\frac{3[sin(qa) - (qa)cos(qa)]}{(qa)^3}\right\}^2. \tag{2.7}$$

The interparticle structure factor is then written as,

$$S(q) = \frac{\langle I(q)\rangle}{\langle I(q)\rangle_0} \propto \langle \sum_{i,j} exp\left[i\vec{q}.\left(\vec{R}_i - \vec{R}_j\right)\right]\rangle. \tag{2.8}$$

In Rayleigh Gans regime, the scatterd intensity can be written as,

$$I(q) = AP(q)S(q), \tag{2.9}$$

where *A* is the constant given by [3],

$$A = \frac{16\pi^4 N a^6}{\lambda^4}\left[\frac{\mu_r^2 - 1}{\mu_r^2 + 2}\right]\frac{I_0}{P^2}. \tag{2.10}$$

where I_0 Intensity of the incident light, *P* is the distance between sample and the detector and $\mu_r = \mu_p / \mu_s$ is the relative refractive index of the particle with respect to medium.

2.1.2 Dynamic light scattering

In a suspension, colloidal particles exhibit translational, rotational or vibrational motions due to thermal motion of solvent molecules [2]. Because of this, the intensity of the scattered light fluctuates in time. Thus, fluctuations in intensity, carries information about positions and orientations of the colloidal particles and hence can be used to obtain the information about the dynamics of colloidal particles. The time dependent correlation function of fluctuating property provides concise way to extract the information about the dynamics of the system.

In general, any fluctuating property *A(t)*, which fluctuates in time, displays following features: *A* at time *t* and $t+\tau$ can have different values, so that $A(t) \neq A(t+\tau)$. For small values of τ, *A(t)* is very close to $A(t+\tau)$. As τ increases, deviation of *A(t)* from $A(t+\tau)$ is more likely to be nonzero. Thus we can say that, the value $A(t+\tau)$ is correlated with *A(t)* when τ is small but this correlation is lost when τ becomes large compared to the period of fluctuations. A measure of this correlation is the auto correlation of the property, A which is defined as,

$$\langle A(0)A(\tau)\rangle = \lim_{T\to\infty}\frac{1}{T}\int_0^T dtA(t)A(t+\tau) \tag{2.11}$$

and the average of *A(t)* is given by,

$$\langle A\rangle = \lim_{T\to\infty}\frac{1}{T}\int_0^T dtA(t)\,. \tag{2.12}$$

The discrete form of these equations is written as,

$$\langle A(0)A(\tau)\rangle = \lim_{\upsilon\to\infty}\frac{1}{\upsilon}\sum_{j=1}^{\upsilon} A_j A_{j+m} \tag{2.13}$$

and

$$\langle A\rangle = \lim_{\upsilon\to\infty}\frac{1}{\nu}\sum_{j=1}^{\upsilon} A_j \tag{2.14}$$

where A_j is the value of the property at j^{th} interval and $T = \nu\Delta t$, $t = j\Delta t$ and $\tau = m\Delta$t.

From Eq. (2.13), it can be shown that,

$$\lim_{\tau\to 0}\,\langle A(0)A(\tau)\rangle = \langle A(0)^2\rangle = \langle A^2\rangle \tag{2.15}$$

and

$$\lim_{\tau\to\infty}\,\langle A(0)A(\tau)\rangle = \langle A\rangle^2. \tag{2.16}$$

Thus, the time correlation function of nonperiodic property decays from $<A^2>$ to $<A>^2$ in the course of time. In many applications autocorrelation function decays like single exponential so that,

$$\langle A(0)A(\tau)\rangle = \langle A\rangle^2 + \{\langle A^2\rangle - \langle A\rangle^2\}\exp(-\tau/\tau_c) \tag{2.17}$$

where, τ_c is called the “ relaxation time of correlation function”.

In light scattering experiments, instantaneous electric field of the scattered light at a given scattering wave vector $\vec{q}$ is given by Eq. (2.2). Detector detects the intensity of scattered light which is given as $I(t) = |E_s(t)|^2$, which is fed to the correlator to calculate the intensity-intensity autocorrelation function (also known as homodyne or self beating correlation function), which is defined as,

$$\langle I(q,0)I(q,t)\rangle = B\langle |E_s(q,0)|^2|E_s(q,t)|^2\rangle\,, \tag{2.18}$$

where B is the proportionality constant. Colloidal suspensions for which time averaged intensity of the scattered light is same as ensemble averaged intensity of the scattered light are referred as ergodic colloidal suspensions. In the case of ergodic suspensions, time averaged $g^{(2)}(q,t)$ (measured at one point in the sample) represents the ensemble averaged $g^{(2)}(q,t)$ and hence, can be used to obtain the dynamical information about the system. The normalized intensity autocorrelation function, $g^{(2)}(q,t)$is defined as,

$$g^{(2)}(q,t) \; = \frac{\langle I(q,0)I(q,t)\rangle}{\langle I(q)\rangle^2} \; . \tag{2.19}$$

The normalized electric field autocorrelation function, $g^{(1)}(q,t)$ is defined as,

$$g^{(1)}(q,t) \; = \frac{\langle E_s(q,0)E_s(q,t)\rangle}{\langle E_s(q)\rangle^2} \, . \tag{2.20}$$

With an assumption that the scattering volume can be divided into a large number of statistically independent sub-regions and the scattered electric field is Gaussian random variable, one can relate the $g^{(2)}(q,t)$ and $g^{(1)}(q,t)$using Siegert's relation,

$$g^{(2)}(q,t) = \; 1 + \; \left|\beta_C \, g^{(1)}(q,t)\right|^2 . \tag{2.21}$$

where coherence factor, β_c depends on the coherence area set by the optics of the instrument. For one coherence area the ideal value of β_c = 1. Light scattering experiments, where Gaussian approximation for the scattered electric field is not valid, are performed in heterodyne mode. In heterodyne mode, electric field of scattered light is mixed with that of incident light before the detector, which is further used to calculate heterodyne correlation function.

The electric field correlation function can also be defined as intermediate scattering function or dynamic structure factor, $F(q,t)$ which is related to positions of colloidal particles and is given as,

$$F(q,t) \propto \langle E_s(q,0)E_s(q,t)\rangle \, . \tag{2.22}$$

Eqs. (2.2), (2.9) and (2.22) suggest that, for colloidal suspensions with $P(q)$ = 1

$$g^{(1)}(q,t) = \frac{F(q,t)}{S(q)} \quad ; \qquad S(q) = F(q,0) \tag{2.23}$$

$g^{(1)}(q,t)$ is also called as normalized dynamic structure factor denoted as $f(q,t)$, which are used interchangeably in the following text. When displacement of the colloidal particle, $\Delta\vec{\mathrm{r}}(t)$ in the vicinity $\mathrm{d}^3\mathrm{R}$ of $\vec{R}(t)$ is Gaussian distributed, the $f(q,t)$ is related to the mean square displacement (MSD), $<\Delta r^2(t)>$ of the colloidal particle by following relation [2],

$$f(q,t) = exp(-q^2\langle\Delta r^2(t)\rangle/6). \tag{2.24}$$

MSD obtained using this relation is used to characterize the dynamics of colloidal suspensions as discussed in Chapter 1. In dilute non interacting suspensions, colloidal particles undergo free Brownian motion and the MSD is given by $<\Delta r^2(q,t)> = 6D_0t$, where D_0 is the free diffusion coefficient. Therefore $f(q,t)$ takes the form as,

$$f(q,t) = exp(-D_0q^2t) \quad = \quad exp(-\Gamma\, t), \tag{2.25}$$

where $\Gamma = D_0q^2$ is called decay constant. D_0 is related to the hydrodynamic diameter, d_h of the colloidal particle via Stokes-Einstein relation as $d_h = k_BT/3\pi\eta_sD_0$. When colloidal particles are polydisperse in diameter, Γ has a distribution $G(\Gamma)$ and the corresponding $f(q,t)$ is written as [4],

$$f(q,t) = \int_0^\infty G(\Gamma)\, exp(-\Gamma t)\ d\Gamma. \tag{2.26}$$

$G(\Gamma)$ and hence the particle size distribution can be calculated from the Laplace inversion of $f(q,t)$. Finding the precise functional form for the distribution involves rigorous calculations. Another simplest way to analyze the DLS data to get basic information about size and size polydispersity (SPD), is a method of cumulants. In this method, $\ln[f(q,t)]$ is expressed as cumulant expansion given as [4],

$$\ln[f(q,t)] = -\bar{\Gamma}t + \frac{\kappa_2}{2!}t^2 - \frac{\kappa_3}{3!}t^3 + \cdots, \tag{2.27}$$

where, $\bar{\Gamma}$ is a first cumulant which is related to the average diffusion coefficient, $\bar{D}$ as $\bar{\Gamma} = \bar{D}q^2$ and used to determine the average diameter of colloidal particles using Stokes-Einstein relation defined in the above text. Second cumulant, κ_2 gives the variance of the size distribution relative to average value. Square root is κ_2 is a size polydispersity (SPD), which is given as SPD = standard deviation in diameter / average diameter. In the case of dense interacting suspensions, the motion of colloidal particle at short times ($\tau_B << t << \tau_R$) is characterized by D_S and at long times ($t >> \tau_R$) by D_L as in discussed Chapter 1. The diffusion coefficients measured in DLS experiment depend on q. MSD's corresponding to both the short and long times are defined as $<\Delta r^2(q,t)> = 6D_S(q)t$ and $<\Delta r^2(q,t)> = 6D_L(q)t$, respectively.

2.1.3 Light scattering setup

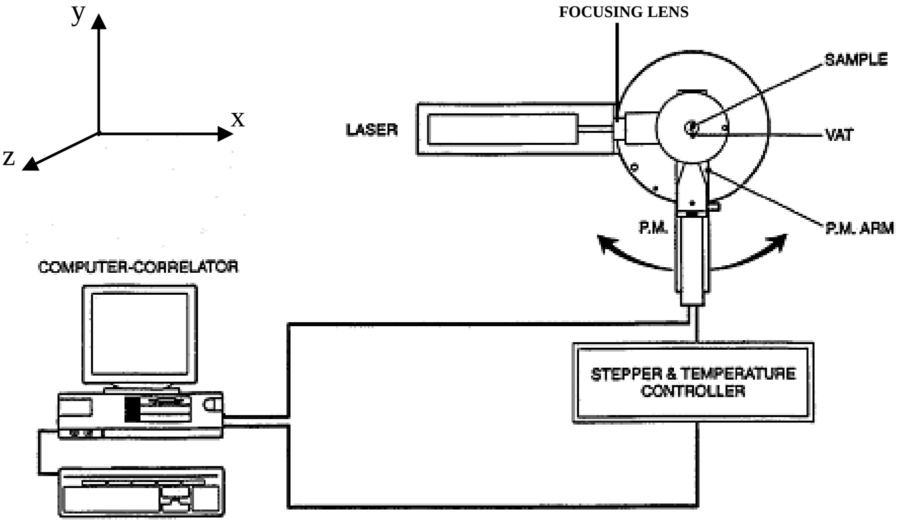

Fig. 2.2 Schematic diagram of light scattering set up (top view) showing various components.

We have carried out static and dynamic light scattering experiments using commercial light scattering set up (Malvern, UK, model 4700). Schematic of the light scattering set up showing various components is shown in Fig 2.2. It consists of a laser as light source (solid state laser, λ = 532 nm), polarizer and analyzer, lenses, vat, detector and correlator. Polarizer and analyzer have been used to select V-V (vertical – vertical) or V-H (vertical – horizontal) scattering geometries. In V-V geometry vertically polarized light is made to incident on sample and vertical component of scattered light is detected. In V-H geometry vertically polarized light is made to incident on sample and horizontal component of scattered light is detected. V-H geometry is also known as depolarized light scattering geometry. The light scattering set up consists of a Goniometer with an arm to mount a detector, a vat (containing index matching liquid - toluene), sample holder to hold sample inside the vat and a heater to raise the sample temperature from 10 °C to 60 °C with temperature stability of ± 0.1 °C. Vat with toluene serves as index matching medium and as constant temperature bath. Goniometer is moved using spectrometer motor which moves the detector in scattering plane (x-y) with an angular resolution of 0.1°. Photomultiplier tube (PMT) is used as the photon detector in single photon counting mode. A pin hole with an adjustable aperture placed before the PMT is used to vary the detector area exposed to the scattered light. Intersection of the detector cross section and the laser beam at the center defines the scattering volume. In order to enhance the coherence factor, β_c scattering volume is reduced by focusing the incident light at the center of the vat and by decreasing the pin hole size placed before detector.

The signal coming from the PMT is processed by the correlator and then passed to the computer for final analysis and display. Generally, a correlator stores the successive signals from the sample and multiplies every sample signal by the next value of the signal as it is measured. These products are accumulated in ‘store channels’. The change in the value of the ‘correlation coefficient’ measured by each channel is characteristic of the fluctuations in the signal. These fluctuations and the number of channels available dictate the choice of the ‘sample time’. Model 7132 correlator is used in our DLS set up. The 7132 correlator has dual correlator architecture. It has fast 64 channels, which can operate as a linear correlator or a log correlator operating in 8 × 8 groups. It has a slower correlator, which can operate as a 256 channel linear correlator with a minimum sample time of 10 μsec or a log correlator operating in 16 × 8 or 24 × 8 groups with a fundamental sample time of down to 4 μs. For a general operation, 192 channels are used among which 64 (8 × 8) are fast channels and 128 (16 × 8) are slow channels. In the fast channel, the minimum sample time is from 50 ns and for slow channel, the minimum sample time is 4 μs. The time required to do an experiment is set through the computer. For those experiments, where the relaxation time of the sample exceeds the time period of operation of 192 channels with highest sample time, the experiments are performed with extended channels. The dynamic range of our correlator (in log mode) is 10^{11} seconds starting from 50 nsec.

Light scattering set up is equipped with the translation (in x,y,z directions) and rotation (about z axis) stage, which used for positioning and orienting the sample cell with respect to incident laser beam.

2.1.4 Alignment Procedure

a) First the laser beam is aligned using the translational, horizontal and vertical screws so that the beam exactly passes through the crosswire placed on the PMT arm and falls on the opposite wall and the position of the beam is marked on the wall. This ensures that the laser is parallel to the plane of the table.

b) Then the vat is placed in the ring so that the beam passes through the center of the flat portion of the vat and exits out through the other end. Finally, the three leveling screws are tightened.

c) The vat cover is placed on the top and tightened. Then the vat is filled with water from the top. Further the beam is once again checked that it should pass through the pinhole, crosswire and then falls on the previously marked position.
d) Then the focusing lens is placed at the proper position and the three screws are tightened. After that if the beam is still not passing through the pinhole and crosswire, then using the fine screw on the focusing lens, the beam is made to pass through the crosswire.
e) Finally, the diffraction fringes are verified by inserting a thin platinum wire exactly perpendicular to the beam. If the beam is in a straight line, then the diffraction fringes will be symmetric on both sides of the center. This completes the procedure for aligning the beam. Finally the crosswire is removed and the PMT is placed on the PMT arm and tightened properly.

Checking of the Alignment with Toluene

A good basic check that the instrument is aligned properly for an angular intensity scattering (i.e. $I(\theta)$ vs θ) is to compare the count rate from the toluene sample at scattering angles of 30^o, 90^o and 150^o. The PMT optics “sees” a longer path length at oblique scattering angles, so that the observed count rate should rise in proportion to the *sin* of the scattering angle (θ). A correction for this effect is automatically made in angular scan measurement provided the alignment is made to satisfy, Count rate at 30° = Count rate at 150° = 2(Count rate at 90°). This relation holds good to within 5% for a good alignment. Figure 2.3 shows the scattered intensity as a function of scattering angle for toluene in 10 mm cell. One can see that the scattered intensity remains constant from 20° to 150°. This represents good alignment for the instrument. Most of the results presented in this thesis correspond to 10 mm cell.

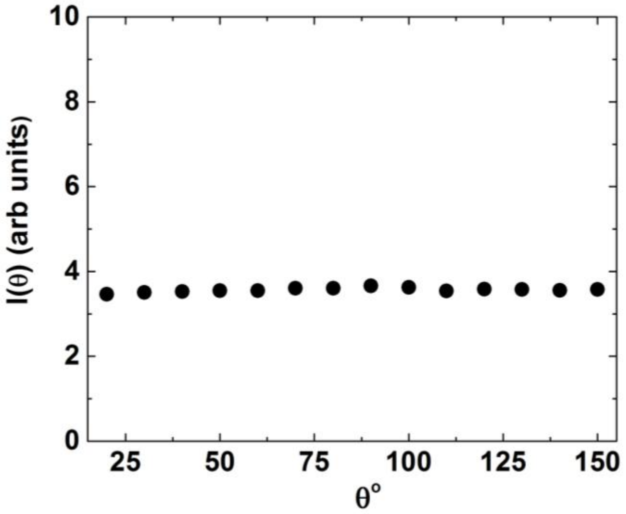

Fig. 2.3 Scattered intensity as a function of scattering angle, θ measured for toluene.

2.1.5 Cross-correlation based 3D dynamic light scattering technique for turbid colloidal suspensions

Light scattering technique discussed in the preceding sections is based on the single scattering of light, *i.e* photon scattered by a particle reaches the detector without undergoing scattering from other particles. In the case of colloidal suspensions with higher concentration (particle density) and / or higher refractive index contrast multiple scattering of light becomes a problem [5]. Light scattering technique based on cross-correlation method provides a way to measure singly scattered light in to presence of the multiply scattered light and hence can be effectively used to characterize the turbid colloidal media [6-7]. Cross-correlation light scattering technique is also known as 3D light scattering (3D DLS and 3D SLS) as it detects the light scattered from same sample in two different scattering planes (Fig. 2.4(a)) by performing two different light scattering experiments. Two light scattering experiments are performed by using two laser beams, having incident wave vectors $\bar{k}_{i1}$ and $\bar{k}_{i2}$, which cross each other at angle, ψ at the centre of the vat and scattered light from corresponding beams is detected at wave vectors $\bar{k}_{s1}$ and $\bar{k}_{s2}$, respectively using two detectors. Two detectors are mounted on the Goniometer arm in such a way that with respect to single scattered light both the detectors see same scattering wave vector, $|\bar{q}| = |\bar{k}_{i1} - \bar{k}_{s1}| = |\bar{k}_{i2} - \bar{k}_{s2}|$. Intensity of the scattered light measured by two detectors is then correlated with each other to obtain the intensity cross-correlation function, $g_{12}^{(2)}(q, \tau)$ which is given as

$$g_{12}^{(2)}(q, \tau) = \frac{\langle I_1(q, t') I_2(q, t' + \tau) \rangle}{\langle I_1(q) \rangle \langle I_2(q) \rangle} \,. \tag{2.28}$$

Scattered light detected by each detector consist of single plus multiply scattered component. In case of multiple scattering, photon undergoes scattering from several particles before reaching the detector, thus each detector sees several different $\vec{q}$. Intensity of light scattered at same $\vec{q}$ is temporally correlated, whereas that for different q is decorrelated. Therefore, upon cross-correlation of intensity of scattered light from two different detectors, multiply scattered light produces constant background and only contribution from singly scattered light survives, removing the effect of multiple scattering on correlation function. $f(q, t)$ can be obtained from $g_{12}^{(2)}(q, t)$ using Siegert's relation, $g_{12}^{(2)}(q, t) = 1 + |\beta f(q, t)|^2$. Where β is net coherence factor given as, $\beta = \beta_m \beta_{12} \beta_c$ with β_m, β_{12} and β_c are the factors arising due to multiple scattering, overlap of two laser beams used in cross-correlation and alignment of the optics, respectively. For dilute sample, where the multiple scattering is absent, $\beta_m = 1$. Time averaged intensity of the single scattered light from turbid colloidal suspensions can be obtained as $I(q) = \sqrt{I_1^M I_2^M \beta^{conc} / \beta^{dilute}}$ [6]. Where I_1^M and I_2^M are the intensity detected by two detectors, respectively.

Figure 2.4 (b) shows schematic diagram of 3D light scattering set up. The photograph of 3D DLS setup (LS Instruments AG, Fribourg, Switzerland) used for probing turbid samples are shown in Fig. 2.4 (c). The 3D light scattering setup is equipped with 633 nm He-Ne laser as a light source, Avalanche photo diodes (APD) as photon detectors and a multi-tau correlator. Here, decaline is used as index matching fluid instead of toluene as in previous case. Sample temperature is controlled to accuracy of ± 0.1 °C by circulating heat exchanger fluid around the vat.

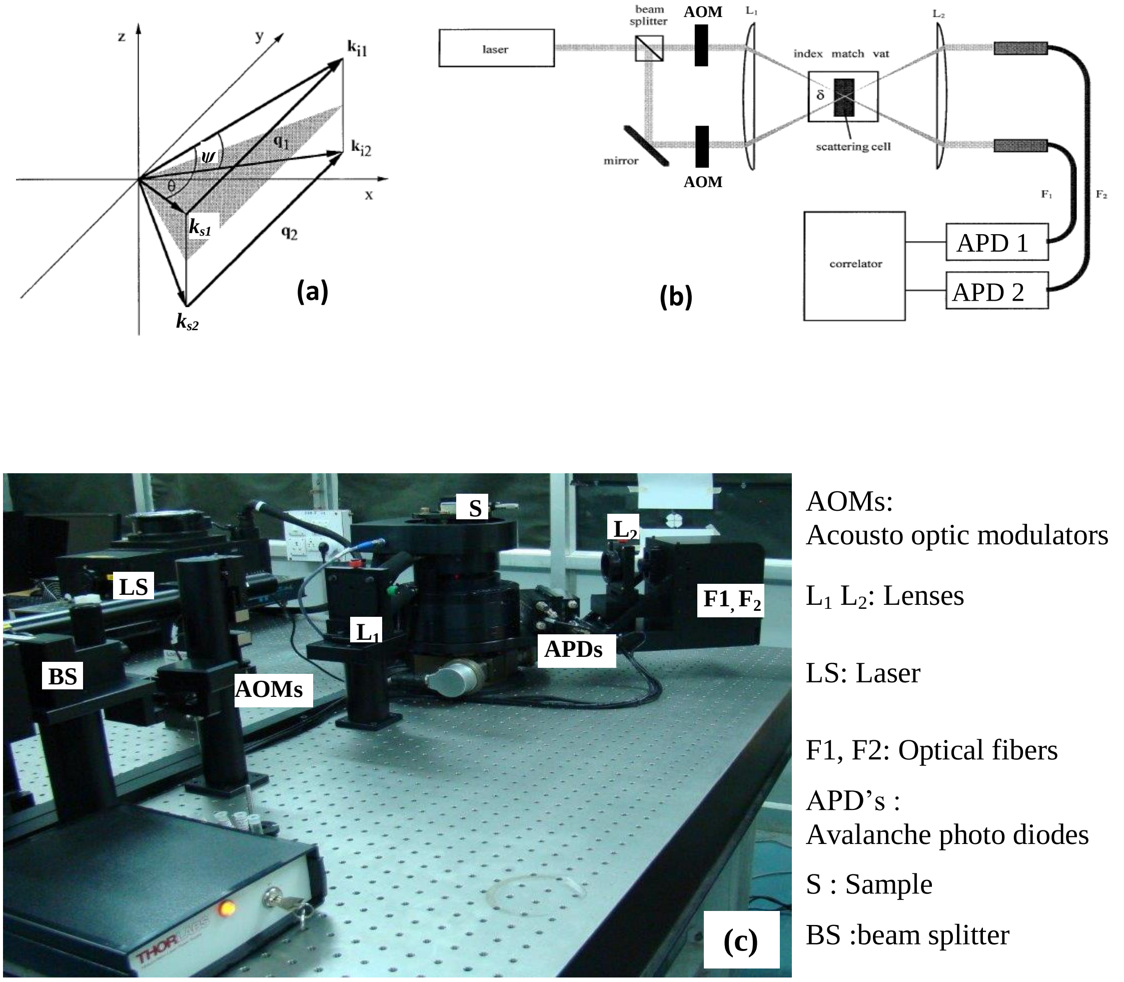

AOMs:
Acousto optic modulators

L_1 L_2: Lenses

LS: Laser

F1, F2: Optical fibers

APD's :
Avalanche photo diodes

S : Sample

BS :beam splitter

Fig. 2.4 (a) Ray diagram showing scattering geometry of 3D light scattering setup, (b) Schematic diagram of the cross-correlation light scattering setup, (c) photograph of cross-correlation light scattering setup.

Fig. 2.5(a) shows the $I(\theta)$ vs θ for toluene on 10 mm cell which is observed to be constant over θ range of 30° (q = 0.68 x 10^5 cm^{-1}) to 150° (q = 2.54 x 10^5 cm^{-1}), ensuring the good alignment of the optics of the light scattering instrument. In cross-correlation light scattering, intercept of intensity correlation function decreases to ideal value of 0.25 from its ideal value of 1 in auto correlation, due to overlap of two laser beams. The laser beams are aligned such that $g_{12}^{(2)}(q,0)$ = 0.23 is achieved in cross-correlation mode. In order to increase this intercept, acousto-optic modulators (AOMs) are used. AOMs switch the laser beams on and off alternately at interval of 3μ sec, thus avoiding the overlap of the beams. With AOMs, $g_{12}^{(2)}(q,0)$ is observed to increase up to 0.74. Intensity correlations measured in auto and cross-correlation mode for dilute suspension of polystyrene particles (diameter 70 nm) are shown in Fig. 2.5(b).

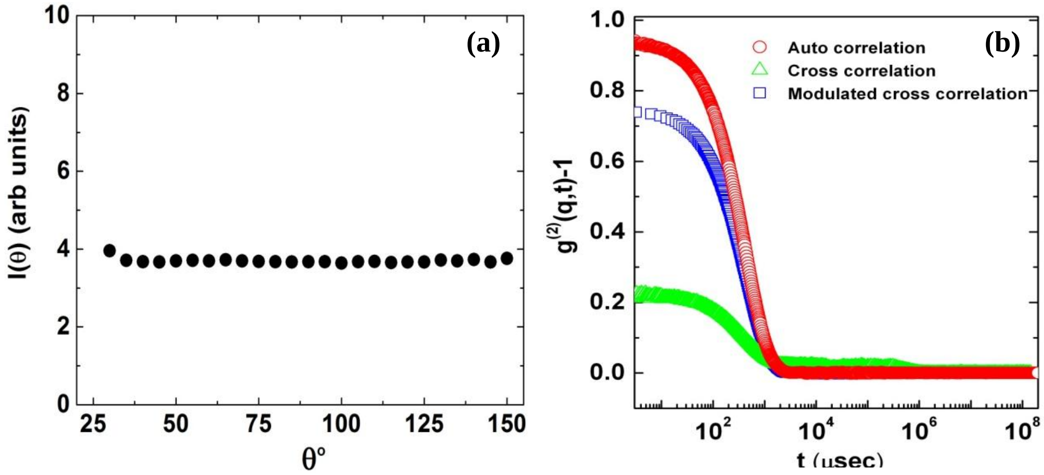

Fig. 2.5 (a) Scattered intensity as a function of scattering angle measured for toluene, and (b) Intensity cross-correlation functions measured in auto and cross-correlation mode on dilute polystyrene (70 nm diameter) suspension.

2.1.6 Light scattering from non-ergodic colloidal suspensions

The colloidal suspensions for which time averaged intensity of the scattered light (at a given q) differs from ensemble averaged intensity of the scattered light, are referred as non-ergodic. In the case of non-ergodic colloidal suspensions, time averaged $g^{(2)}(q,t)$ measured at different sample locations, differ from each other. True ensemble averaged $g^{(2)}(q,t)$ can be obtained by actually averaging the time averaged $g^{(2)}(q,t)$ measured at different sample locations, which is very time consuming process. Instead, Pusey and Van magen [8] have developed a method to obtain $f(q,t)$

for non-ergodic samples, using time averaged $g^{(2)}(q,t)$ measured at single sample location. According to which,

$$f(q,t) = \frac{Y-1}{Y} + \frac{\sqrt{g^{(2)}(q,t) - \ \sigma_I^2}}{Y}\ , \tag{2.29}$$

where Y is called as non-ergodicity factor which is given as

$$Y = \frac{\langle I(q)\rangle_E}{\langle I(q)\rangle_T}\ ; \qquad \text{and} \qquad \sigma_I^2 = \frac{\langle I^2(q)\rangle - \langle I(q)\rangle^2}{\langle I(q)\rangle^2} = \ g^{(2)}(q,0) - 1$$

here, σ_I^2 is mean square fluctuation of the scattered intensity. $<I(q)>_E$ and $<I(q)>_T$ represents ensemble averaged and time averaged intensities of scattered light. $<I(q)>_T$ is obtained by time averaged measurements at one location in sample, whereas $<I(q)>_E$ is obtained by measuring the scattered light intensities from different sample locations by rotating or translating the sample during the measurements.

In the case of turbid non-ergodic colloidal suspensions, the $f(q,t)$ is obtained as [9],

$$f(q,t) = 1 + \frac{1}{Y}\left\{\left[\frac{g_{12}^{(2)}(q,t) - g_{12}^{(2)}(q,0)}{\beta^{dilute}} + 1\right]^{1/2} - 1\right\}, \tag{2.30}$$

where $Y = [(<I_1(q)>_E <I_2(q)>_E)/(<I_1(q)>_T <I_2(q)>_T)]^{1/2}$, E- ensemble average and T- time average.

Figure 2.6(a) shows the time averaged $g^{(2)}(q,t)$ measured on dense PNIPAM microgel glass (ϕ = 0.7) at different sample locations. $g^{(2)}(q,t)$ is seen to be different at different sample locations indicating non-ergodic nature of sample. The ensemble averaged $f(q,t)$ is obtained from these time averaged $g^{(2)}(q,t)$ using method described above, which is shown in Fig. 2.6(b). The ensemble averaged intensity, $<I(q)>_E$ is collected by rotating the sample at speed of 10 revolutions per 15 minutes. The $f(q,t)$ at different sample locations, obtained by performing non-ergodic analysis, is found to overlap, indicating the validity of above method for our measurements. Same methodology has been followed for analyzing all non-ergodic samples.

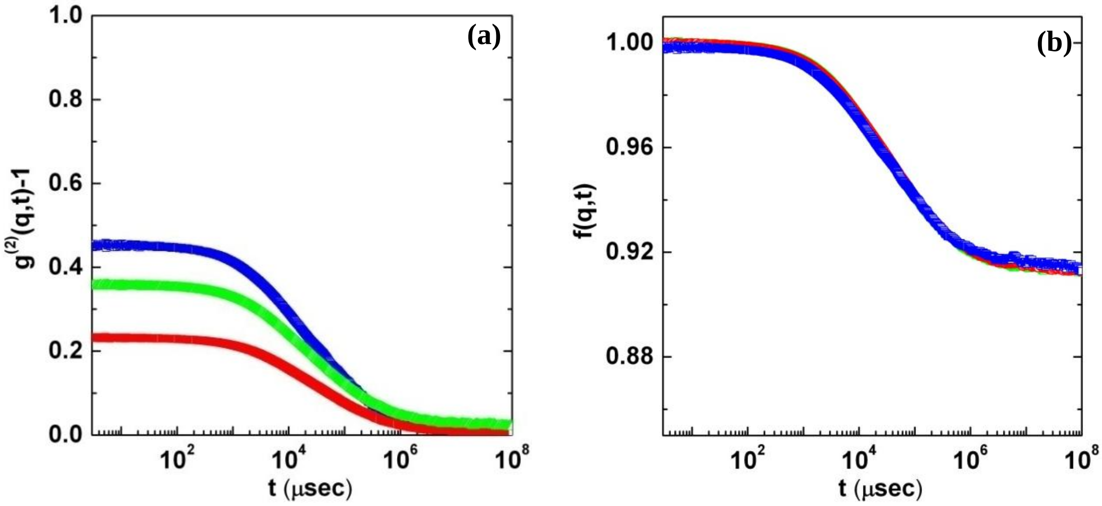

Fig. 2.6 (a) time averaged $g^{(2)}(q,t)$ at different sample locations, for PNIPAM microgel suspension having ϕ = 0.7 (at 20°C), (b) ensemble averaged $f(q,t)$, obtained from $g^{(2)}(q,t)$ at different sample locations, using Eq. (2.29).

2.2 UV visible spectroscopy

In the case of colloidal crystals having near neighbour separation smaller than ~ 200 nm or larger than ~ 2000 nm, the Bragg diffraction cannot be recorded using SLS, as the Bragg peaks fall out of the accessible q range. The Bragg diffraction from these colloidal crystals can be recorded using UV-Vis spectrometer, in which the incident wavelength is varied from UV to Visible and further to near Infrared (IR) by keeping angle of measurement constant. JASCO 650 UV-Visible spectrophotometer is employed to record the Bragg diffraction from PNIPAM microgel crystals. Schematic setup of UV-Visible spectrophotometer is shown in the Fig. 2.7. When the light is made incident on the sample, part of the light is attenuated due to scattering and absorption, a part is reflected and the remaining is transmitted. According to Beer-Lambert law, the attenuation at a given wavelength is given by,

$$\log\left(\frac{I_0}{I}\right) = \varepsilon C' z \,, \tag{2.31}$$

where I_0 is the incident intensity, I is the transmitted intensity of the light, ε is the molar absorbance, C' is the molar concentration of the absorbing molecules and z is the optical path length of the sample. This spectrophotometer is a double beam, direct radiation measuring system. A deuterium lamp and a halogen lamp are the sources covering ultraviolet region and visible region respectively. It has a grating type double monochromator to disperse the measuring light in to constituent wavelengths. Using a chopper mirror the incident beam is split into reference and sample beams. The reference beam is used to nullify the effect of sample cell and solvent. This instrument has two detectors (PMTs); one for measuring the reference beam and other for the sample beam. The wavelength range covered in this instrument is from 900 nm - 200 nm with resolution of 0.1 nm. We have recorded UV- Visible spectra of PNIPAM microgel crystals contained in quartz cells of optical path length 2 mm. All spectra reported in thesis correspond to normal incidence.

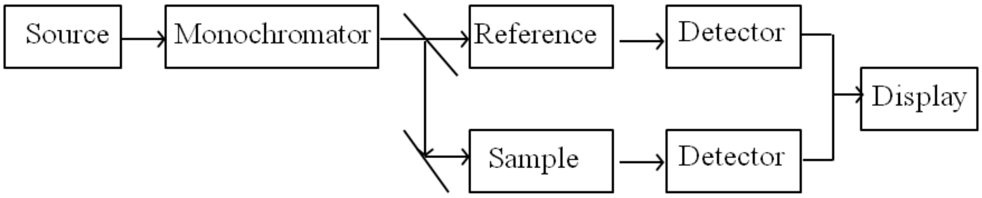

Fig. 2.7 Schematic diagram of UV-Vis Spectrometer.

2.3 Rheology

Rheology is the study of flow and deformation behavior of the materials under the applied shear stress. An instrument used to study the rheological behavior of the materials is called a rheometer. Rheological measurements on dense PNIPAM microgel suspensions have been carried out using a MCR 301 rheometer (M/s Anton

Paar, Germany). It consists of a measuring cell which is held static and a measuring tool which is either rotated or oscillated during course of measurements, for the application of shear. Rotation or oscillation of the tool is achieved with the help of a electromagnetic motor which operates on air bearings to produce finest movements. Required air is pumped via external compressor. This rheometer can be operated in controlled stress or controlled strain modes. Rheological measurements presented in this thesis correspond to controlled strain mode. The rheometer can apply torque in the range of 0.1 μNm – 200 mNm with a resolution of 0.001 μNm and a frequency in the range of 10^{-4}-10^{2} Hz. Measuring cell and measurement tools are available in the form of cone and plate, parallel plates, double gap, cup and bob etc. The choice of the geometry depends on sample viscosity.

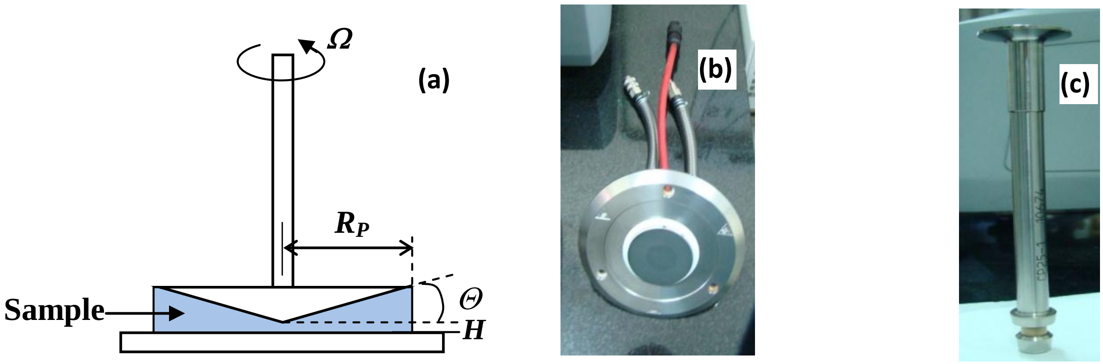

Fig. 2.8 (a) Schematic diagrams of the cone and plate geometry with cone of angle, Θ and radius, R_P. (b) and (c) show photographs of the rheometer plate and cone, respectively.

We have performed rheological measurements using cone & plate geometry with a cone of angle, $\Theta = 1°$, radius, $R_P = 12.5$ mm and cone truncation at $H = 0.051$ mm. Schematic of cone and plate geometry is shown in Fig. 2.8(a). Photographs of plate and cone are shown as Fig. 2.8(b) and (c), respectively. Cone and plate is geometry suits for high viscous samples. Plate acts as measuring cell which is held static and cone act as measuring tool which is connected to the motor for vertical as well as rotation/oscillation movements. Sample to be sheared is sandwiched between cone and plate. Open area of the sample is sealed with silicon oil (viscosity 99 cp) in order to prevent the evaporation of the water during the course of measurements. Temperature of the sample is varied using Peltier unit associated with measuring plate which is cooled by circulating water using a external circulator. Peltier element allows the variation of temperature from -20 °C to 200 °C with a temperature stability of ± 0.01°C.

The rheometer can be operated either in rotation or oscillation mode. In rotational measurements, cone rotates on the sample in which speed of rotation is proportional to the shear rate. In order to ensure uniform shear rate the cone angle is kept small (~ 1 to 4°) [10]. The distance between the bottom plate and the cone tip is H. When sample is sheared with an angular speed of Ω, the shear rate, $\dot{\gamma}$ (experienced by suspension) is given by the expression, $\dot{\gamma} = \Omega/tan\Theta$. For small Θ, $\dot{\gamma} = \Omega/\Theta$. Thus, the shear rate is dependent only on the rotational speed and provides constant shear rate throughout the sample. The corresponding shear stress is given by $\sigma = 3M/(2\pi R_p^3)$ where, M is the applied torque for generating the given stress. Using rotation mode one can study the flow behavior of the material.

On the other hand, oscillatory measurements are used to study viscoelastic response of the materials [10]. The parameters for viscoelastic materials are written in complex domain where the real and imaginary parts represent elastic and viscous contributions of a material, respectively as,

$\sigma^* = G^*\gamma^*$, with $\gamma^* = \gamma' + i\gamma''$; $\sigma^* = \sigma' + i\sigma''$; $G^* = G' + iG''$.

Here $*$ represents complex quantities, with $'$ and $''$ as real and imaginary parts, respectively. In oscillatory rheological measurements, oscillatory strain, $\gamma^* = \gamma_0 \exp{(i\omega t)}$ with amplitude, γ_0 and angular frequency of oscillation, ω, is applied on the sample and oscillatory stress, $\sigma^* = \sigma_o \exp i[\omega \mathrm{t} - \delta(\omega)]$ with amplitude, σ_0 and phase shift $\delta\,(\omega)$, is measured. The phase shift between applied strain and measured stress is shown schematically in Fig. 2.9(a). From the strain and stress, complex modulus is obtained as

$$G^* = ({\sigma_0}^*/{\gamma_0}^*) = (\sigma_0/\gamma_0)\exp[i\delta(\omega)] = (\sigma_0/\gamma_0)\,[\cos\delta(\omega) + i\sin\delta(\omega)],$$

which is further resolved in to G' and G'', using $\delta(\omega)$ (Fig. 2. 9(b)) as follow,

$G' = (\sigma_0/\gamma_0)\cos\delta(\omega)$, $G'' = (\sigma_0/\gamma_0)\sin\delta(\omega)$ and $\tan\,\delta(\omega) = G''/G'$ is a damping factor.

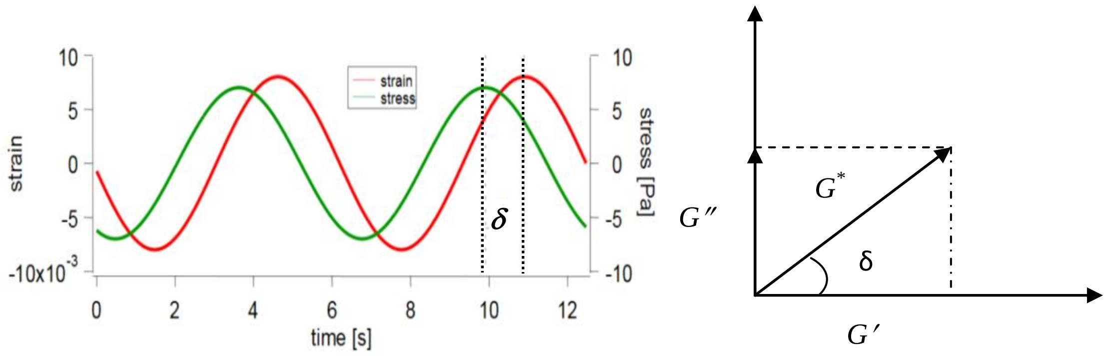

(a) **(b)**

Fig 2.9 (a) Phase difference, δ in strain (γ) and stress (σ) for a visco-elastic materials and (b) Vector representation of complex modulus for visco-elastic materials.

G' and G'' are used to determine the physical state of the material. When $G' > G''$, material is said to be viscoelastic solid and when $G' < G''$, material is said to be viscoelastic liquid. At small γ_0, viscoelastic solids deform linearly, where as for large γ_0 deformation becomes non-linear (*e.g.* Fig. 1.7). Using linear deformation behavior (where G' and G'' are measured as a function of ω by keeping γ_0 to be constant and small) the physical state and relaxation times of the material can be determined (Fig. 1.8). On the other hand, using non-linear deformation behavior (where G' and G'' are measured as a function of γ_0 by keeping ω constant), yielding behavior of the materials can be studied (Fig. 1.7). We have performed linear viscoelastic measurements on PNIPAM microgel glasses by applying constant γ_0 (< 5%) and by varying the ω from 0.1 to 100rad/sec. Non-linear rheological measurements have been carried out using dynamic strain sweep (DSS), in which γ_0 is varied between 1 - 1000% by keeping ω constant. Results of linear and non-linear rheological measurements on dense PNIPAM microgel glasses are presented in Chapter 5.

2.4 Synthesis and purification of PNIPAM microgel suspensions

PNIPAM microgel particles have been synthesized using free radical precipitation polymerization method [11-13]. Key ingredients in the synthesis includes monomer (N-isopropyl acrylamide - NIPAM), initiator (potassium per sulphate - KPS), crosslinker (N, N′-methelene bisacrylamide - BIS) and surfactant (sodium dodecyl sulphate - SDS). All the chemicals used in synthesis are of analytical grade reagents and used as supplied. Synthesis is carried out as one pot synthesis. A pre-gel solution is prepared by dissolving NIPAM, SDS and BIS in ultrapure deionized (Milli-Q) water. Dust particles can act as nucleation center while polymerization leading to formation of polydisperse microgel particles. The pre-gel solution is then filtered through 0.22 μm syringe filter (Millex) for removal of dust. Filtered pre-gel solution is transferred to round bottom flask and degassed through constant Argon purging for one hour under rigorous stirring. Degassing is essential to remove the oxygen present in the solution, which can affect the polymerization. While Argon purging was on, pre-gel solution is heated to 70°C. In aqueous solution SDS forms spherical micelles (self aggregates of

SDS molecules), which contains monomer and act as monomer droplets. The initiator (KPS) is dissolved separately in Milli-Q water at 70 °C and added to the degassed reaction mixture. KPS forms free radicals at 70 °C, which initiates the polymerization reaction within monomer droplet. KPS radicals bind to the monomer and transfers charge on to it. Monomer with charge binds with another monomer forming dimer and transfers charge on to it. In this way, polymerization reaction proceeds with formation of trimers and higher oligomers. Polymerization gets terminated by the joining of oligomers. During the polymerization process, BIS binds two polymer chains together creating the network structure of polymers, which is essential for formation of microgel. Polymerization is allowed to proceed for six hours. During polymerization, temperature of the solution is maintained at 70 ± 2 °C. Polymerization is carried out under continuous purging of Argon gas and rigorous stirring of the solution. Fluctuations in the temperature, stirring speed and gas purging during polymerization can cause aggregation of microgel particles. Upon completion of polymerization, microgel suspension is cooled back to room temperature. The size of PNIPAM microgel particles can be varied by varying the amount of the SDS and crosslinker (BIS). Variation of SDS amount leads to variation of size of micelle and hence that of microgel particle. In absence of the SDS, monomer themselves form droplets. On the other hand, increase in crosslinker concentration makes polymer network more compact, resulting in decrease in the size of the particles. At higher crosslinker, due to compaction of polymer network, PNIPAM microgel particles become more rigid than those with lesser crosslinker. In the absence of the crosslinker (BIS), polymer chains join together via self cross linking [13].

Monodisperse PNIPAM microgel particles of various sizes have been synthesized by varying SDS and BIS. Details of the chemical compositions used for synthesis are listed in Table 2.1. As synthesized suspension of PNIPAM microgels are subjected to dialysis using dialysis membrane (10 kDa, M/s Hi-media, India) against Milli-Q water for several days. Dialysis is stopped when conductivity of the dialyzed water reduces to that of ultrapure water. Variation of the hydrodynamic diameter, d_h with temperature, measured on dilute suspensions using DLS, for PNIPAM microgels, synthesized with various SDS and BIS combinations are shown in Fig. 2.10

Table 2.1: Details of reagents used in synthesis of PNIPAM microgels along with the hydrodynamic diameter, d_h of PNIPAM microgels at 25 °C and corresponding size polydispersity (SPD).

Sr. No.	NIPAM	BIS	SDS	KPS	d_h at 25 °C	*SPD*
1.	139mM	1.96mM	25mM	2.22mM	238nm	5.5%
2.	139mM	1.96mM	19mM	2.22mM	273nm	3.0%
3.	139mM	1.96mM	10mM	2.22mM	353nm	6.0%
4.	073mM	0.00mM	00mM	1.39mM	560nm	6.0%

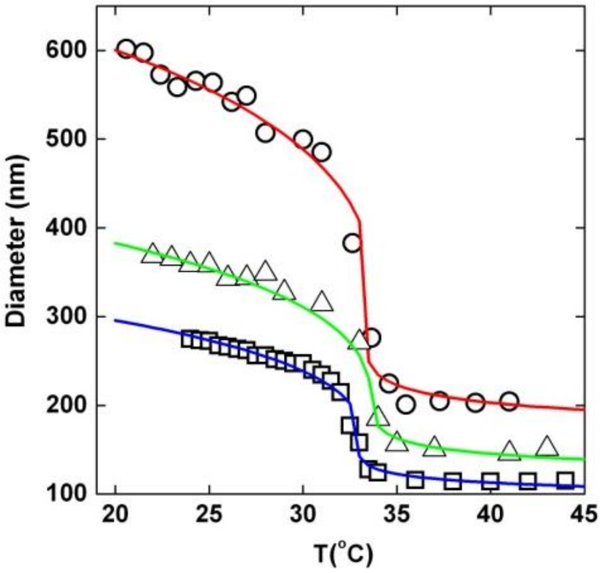

Fig. 2.10 Hydrodynamic diameter, d_h as function of temperature, *T* for PNIPAM microgel particles synthesized with different combinations of SDS and BIS; circles (BIS - 0 mM, SDS - 0 mM), triangles (BIS - 1.96mM, SDS -10 mM), squares (BIS - 1.96 mM, SDS – 25 mM). Continuous lines are fits of the experimental data to Flory Rehner theory, which is discussed in Chapter 3.

2.5 Preparation PNIPAM microgel crystals and glasses

Dialyzed suspensions of PNIPAM microgels are concentrated using a stirred cell equipped with an ultra-filtration membrane. Details of the stirred cell ultra-filtration set up are given in Chapter 3. During the course of concentration, samples with different concentrations are collected. When concentrated samples are kept steady for 24 hrs, moderately dense samples showed crystallization by exhibiting iridescence under white light illumination. Whereas, highly dense samples did not show iridescence indicating lack of crystallization. The volume fractions for moderately dense crystalline samples determined from Bragg peak position are found to be ~ 0.5 - 0.6. The procedure for determination of ϕ from Bragg peak position is discussed in Chapter 3. These ϕ values have been used to determine the volume fractions for higher concentration samples. Samples with $\phi > 0.7$ did not show iridescence even after leaving undisturbed for a week. In order to prepare the PNIPAM microgel crystals with $\phi > 0.7$, samples are heated to the temperatures close to VPT and cooled back slowly (0.5°C/hour). When samples are heated, PNIPAM microgel particles shrink in size creating space for their movements. When cooled slowly, particles get enough time to arrange themselves into an ordered state before they swell back [11, 14]. After repeated heating and cooling cycles, suspensions with ϕ between 0.7-1.0 showed iridescence. Photographs showing iridescence from PNIPAM microgel crystals under visible light illumination are shown in Fig. 2.11.

Fig.2.11. Photographs of PNIPAM microgel crystals showing iridescence under visible light illumination, at 22 °C, (a) $\phi = 0.49$, $d_h = 243$ nm, left undisturbed for 24 hours (b) $\phi = 0.87$, $d_h = 362$ nm, cooled at 0.5 °C/hour.

When samples are cooled rapidly (1.0°C/min), no iridescence was observed. Samples with ϕ >1.0 did not show iridescence even after slow cooling of 0.5°C/hour. The dense PNIPAM microgel suspensions not showing iridescence are characterized to be in glassy state (as discussed in Chapter 5). In dense suspensions, dynamics of the PNIPAM microgel particles becomes extremely slow. Therefore, when suspensions are cooled rapidly, microgel particles get kinetically arrested leading to a glassy state. For light scattering studies, samples have been prepared in cylindrical glass cell of 8 mm optical path length. For UV- Vis study samples have been prepared in quartz cell of 2 mm optical path. The sample cells were cleaned thoroughly before preparing the sample and care has been taken that no dust enters into the sample during the sample preparation.

References

1. B.V.R. Tata, in “Statistical Physics of complex Fluids”, edt. S. Maruyama and M. Tokuyama, Tohoku university press, Sendai, Japan (2007).
2. Berne and Pecora, “dynamic light scattering”, A Wieley-Interscience Publication, USA.
3. M. Kerker, “scattering of light and other electromagnetic radiation”, Academic Press, New York (1969).
4. B.J. Frisken, Applied Optics 40, (2001) 4087-4091.
5. F Grüner and W Lehmann, J. Phys. A: Math. Gen. 13, (1980) 2155-2170.
6. C. Urban and P. Schurtenberger, J. of colloid and int. sci. 207, (1998) 150-158.
7. P.N. Pusey, Current Opinion in Colloid & Interface Science 4, (1999) 177-185.
8. P.N. Pusey and W. Van Megen, Physica A 157, (1989) 705-741.
9. C. Haro-Pérez, G. J. Ojeda-Mendoza, and L. F. Rojas-Ochoa, J. Chem. Phys. 134, (2011) 244902.
10. C. W. Macosko, Rheology Principles Measurements and Applications, WILEY-VCH, New York (1994) ; T. A. Mazder, Rheology Handbook, Vincentz Network GmbH & Co, K.G.

11. J. Brijitta, Ph. D thesis, Pondicherry University, (2012).

12. J. Gao and B. J. Frisken, Langmuir 19, (2003) 5217-5222.

13. I. Varga, T. Gilányi, R. Mészáros, G. Filipcsei and M. Zrínyi, J. Phys. Chem. B 105, (2001) 9071-9076.

14. J. Brijitta, B. V. R. Tata and T. Kaliyappan, J. Nanosci. Nanotechnology 9, (2009) 5323-5328.

CHAPTER 3

EFFECT OF OSMOTIC PRESSURE ON DESWELLING BEHAVIOR OF MICROGEL PARTICLES IN DENSE PNIPAM MICROGEL CRYSTALS

3.1 Introduction

PNIPAM microgel particles are known to be thermo-responsive, where the size of PNIPAM microgel particle decreases with increase in temperature, with a sudden jump at ~ 34°C, which is known as volume phase transition, VPT [1-3]. In addition to being thermo-responsive, PNIPAM microgel particles are also known to undergo compression upon application of osmotic pressure, where the osmotic pressure is applied by adding a non-adsorbing polymer to their suspensions under dilute conditions [4]. Fernández-Nieves *et al.* [4] have shown that at low osmotic pressure, size of microgel remains constant and starts decreasing beyond a critical osmotic pressure (~ kPa). Bulk modulus of PNIPAM microgel particles, determined from the variation of the particle size with osmotic pressure in a dilute suspension, has been found to be of the order of kPa [5]. In a suspension, PNIPAM microgel particles can also experience an osmotic pressure due to its own surrounding particles, which increases with increase in particle number density, n_p of the suspension. In addition, dense suspensions (high n_p) of PNIPAM microgel particles exhibit structural ordering (liquid-like, crystalline, glassy) [1, 3], which leads to increase in the osmotic pressure of the suspension [6]. The effect of osmotic pressure arising from its own surrounding particles on deswelling of PNIPAM microgel particles under dense conditions has not been investigated.

In this chapter we report the experimental evidence for the compression of PNIPAM microgel particles in structurally ordered dense suspensions, due to osmotic pressure exerted by its own PNIPAM microgel particles. Our experiments of osmotic compression of PNIPAM microgel particles in dense suspensions are equivalent to that of Fernández-Nieves *et al.* [4] on dilute suspensions, with polymer (dextran) chains being replaced by microgel particles themselves. Unlike dilute suspensions, DLS cannot be used to measure the size of the microgel particle in dense suspensions due to structural ordering. Here, we use the structural ordering of PNIPAM microgel particles itself to measure near-neighbour separation and hence particle size in close packed conditions, by recording the diffraction pattern on structurally ordered microgel suspension. Towards this we have prepared dense PNIPAM microgel crystals of varying osmotic pressure by varying the volume fraction (number density) of the suspension using stirred cells. Another method for increasing the volume fraction of the suspension is by centrifugation. But, centrifugation gives poor control over variation of volume fraction of the PNIPAM microgel suspensions. Centrifugation at low speeds does not concentrate the suspension due to low density (low polymer content) of PNIPAM microgel particles, whereas centrifugation at high speeds lead to the formation of lumps (aggregates) of microgel particles, which takes long time (more than a month) to re-dissolve back in a solvent. Bragg diffraction of PNIPAM microgel crystals have been recorded using UV-Vis spectrometer. Upon increasing the osmotic pressure (particle concentration), Bragg peak has been found to exhibit a blue shift. The Bragg peak has been used to determine the interparticle separation. Beyond a certain osmotic pressure, interparticle separation is found to be smaller than the size of PNIPAM microgel particle under swollen state (measured using DLS on dilute suspension). In dense PNIPAM microgel crystals, the interparticle separation being lesser than the particle size in its swollen state provides direct evidence for compression (deswelling) of PNIPAM microgel particles under osmotic pressure. Flory-Rehner (FR) theory for swelling/deswelling of gels has been used to understand the experimentally observed swelling/ deswelling behavior of the PNIPAM microgel particles osmotic pressure.

3.2 Experimental details

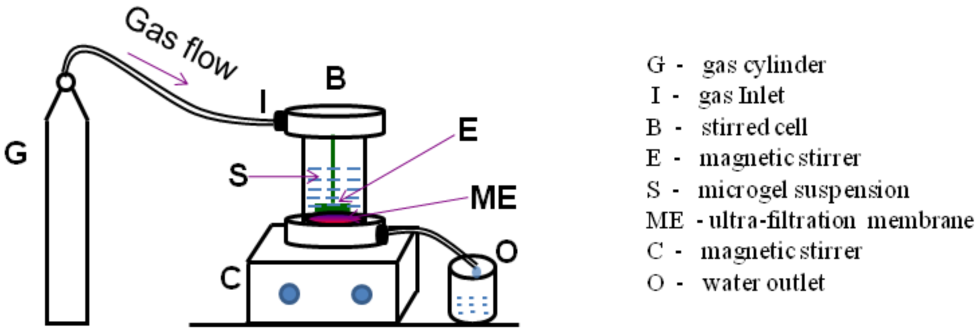

Fig. 3.1 Schematic diagram of Stirred cell ultra-filtration set up.

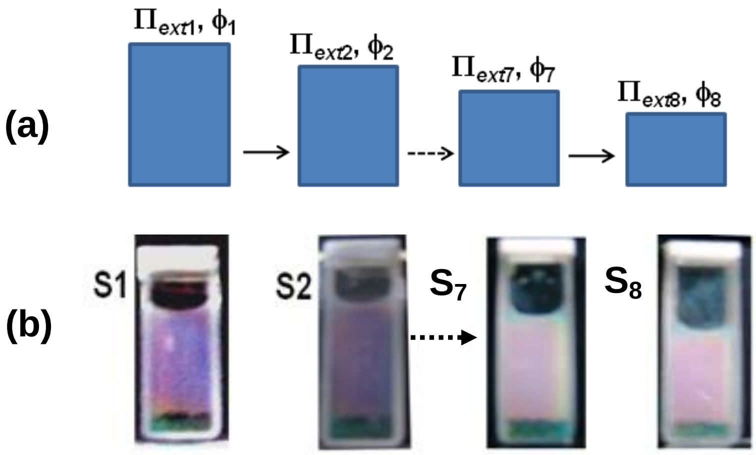

Fig. 3.2 (a) Schematic showing the osmotic compression of PNIPAM microgel suspensions by simultaneous decrease in suspension volume *V* and increase in number of microgel particles *N*. (b) Photographs of the PNIPAM microgel crystals showing iridescence under white light illumination.

For these studies, PNIPAM microgel particles having hydrodynamic diameter, d_h = 353 nm and SPD 6%, at 25°C have been used. Details of synthesis are given in the Chapter 2. In order to prepare the PNIPAM microgel crystals of different volume fractions, purified microgel suspension was subjected to different osmotic compressions using a stirred cell, which is depicted schematically in Fig. 3.1. On the other hand, stirred cell gives a very controlled way for osmotic compression of PNIPAM microgel suspension. Stirred cell uses an ultra-filtration membrane, which allows solvent to pass through but not PNIPAM microgel particles. We used an ultra-filtration membrane having pore size of 10 kDa (pore size ~ 50 nm).

Figure 3.2(a) shows the scheme by which PNIPAM microgel samples subjected to different osmotic compressions (due to change in ϕ) are prepared. We start with purified PNIPAM microgel suspension of known volume (V_1) and having N_1 number of particles, in stirred cell equipped with ultra-filtration membrane. Stirred cell have inlet for passing gas inside stirred cell and outlet for collecting the water passed through membrane. In the suspension with volume V_1 and number of particles N_1, PNIPAM microgel particles experience osmotic pressure, Π_{ext1} proportional to the concentration of the suspension ($n_{p1} = N_1/V_1$). Argon gas was passes via inlet to apply pressure on the suspension for the removal of the water in the suspension (through membrane). By measuring the amount of water collected at the outlet, new volume, V_1' of the suspension inside the stirred cell has been estimated. When suspension is compressed using external pressure against the ultra-filtration membrane that is permeable to solvent but not to PNIPAM microgel particles, microgel particles experience the increase in osmotic pressure due to increase in particle concentration ($n_{p2} = N_1/V_1'$). Part of the sample with particle concentration n_{p2} is collected aside and remaining suspension with volume V_2 and number of particles N_2 is subjected to higher osmotic compression. In this way, we have prepared eight samples of different ϕ, namely S_1 to S_8. These samples were transferred to 2 mm path length quartz cells for

UV-Visible measurement. Quartz cells along with microgel suspensions were heated above VPT and cooled slowly (at rate of 0.5°C/hour) to 22°C. Upon repeated heating and slow cooling (about 3 cycles), samples showed iridescence upon white light illumination (photographs shown in Fig. 3.2(b)) indicating crystallization of PNIPAM microgel suspensions. All the eight samples showed crystallization. These crystalline samples were subjected to the UV-Visible measurements and results are discussed as follows.

3.3 Results and Discussion

UV-Visible spectra for crystalline PNIPAM microgel samples S_1-S_8, recorded using UV visible spectrometer under normal incidence, are shown in Fig. 3.3(a). The peaks in the UV-Vis spectra of PNIPAM microgel crystals are due to the Bragg diffraction satisfying the Bragg condition, $2\mu_s d_{hkl} \sin\theta = n\lambda$. Here μ_s is the refractive index of the solvent, d_{hkl} is inter-planar spacing, λ is incident wavelength and n is the order of diffraction which is taken to be 1. At normal incidence θ = 90°. Notice that the wavelength, λ_B, at which the Bragg peak occur, shifts to lower wavelength (blue shift) with increasing ϕ (*i.e.*from S_1 to S_8). As discussed in Chapter 1, PNIPAM microgel suspensions are known to crystallize into a face centered cubic (fcc) structure [7]. For fcc structure, position of the first peak (arising from the <111> plane of fcc), λ_B is related to the number density, n_p and the interparticle separation, d_{nn} by,

$$n_p = \frac{4}{3\sqrt{3}}\left(\frac{2\mu_s}{\lambda_B}\right)^3 \;\; ; \;\; d_{nn} = \sqrt{\frac{3}{2}}\left(\frac{\lambda_B}{2\mu_s}\right). \tag{3.1}$$

Figure 3.3(b) shows variation of ϕ and d_{nn}/d_h with n_p. Value of ϕ, determined from $\phi = n_p \pi d_h^3/6$, for samples S_1 to S_3 is found to be lesser than 0.74, whereas for samples S_4 to S_8 it is larger than 0.74. The ϕ values being larger than 0.74 are unphysical, as the highest possible ϕ for fcc structure of spheres is 0.74. d_{nn}/d_h for samples S_1 to S_3, is found to be greater than 1.0. Whereas, for samples S_4 to S_8, d_{nn}/d is found to be smaller than 1.0. The reduction of d_{nn}/d_h to values less than 1.0 indicates that the PNIPAM microgel particles have undergone compression in dense suspensions. The unphysical values of ϕ for samples S_4 to S_8 are due to the use of d_h measured under dilute condition, where particles are known to be in swollen state. In dense suspensions, PNIPAM microgel particles get compressed (deswell) due to osmotic pressure exerted by surrounding PNIPAM microgel particles, as evident from d_{nn}/d_h being less than 1.0. The ϕ values estimated using d_h and d_{nn} are shown in Fig. 3.3(b). When d_{nn} is used as the diameter of PNIPAM microgel particles, ϕ is found to be 0.74. Any increase in the n_p beyond $\phi = 0.74$ leads to decrease in size of the particles such that volume fraction remains constant (0.74), which is shown schematically in Fig. 3.4.

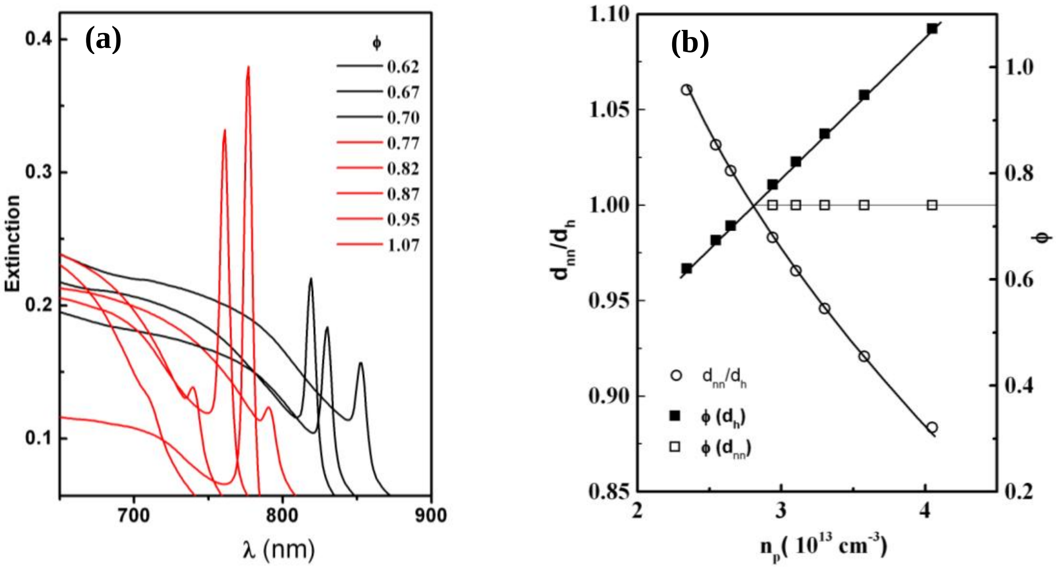

Fig. 3.3 (a) UV-Visible spectra from PNIPAM microgel crystals with different ϕ (Increasing volume fraction from right to left). Black and red lines indicate the samples with uncompressed ($\phi < 0.74$) and compressed ($\phi > 0.74$) microgel particles, respectively. (b) d_{nn}/d_h and ϕ estimated using d_h *and* d_{nn} as a function of n_p for samples S_1-S_8. Continuous lines are guides to the eye. All spectra recorded at $T = 22°C$.

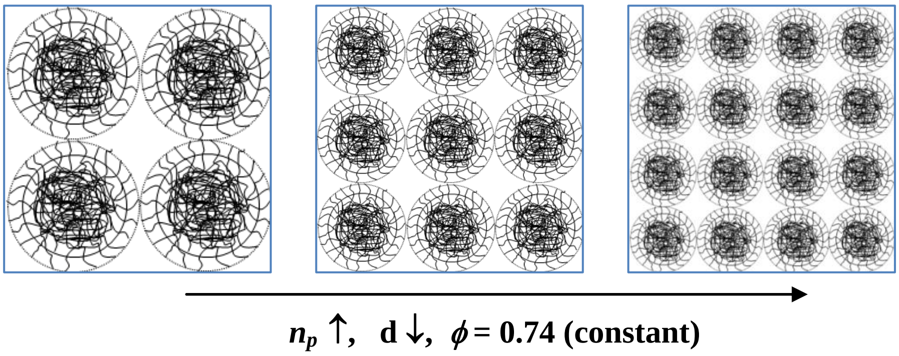

Fig. 3.4 Schematic presentation of the deswelling of PNIPAM microgel particles with increasing n_p beyond the close packing densities.

We have determined the osmotic pressure, Π_{ext} associated with PNIPAM microgel crystals using the equation of state (EoS) for fcc crystals [9] which is given as,

$$\frac{\Pi_{ext} V}{N k_B T} = \left(\frac{3}{1 - Z}\right) - \frac{a(Z - b)}{(Z - c)} \quad . \tag{3.2}$$

where N is number of particles, V is the volume of the crystal, $Z = 6\phi/\sqrt{2}\pi$. For fcc structure the parameters a = 0.6207, b = 0.7081 and c = 0.5916 [9]. At ϕ = 0.74, where particles are in close contact, Π_{ext} is found to attain the value of ~ kPa, which is of the order of osmotic pressure observed in compression of PNIPAM microgels in dilute suspensions [4, 5]. Thus, at ϕ = 0.74 PNIPAM microgel particles come into contact with each other, experience the osmotic pressure of ~ kPa (which is more than the Bulk modulus of the PNIPAM microgel particles) and undergo compression.

3.4 Flory-Rehner theory for deswelling of PNIPAM microgels

Flory - Rehnar (FR) theory describes the swelling or deswelling behavior of gels under external stimuli [8]. FR theory considers gel to be a homogeneous, elastic network of crosslinked polymer chains immersed in a solvent. Upon mixing the polymer network into the solvent, polymer chains have a tendency to disperse due to osmotic pressure, Π_{mix} arising from mismatch of polymer density between polymer rich and polymer poor region and hence gel undergo swelling. While swelling, polymer chains between crosslinked network junctions get stretched and experience osmotic pressure due to elasticity of polymer network, Π_{ela} which opposes the swelling of gel. Any external pressure on the gel is balanced by the Π_{mix} and Π_{ela} as,

$$\Pi_{mix} + \Pi_{ela} = \Pi_{ext}. \tag{3.3}$$

FR theory considers gel to be homogeneous network of polymer chains, but in practice it contains inhomogeneities due to crosslinking of polymer chains. Such inhomogeneities are shown schematically in Fig. 3.5.

Homogeneous gel **Inhomogeneous gel**

Fig. 3.5 Schematics showing homogeneous and inhomogeneous gel networks.

Empirical corrections have been incorporated in modified FR theory to take into account these inhomogeneities [10, 11], according to which modified FR equation is given as,

$$[\Phi + ln(1 - \Phi) + \chi\Phi^2] + \frac{\Phi_0}{m}\left[\frac{1}{2}\left(\frac{\Phi}{\Phi_0}\right) - \left(\frac{\Phi}{\Phi_0}\right)^{1/3}\right] = \Pi_{ext}\,. \tag{3.4}$$

The first term in above equation represents the mixing contribution to osmotic pressure (Π_{mix}) and second represents elastic contribution (Π_{ela}). Here, Φ is the polymer volume fraction within microgel particle. χ is the Flory's polymer-solvent interaction parameter which depends on temperature and Φ which is given as,

$$\chi = \chi_1 + \chi_2\Phi$$

where, $\chi_1 = (\Delta H - T\Delta S)/k_B T$ with ΔH = -12.46 x 10^{-21} J and ΔS = -4.717 x 10^{-23} J/K. Here, ΔH is enthalpy change and ΔS is entropy change per monomeric unit of network related to volume phase transition [11]. Φ_0 and m are the volume of microgel particle in its collapsed state and effective number of crosslinks per unit volume of gel, respectively.

FR theory has been successfully applied to describe the deswelling of microgels under osmotic pressure in dilute suspensions [4]. Here, we apply it for describing the deswelling in dense suspensions with Π_{ext} being osmotic pressure from surrounding microgel particles. Equation 3.4 can solved for getting Φ/Φ_0 in balanced condition of the gel, which can be further used to determine the diameter of PNIPAM microgel particle using the relation,

$$\frac{\Phi}{\Phi_0} = \left(\frac{d_0}{d}\right)^3. \tag{3.5}$$

Equations 3.4 and 3.5 are used to fit the experimentally measured data on variation of PNIPAM microgel particle diameter with respect to temperature and osmotic pressure. During the fitting process, χ_2 , m, and Φ_0 are used as fitting parameters. In order to maintain the consistency between parameters with respect to temperatures and pressure, χ_2 , m, and Φ_0 are obtained by fitting the data on variation of d_h with respect to temperature measured using DLS on dilute suspension and the same are used to determine the size variation of particles with osmotic pressure. In dilute suspension, Π_{ext} due to surrounding microgel particles is negligible. Thus,

$$\Pi_{mix} + \Pi_{ela} = 0. \tag{3.6}$$

Variation of d_h for PNIPAM microgel particles with temperature along with the its fit to FR theory is shown in Fig 3.6(a). The best fit to experimental data is obtained at χ_2 = 0.51, m = 2171 and Φ_0 = 0.43. Value of χ_2 is consistent with earlier reports for

PNIPAM in water [12]. In collapsed state, PNIPAM microgels have been observed to contain about 50% of water [13], hence value of Φ_0 = 0.43 is reasonable. The parameters χ_2, m, and Φ_0 thus obtained, have been used to estimate the variation in the size of the PNIPAM microgel particles with Π_{ext}, which is shown in Fig. 3.6(b). It can be seen that, PNIPAM microgel particles starts deswelling beyond certain critical osmotic pressure (Π_{ext} ~ kPa).

Experimentally measured sizes of the PNIPAM micorgel particles for low Π_{ext} (*i.e.* in dilute suspensions) and for high Π_{ext} (*i.e.* in suspensions with $\phi \geq 0.74$) are also shown in Fig. 3.6(b). In dilute suspensions, the diameter of PNIPAM microgel particle has been measured directly using DLS. At intermediate Π_{ext} (*i.e.* in moderately dense suspensions with $\phi < 0.74$), diameter of PNIPAM microgel particles cannot be determined directly either from DLS or UV visible spectra, as suspensions are interacting. Since the inetrparticle interactions in PNIPAM microgel suspensions are unknown, determination of the structure factor and hence the particle size is difficult in ordered suspensions. Nonetheless, critical osmotic pressure (equal to Bulk modulus of the microgel particle) required to compress the PNIPAM microgels is attained in a crystalline state at $\phi = 0.74$. Hence, compression of these PNIPAM microgels is expected to occur only when particles touch each other (*i.e.* at $\phi = 0.74$ for fcc crystals). Therefore for $\phi \geq 0.74$, d_{nn} (determined from Bragg peak) is considered as diameter of the PNIPAM microgel particle. Critical osmotic pressure predicted by FR theory is found to match with that determined form the experiments, beyond which microgel particle size decrease with increase in osmotic pressure. But, the experimental size of microgel particles is seen to decrease suddenly as compared to that determined from FR theory (Fig. 3.6). The sudden decrease of the experimental microgel particle's size as compared to that from FR theory (Fig. 3.6) is due to an approximation in Eq. (3.2) that particles behave as hard spheres. As the microgel particles are made of polymeric chains, consideration of polymeric contribution to the Π_{ext} may help to obtain better match between results of experiments and FR theory.

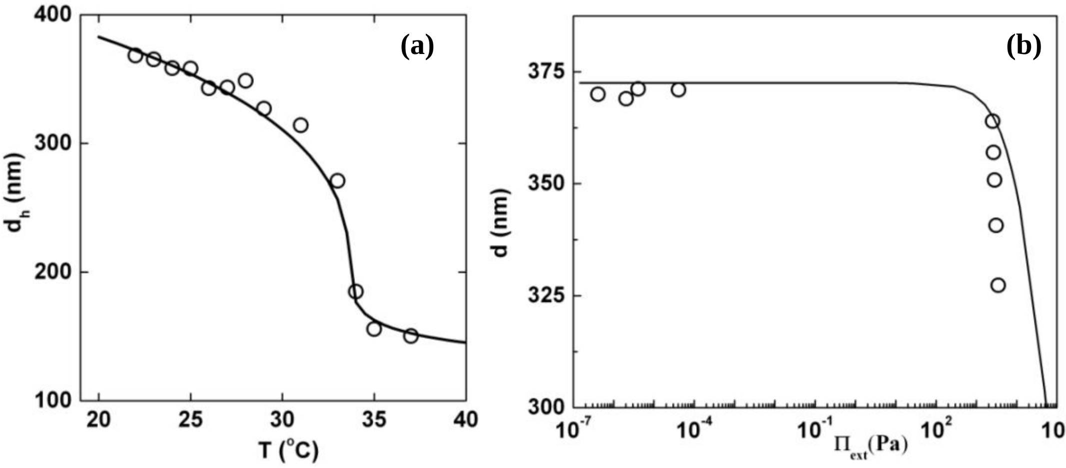

Fig. 3.6 (a) hydrodynamic diameter of PNIPAM microgel particles, as function of temperature (*T*), (b) variation of PNIPAM microgel diameter with osmotic pressure, Π_{ext}. Continuous lines are obtained from Flory-Rehner theory with fitting parameters to be $\chi_2 = 0.51$, $m = 2171$ and $\Phi_0 = 0.43$.

3.5 Summary

Dense PNIPAM microgel crystals with different volume fractions have been prepared by compressing the suspensions osmotically. Bragg diffraction of these crystals has been recorded using UV-Vis spectrometer. Upon increasing the osmotic pressure (particle concentration), Bragg peak is found to exhibit a blue shift. The Bragg peak has been used to determine the interparticle separation. Beyond a certain osmotic pressure, interparticle separation is found to be smaller than the size of PNIPAM microgel particle under swollen state (measured using DLS on dilute suspension). The observation of interparticle separation being less than the particle size in its swollen the state, provides direct evidence for shrinking (deswelling) of PNIPAM microgel particles under osmotic compression in a crystalline state. The experimentally observed swelling/ deswelling behavior of the PNIPAM microgel particles with pressure is understood using Flory-Rehner (FR) theory. Only qualitative agreement has been observed between theory and experiments. Results reported here suggest the need for incorporation of the core-shell structure of PNIPAM microgel particles, for improvement of FR theory.

References

1. J. Brijitta, B. V. R. Tata and T. Kaliyappan, J. Nanosci. Nanotechnology 9, (2009) 5323-5328.
2. M. Ballauff, Y. Lu, Polymer 48, (2007) 1815-1823.
3. J. Wu, B. Zhou and Z. Hu, Phys. Rev. Lett. 90, (2003) 048304.
4. A. Fernández-Nieves, A. Fernández-Barbero, B. Vincent and F. J. de las Nieves, J. Chem. Phys. 119, (2003) 10383-10388.
5. B. Sierra-Martín, Y. Laporte, A. B. South, L. A. Lyon and A. Fernández-Nieves, Phys. Rev. E 84, (2011) 011406.
6. Markus Deserno and H. von Grünberg, Phys. Rev. E 66, (2002) 011401.
7. J. Brijitta, B. V. R. Tata, R. G. Joshi and T. Kaliyappan, J. Chem. Phys. 131, (2009) 074904.
8. P. J. Flory. Principles of Polymer Chemistry Carnell University Press Ithaca, New York (1953).
9. R. J. Speedy, J. Phys; Cond.Mat. 10, (1998) 4387.
10. J. Wu and Z. Hu, Dekker Encyclopedia of Nanoscience and Nanotechnology DOI: 10.1081/E- ENN 120014140, (2004) 1967-1976.
11. S. Takata, K. Suzuki, T. Norisuye and M. Shibayama, Polymer 43, (2002) 3101-3107.
12. J. J. Lietor-Santos, B. Sierra-Martin, R. Vavrin, Zhibing Hu, U. Gasser and A. Fernandez-Nieves, Macromolecules 42, (2009) 6225–6230.
13. B. R. Saunders, Langmuir 20, (2004) 3925-3932.

CHAPTER 4

DYNAMICS ACROSS MELTING OF THERMO-RESPONSIVE MICROGEL CRYSTALS

4.1 Introduction

Melting of a crystal into a liquid or freezing of a liquid into a crystal is the best example for a first order transition with spontaneous breaking of continuous translational symmetry. Though there have been several studies in the past, there exist only two important empirical rules to identify melting/freezing transition. The first phenomenological criterion was given by Lindemann [1], according to which the ratio of the root mean-square (rms) displacement of the atoms to the lattice constant at the melting of the crystal has a value of ~ 0.1. Here the lattice constant sets the scale for rms displacement. The second criterion was formulated by Hansen and Verlet [2] based on computer simulations of Lennard-Jones liquid undergoing freezing. They found that the height of the first peak in structure factor $S(q)$, S_{max}, has a value $\cong 2.85$ near freezing. The applicability of these criteria for colloidal liquids (crystals) undergoing freezing (melting) has been verified. In the case of charged colloids, the Lindemann parameter was found to deviate by 20% from 0.1 whereas S_{max} at freezing was found to be as high as 3.2. [3-4]. Though colloidal systems mimic atomic systems in structural ordering, they differ in dynamics due to the presence of background solvent. The dynamics in atomic systems is ballistic, whereas Brownian motion governs the dynamics in colloidal systems. Realizing this fact, Löwen *et al.* [4] have proposed a phenomenological dynamical criterion for freezing of colloidal liquids in to a crystalline order. The dynamical criterion states that the ratio of long time self diffusion coefficient (D_L) to the short time self diffusion coefficient (D_S), at the freezing point, is a universal number ($D_L/D_S \sim 0.1$). As discussed in Chapter 1, the dynamics in colloidal liquids (i.e. liquid like-ordered suspensions) is characterized by short-time and long-time diffusion coefficients and as a colloidal liquid freezes into a colloidal crystal, it is the long-time diffusion that decreases and slows down near freezing. Thus monitoring D_L helps in identifying the freezing transition and D_S sets the scale to measure the value of D_L at freezing/ melting. Thus Löwen's criterion is a measure of the value of D_L (in units of D_S) at freezing/melting and constitutes a dynamical analog to Lindemann criterion [1] which is based on static properties of the system. Further, the validity of Löwen's criterion implies that the self-diffusional behavior in the colloidal fluids at freezing is universal and allows locating the freezing/melting transition by a single self-diffusion measurement. The dynamical criterion is confirmed both by Brownian dynamics simulations of a Yukawa liquid and by forced Rayleigh Scattering experiments on dilute charged colloidal suspensions [4]. Recently, Holmqvist and Nägele [3] have verified the applicability of this rule for freezing of concentrated charged colloidal suspensions by performing dynamic light scattering (DLS) measurements. They found that at the freezing concentration the ratio $D_L / D_S \approx D_L(q_m)/D_S(q_m) \approx 0.12$, which is in close agreement with dynamical criterion proposed by Löwen *et al.* [4]. $D_L(q_m)$ and $D_S(q_m)$ represent the long time and short time diffusion coefficients measured at first peak position, q_m of $S(q)$. They also verified for charged colloids the ratio $D_L(q)/D_S(q)$ is to be q independent (*i.e.* $D_L(q_m)/D_S(q_m) = D_L / D_S$, for $q > 0.8q_m$).

Though dynamical criterion for freezing is found to be applicable for hard-sphere and charged colloidal fluids undergoing freezing [4], its validity for PNIPAM microgel dispersions is not yet verified. Unlike hard-sphere and charge stabilized colloidal particles, PNIPAM microgel particles are inhomogeneous in structure in the form of a fuzzy shell consisting of dangling polymer chains and a dense polymer core (as shown in Fig 1.4(b)) [5-6]. In dense suspensions, where interparticle separations are of the order of the particle diameter, such complex inhomogeneous intra-particle structure is expected to influence particle dynamics due to overlapping of the fuzzy surfaces and soft interparticle interactions. This chapter reports the results on dynamics in dense PNIPAM microgel crystals across their melting transition, carried out towards the verification of dynamical criterion for melting of PNIPAM microgel crystals using DLS. Melting transition of the crystals is identified by monitoring the Bragg peak intensity as a function of temperature. In dense PNIPAM microgel crystals undergoing melting, the ratio D_L/D_S is found to be less than 0.1. This deviation is found to be larger in the suspension with higher ϕ. Possible reasons for the observed deviation in D_L/D_S are discussed in this chapter. Careful analysis of the mean square displacement (MSD) of PNIPAM microgel particles at short times show that, close to the melting transition of PNIPAM microgel crystals, motion of the microgel particle is subdiffusive. The observed subdiffusive behavior of MSD at shorter times is understood in terms of entanglement of dangling polymer chains between the shells of neighboring PNIPAM microgel particles and argued to be the reason for the observed deviation (i.e. $D_L/D_S < 0.1$).

4.2 Experimental details

PNIPAM microgel crystals having volume fractions 0.49 (S1) and 0.79 (S2) at 23 °C, with particle diameters, d_h to be 241 nm and 276 nm, respectively are used for these studies. Details of synthesis are given in Chapter 2. PNIPAM microgel crystals have been prepared in cylindrical glass cells of 8 mm optical path length using the method discussed in Chapter 2. Light scattering measurements have been carried out using Malvern 4700 (UK) light scattering instrument. Details of light scattering measurements are discussed in Chapter 2. The Bragg intensity from PNIPAM crystals in the scattering volume is captured using PMT, and maximized by adjusting the crystal orientation and position using a rotation and translation stage respectively. Concentrated suspensions of PNIPAM microgels are known to crystallize into an fcc structure [7] and the first Bragg peak position, q_m was used for estimating the lattice constant, $l_a = 2\sqrt{3}\pi/q_m$, particle number density, $n_p = \left(4/3\sqrt{3}\right)(q_m/2\pi)^3$ and volume fraction, $\phi = n_p\,\pi d_h^3/6$. The sample temperature is maintained to an accuracy of ± 0.1°C.

4.3 Results and Discussion

4.3.1 Identification of melting

Bragg peaks recorded from PNIPAM microgel crystals of samples S1 and S2 using SLS are shown in Fig. 4.1(a). The Bragg peak position, q_m is used to determine the n_p and ϕ of the crystals. For samples S1 and S2, n_p and ϕ are found to be 6.71×10^{13} cm^{-3}, 7.11×10^{13} cm^{-3} and 0.49, 0.79 respectively, at 23 °C. For sample S2, the unphysical value of volume fraction (0.79) arises due to the use of d_h of PNIPAM microgels measured under dilute condition. In dense suspensions, PNIPAM microgels undergo compression due to osmotic pressure from the surrounding particles (discussed in Chapter 3). Upon increasing the temperature, iridescence from samples S1 and S2 disappeared indicating loss of crystalline order. The scattering profiles for samples S1 and S2 at higher temperatures showed a broad peak (Fig. 4.1(b)) indicating the melting of the PNIPAM crystals into a liquid like order. In order to identify the temperature at which melting occurs, we monitored the Bragg peak intensity, $I(q_m)$ as a function of T for S1 and S2, which is shown in Fig. 4.2(a). It may be mentioned here that Bragg peak intensity at the given temperature is monitored for 15 minutes (more than the measurement time of correlation function) and found to be almost constant suggesting that crystallites are stationary in the scattering volume during the measurement. With increase in T, $I(q_m)$ showed a gradual decrease followed by a sudden jump around 24 °C and 26 °C for samples S1 and S2 respectively (Fig. 4.2(a)). Temperature at which the sudden jump occurs is identified as the melting transition of PNIPAM microgel crystals. The jump in the $I(q_m)$ is due to jump in structure factor, $S(q_m)$ which changes discontinuously upon structural transition from crystal to liquid state. Upon cooling, molten samples are found to recrystallize at same temperature, suggesting no measurable hysteresis at melting/freezing transition. Further, no shift in Bragg peak position has been observed. The reduction in the intensity up to melting is due to Debye-Waller effect and also due to a small reduction in particle size with increase in temperature.

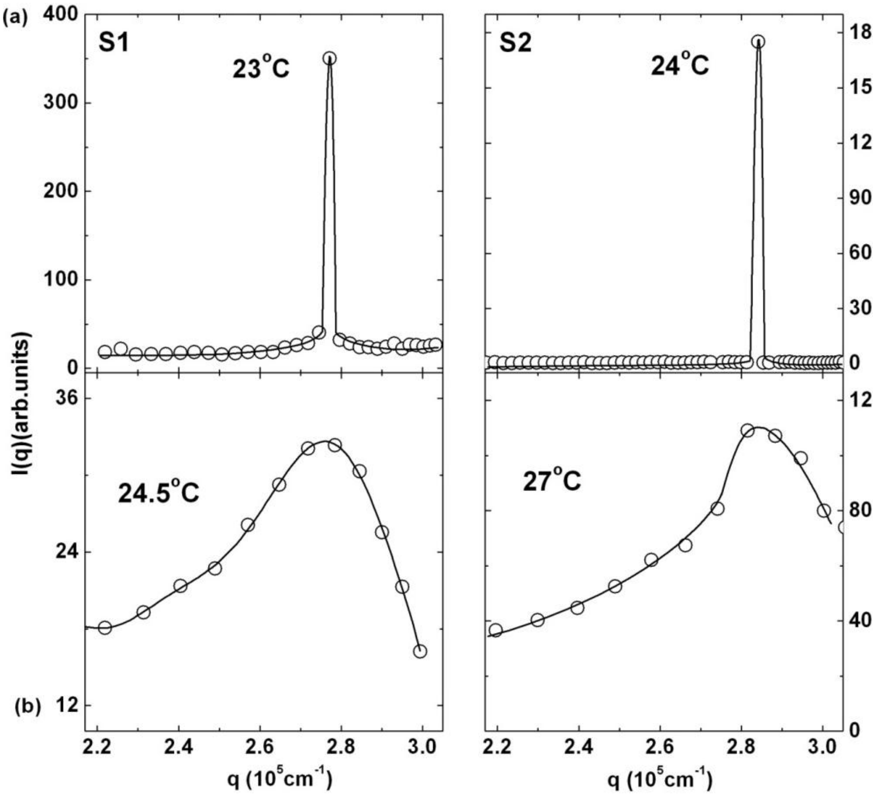

Fig. 4.1 Scattered intensity $I(q)$ vs q for (a) Upper panel - PNIPAM microgel crystals showing Bragg peaks at q_m= 2.78 × 10^5 cm^{-1} and 2.84 × 10^5 cm^{-1} respectively for samples S1 and S2 , (b) Lower panel - liquid like order upon melting of these crystals at elevated temperatures. Lines drawn are guide to the eye.

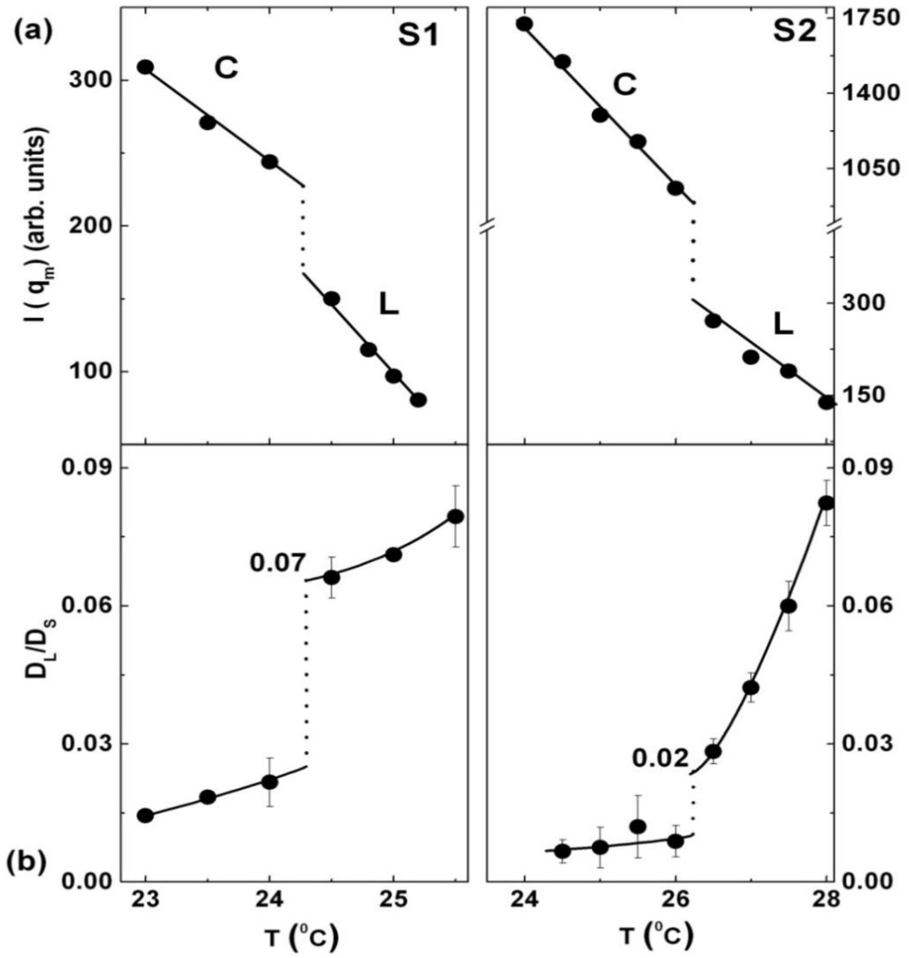

Fig. 4.2. (a) Upper panel - Bragg peak intensity, $I(q_m)$ and (b) Lower panel - D_L/D_S, measured as function of T for PNIPAM microgel samples S1 and S2. Lines drawn are guide to the eye. Dotted lines represent melting transition of PNIPAM crystal (C) to liquid like order (L) upon melting.

4.3.2 Dynamics across melting

We have performed detailed DLS measurements at Bragg peak position, q_m across melting of the PNIPAM microgel crystals with an aim to verify the validity of Löwens criterion across melting of PNIPAM microgel crystals. The PNIPAM microgel samples S1 and S2 were heated in steps of 0.5 °C and allowed to equilibrate at each temperature for 10 minutes. Upon equilibration at each temperature, $g^{(2)}(q,t)$ was collected for 5 minutes and measurements have been repeated for three times. The field correlation, $f(q,t)$ obtained from $g^{(2)}(q,t)$ was used to determine MSD using Eq. (2.24). MSD in the liquid state at T = 27 °C and crystalline state at T = 23 °C for the sample S2 is shown in Fig. 4.3. Short time and long time regime of MSD have been identified with respect to cage rearrangement time, τ_R. τ_R, determined from the expression d_h^2/D_0, is found to be ~ 500 μsec for both the samples. Notice in Fig. 4.3 that at shorter times MSD increases with time in the liquid as well as in the crystalline state.

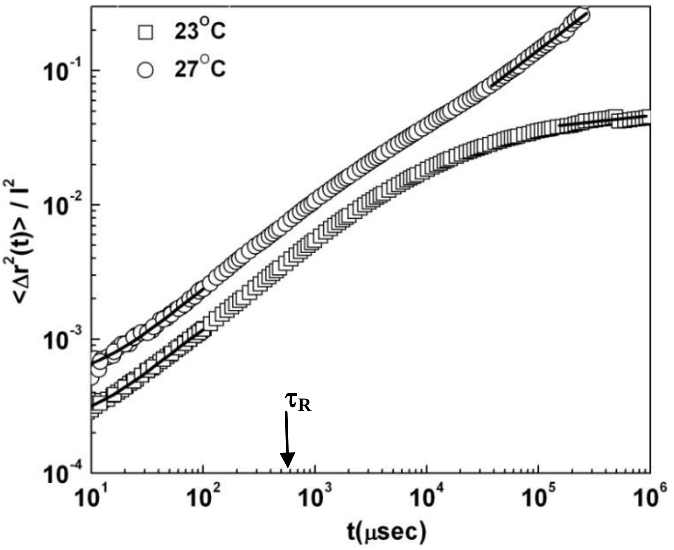

Fig. 4.3. Mean square displacement (MSD), $<\Delta r^2(t)>$, expressed in the units of the average interparticle separation ($l = n_p^{-1/3}$), as function of time, t for sample S2 in the liquid (L) and crystalline (C) state. Lines represent short and long time regimes used for the determination of D_S and D_L, respectively.

At longer times, MSD shows tendency towards saturation in the crystalline state, whereas it increases with time in the liquid state. $D_L(q_m)$ is obtained by linear fitting of long time MSD data. To obtain $D_S(q_m)$, MSD data within 10-100 μsec is subjected to cumulant analysis [8] and the first cumulant is taken as $D_S(q_m)$. D_L and D_S values for samples S1 and S2 have been determined by analyzing the respective MSD data. We have also performed the measurements at another value of q ($> q_m$) and found that $D_L(q)/D_S(q)$ is same as $D_L(q_m)/D_S(q_m)$, suggesting q independence of $D_L(q)/D_S(q)$. Figure 4.2(b) shows the ratio D_L/D_S as a function of T for samples S1 and S2 respectively. For both the samples D_L/D_S is found to increase with increase in T with a sudden jump occurring at the melting/freezing transition temperature. For samples S1 and S2, the values of D_L / D_S at melting/freezing transition are found to be 0.07 and 0.02, respectively. Thus the ratio D_L/D_S determined at the melting of PNIPAM microgel crystals is found to deviate considerably from the dynamical criterion $D_L/D_S \sim 0.1$, proposed by Löwen *et al.* [4]. The deviation from 0.1 is much larger in the case of higher volume fraction sample (*i.e* sample S2). We discuss below the possible reasons for this deviation.

4.3.3 Experimental artifact or not

In order to verify that whether the observed low value of D_L/D_S at melting of PNIPAM microgel crystals is an experimental artifact or not, we have performed DLS experiments on dilute colloidal crystals of charged silica particles under identical experimental conditions. We have prepared colloidal crystals of charged silica particles of size 118 nm and SPD 4% with $\phi = 0.0025$. Mixture of ethylene glycol-water (EGW) in the proportion 80:20 is used as solvent for index matching of the silica particles with the refractive index of the solvent. Index matching minimizes the turbidity of the suspension, hence multiple scattering [9]. The silica colloidal crystals were shear melted into liquid. DLS measurements have been carried out on shear melted colloidal liquid as a function of time. The time count was started immediately after shearing of the sample was stopped. Shear melted colloidal liquid is found to crystallize in 18th minute in to a bcc structure. Figure 4.4 shows the ratio D_L/D_S measured as a function of time while the shear melted liquid is undergoing freezing. The sudden jump observed in D_L/D_S at around 18 minutes corresponds to the freezing of the sample into a crystalline state. Notice that D_L/D_S is 0.09 at freezing which is close to 0.1. We have followed the same methodology for determining the ratio D_L/D_S in samples S1 and S2, but observed deviation from 0.1. Thus we rule out experimental artifact as the reason for the observed deviation in D_L/D_S of PNIPAM microgel suspensions at melting/freezing.

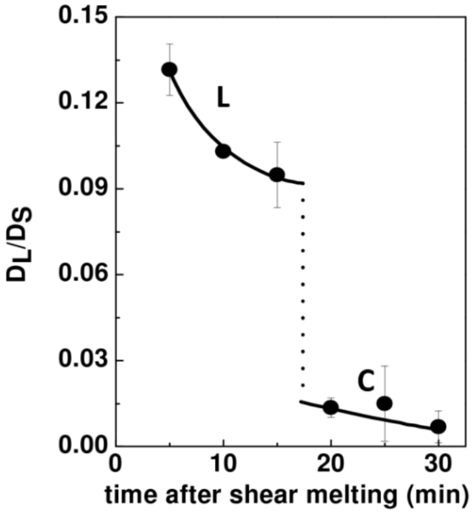

Fig. 4.4 D_L/D_S measured as a function of time, while shear melted charged silica suspension undergoes liquid (L) to crystal (C) transition.

4.3.4 Effect of Multiple scattering

It is known that in dense suspensions multiple scattering of light influences the DLS data [10]. We have estimated the amount of multiple scattering in dense PNIPAM microgel samples S1 and S2 by measuring the scattered intensity in the *VV* and *VH* geometries at scattering wave vector, q_m. Here, *VV* and *VH* geometries correspond to the vertical-vertical (VV) and vertical-horizontal (VH) polarizations of incident and scattered light respectively. For both the samples S1 and S2, the ratio, $I_{VV}(q_m)/I_{VH}(q_m)$ at melting temperature is found to be greater than 100. Also, we have not observed significant reduction in the coherence factor. These observations suggest that multiple scattering is not significant in our samples. As discussed in Chapter 1, PNIPAM microgel particles in the swollen state (*i.e.* below VPT) are closely matched in their refractive index with that of solvent (water) as they contain about 97% of water and rest polymer [5]. The close matching of refractive index of the particles with the solvent is responsible for negligible multiple scattering in sample S1 and S2 despite they are dense. Hence multiple scattering of light is ruled out as the cause for the observed low values of D_L/D_S at melting.

4.3.5 Effect of hydrodynamic interactions

In dense colloidal suspensions hydrodynamic interactions (HIs) i.e. interparticle interactions mediated via solvent velocity field, are known to affect the particle dynamics [11-12]. Dynamical criterion, when measured as D_L/D_0 in dense suspensions, was found to deviate from 0.1. But its validity was regained through hydrodynamic scaling, proposed by Medina-Noyola [13] and verified experimentally by van Blaaderen *et al.* [14], for hard sphere and charged colloidal systems. Thus, for HS and charged colloidal systems dynamical criterion is unaffected by the presence of HIs. Eckert and Richtering [15] have carried out DLS studies on concentrated PNIPAM microgel dispersions and determined the q-dependence of HIs and compared with hard sphere theory. At high concentrations and for q values greater than the first peak, the difference between theory and experiment was found to be small and attributed to the differences in particle structure of microgels versus hard spheres. Since the differences are small the ratio D_L/D_S is expected to remain unaffected by HIs. Hence we rule out HIs being responsible for D_L/D_S being less than 0.1 at melting in PNIPAM microgel suspensions.

4.3.6 Influence of entanglement of interparticle polymer chains on dynamics

As discussed in Chapter 1, the PNIPAM microgel particles have inhomogeneous intra-particle structure. Such inhomogeneous structure not only complicates the modeling of interparticle interactions but also the particle dynamics [6, 16]. Eckert and Richerting [15] have shown through DLS experiments that the short-time collective diffusion coefficient of PNIPAM particles in a liquid-like ordered suspension deviates considerably from that of hard-spheres in the low-q limit and was attributed to the structure of microgel surface (*i.e.* the fuzzy particle surface with dangling polymer chains).

In order to look at the effect of inhomogeneous structure of PNIPAM microgel particles on their dynamics in dense suspensions, we carefully analyzed the MSD of PNIPAM microgel crystals close to their melting transition in different time regimes (short, intermediate and long). Figure 4.5(a) shows MSD behavior of PNIPAM microgel particles at temperatures close to the melting transition of PNIPAM microgel crystals of samples S1 and S2. For the sake of comparison, the MSD of silica particle in shear melted colloidal liquid close to freezing is also shown in Fig. 4.5(a).

At long times ($t >> \tau_R$), we observe the usual diffusive behavior ($<\Delta r^2(t)> \propto t^{\alpha}$ with $\alpha = 1$ as shown in the Fig. 4.5(a)) with D_L as the long-time diffusion coefficient for all three samples (*i.e.* silica suspension and PNIPAM samples S1, S2). At intermediate times ($t \sim \tau_R$), behavior of MSD is subdiffusive, which is expected in the case of a liquid close to its freezing transition [17]. On the other hand, we observe an unusual behavior of MSD for samples S1 and S2 at short-times, which is shown as inset in Fig. 4.5(a). Notice that in silica suspension the particle motion at short times is diffusive (i.e. $\alpha \sim 1$) but in the case of PNIPAM samples S1 and S2 it is subdiffusive ($\alpha < 1$) at short-times and the value of α depends on the volume fraction (*i.e.* 0.8 for sample S1 and 0.6 for sample S2). The subdiffusive short time dynamics have been reported in colloidal suspensions with attractive interparticle interactions [18-19] where particles are bound to each other, whereas in the same systems when interparticle interactions are repulsive, short time dynamics was found to be diffusive [18-19]. Joris Sprakel *et al.* [20] have shown that the short time dynamics of the colloidal particle dispersed in polymer gel matrix is diffusive when colloidal particle is unbound to the gel network and changes to subdiffusive when the particle is attached to the polymer network. Above reports suggest that colloidal particles exhibit subdiffusive short time dynamics when particles are bound to a network.

Thus observation of subdiffusive dynamics at short time in dense PNIPAM microgel suspensions close to its melting/freezing transition indicates existence of binding between the particles. In case of PNIPAM microgel suspensions, interparticle interactions at temperatures below VPT are known to be soft repulsive [21-22]. Thus there is no attraction between PNIPAM microgel particles that can lead to binding. Binding between microgel particles can arise due to core-shell structure of PNIPAM microgel particles (Fig. 1.4(b)). In dense suspensions (sample S1 and S2), where interparticle separations are of the order of particle diameter (almost touching configuration), dangling polymer chains from the shells of neighboring microgel particles can overlap and get entangled. The entanglement of dangling polymer chains can bind neighbouring PNIPAM microgel particles and lead to subdiffusive behavior of MSD at short times. At short times, microgel particle moves within the cage formed by neighboring particles over distances comparable to the thickness of the shell (~30 nm) of the microgel particle. Schematics depicting the entanglement of dangling polymer chains of neighboring PNIPAM microgel particles in samples S1 and S2 are shown in Fig. 4.5 (b) &(c) respectively. We believe that the observation of subdiffusive behavior at short-times in our samples S1 and S2 constitutes a strong evidence for the entanglement of dangling polymer chains. It may be mentioned here that all earlier studies reporting the self-diffusion of particles at short and long-times in liquid-like ordered colloidal suspensions (hard-sphere as well as charged spheres) is always diffusive and subdiffusive behavior was reported only in super cooled liquids at intermediate time scales [23-24]. Thus the present observation of subdiffusive dynamics at short-times in dense liquid like ordered suspensions of PNIPAM microgel particles is first of its kind and is attributed to the overlapping/entanglement (shown schematically in Fig 4.5(b) & (c)) of dangling chains between neighboring particles. Since Sample S2 is more concentrated than sample S1, the extent of overlapping is expected to be more in sample S2 than in sample S1, hence the particle motion becomes much more subdiffusive (more hindered) clearly reflecting in lower value of α (= 0.6) for sample S2 as compared to that (α = 0.8) for sample S1.

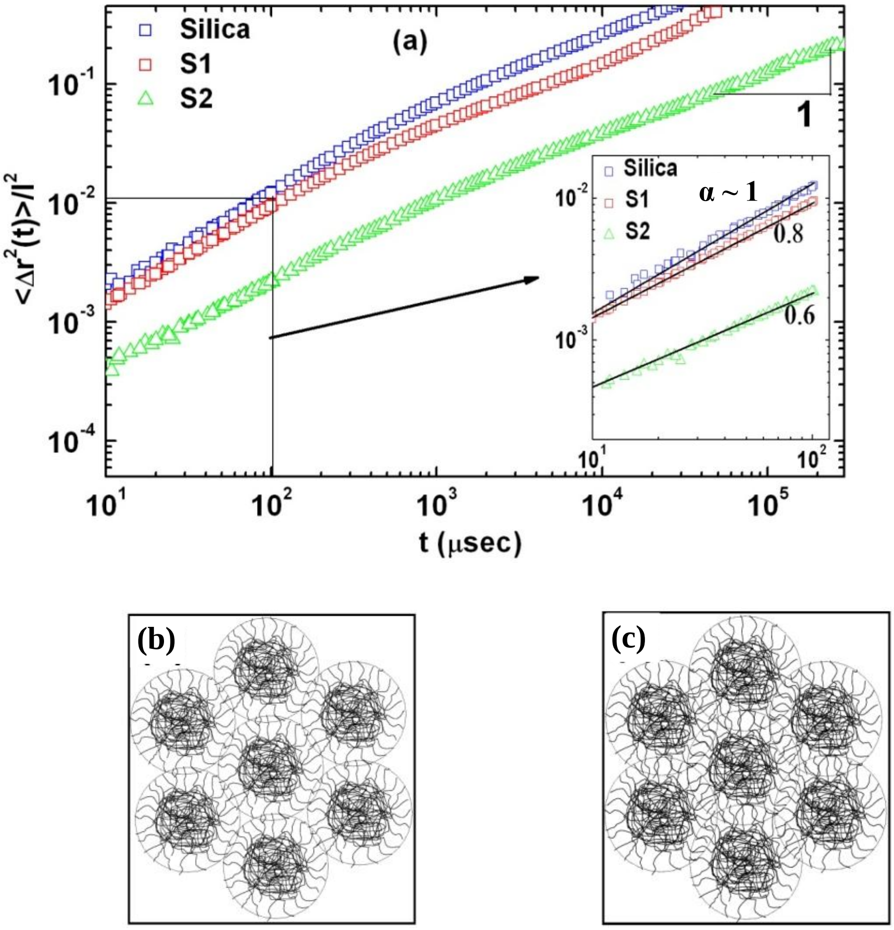

Fig. 4.5. (a) MSD *vs* *t* close to the melting transition of sample S1 and S2 and close to freezing of shear melted silica suspension. Inset in (a): MSD at shorter times; Continuous lines are fits of MSD to t^{α}. Schematic representation of PNIPAM microgel particles depicting the overlapping /entanglement of dangling polymer chains of neighboring PNIPAM particles with less overlap in sample S1(b) and more overlap in sample S2(c).

The assumption that particle dynamics in sample S1 and S2 is diffusive at short-times, leads to the over estimation of D_s. The over estimation of D_S is the cause for the ratio D_L/D_S being low (< 0.1) for samples S1 and S2 at melting (Fig. 4.2(b)). The dynamical criterion of freezing proposed by Löwen *et al.* [4] is for the colloidal liquids where the particles undergo diffusive motion at short as well as at long times. The short-time diffusion sets a suitable scale for the long-time diffusion that a general dynamical freezing criterion holds. Since the short time motion of the particles in dense PNIPAM microgel liquids close to melting/freezing is subdiffusive, there is no suitable scale for D_L.

4.4 Summary

We have prepared PNIPAM microgel crystals with two different volume fractions by synthesizing monodisperse PNIPAM microgel particles with two different diameters. The melting point of these crystals (*i.e.* the temperature at which PNIPAM crystals undergo a transition to a liquid-like order) is identified by monitoring the Bragg peak intensity as function of temperature. We have carried out detailed dynamic light scattering studies on these PNIPAM microgel crystals at different temperatures across melting. We found that the value of the ratio of short-time diffusion coefficient to long-time diffusion coefficient, D_L/D_S at melting is considerably lower than the dynamical criterion of 0.1 reported by Löwen *et al.* for hard-sphere and charged colloidal liquids undergoing freezing. By performing DLS experiments on dilute multiple scattering free shear melted suspension of charged silica particles and depolarized light scattering measurement on PNIPAM suspensions, we ruled out experimental artifacts and multiple scattering of light being the reasons for the observed low values of D_L/D_S in PNIPAM microgel crystals at melting. From the reported experimental and theoretical results on hydrodynamic interactions in hard sphere and PNIPAM suspensions, we argued that hydrodynamic interactions are not responsible for the observed low value of D_L/D_S. Careful analysis of MSD data at short-time and long-times of PNIPAM samples S1, S2 and comparison with that measured on shear melted silica suspension close to freezing have revealed for the first time that short-time dynamics of PNIPAM microgel particles in dense PNIPAM microgel suspensions is subdiffusive and differs from the short time dynamics of hard-sphere and charged colloids. The low values of D_L/D_S at melting and the subdiffusive behavior observed at short times is explained using the core-shell nature of PNIPAM particles. The subdiffusive behavior arises due to the overlapping of dangling chains belonging to the fuzzy shell of neighboring PNIPAM particles. The low value of D_L/D_S is the result of an overestimated D_S from the short-time MSD data. Hence the low values of D_L/D_S measured at the melting point of PNIPAM crystals should not be considered as an evidence for the violation of dynamical freezing rule in colloidal liquids undergoing freezing. However core-shell microgel particles constitute yet another model colloidal system with interesting dynamics. We believe that the present results motivate further experimental and theoretical studies probing the entanglement effect in PNIPAM microgel suspensions, influence of inhomogeneous soft particles with solvent penetrable surfaces on interactions, structure and dynamics of dense suspensions.

References

1. F. A. Lindemann, Physik. Z. 11, (1910) 609.
2. J. P. Hansen and L. Verlet, Phys. Rev. 184, (1969) 151.
3. P. Holmqvist and G. Nägele, Phys. Rev. Lett 104, (2010) 058301 .
4. H. Löwen, T. Palberg, and R. Simon, Phys. Rev. Lett. 70, (1993) 1557-1560.
5. B. R. Saunders, Langmuir 20, (2004) 3925-3932.

6. M. Stieger, W. Richtering, J. S. Pedersen, and P. Lindner, J. Chem. Phys. 120, (2004) 6197 -6206.

7. J. Brijitta, B. V. R. Tata, R. G. Joshi and T. Kaliyappan, J. Chem. Phys. 131, (2009) 074904.

8. B.J. Frisken, Applied Optics 40, (2001) 4087-4091.

9. B.V.R. Tata, P.S. Mohanty, M.C. Valsakumar, and J. Yamanaka, Phys. Rev. Lett. 93, (2004) 268303.

10. F. Grüner and W. Lehmann, J. Phys. A: Math. Gen. 13, (1980) 2155-2170.

11. P. Mazur and U. Geigenmüller, Physica A 146, (1987) 657-661.

12. M. Tokuyama, H. Yamazakib, and Y. Terada, Physica A 328, (2003) 367 -379.

13. M. Medina-Noyola, Phys. Rev. Lett. 60, (1988) 2705-2708.

14. A. van Blaaderen, J. Peetermans, G. Mat-et and J. K. G. Dhont, J. Chem. Phys. 96, (1992) 4591-4603.

15. T. Eckert and W. Richtering, J. Chem. Phys. 129, (2008) 124902.

16. F. Scheffold, P. Dı´az-Leyva, M. Reufer, N.B. Braham, I. Lynch, and J.L. Harden, Phys. Rev. Lett. 104, (2010) 128304.

17. A. V. Indrani and S. Ramaswamy, Phys. Rev. Lett. 73, (1994) 360-363.

18. S. Romer, C. Urban, H. Bissig, A. Stradner, F. Scheffold and P. Schurtenberger, Phil. Trans. R. Soc. Lond. A 359, (2001) 977-984.

19. E. Zaccarellia and W.C. K. Poon, PNAS , (2009).

20. J. Sprakel, J. van der Gucht, M. A. Cohen Stuart, and N. A. M. Besseling, Phys. Rev. Lett. 99, (2007) 208301.

21. J. Wu, B. Zhou and Z. Hu, Phys. Rev. Lett. 90, (2003) 048304.

22. H. Senff and W. Richtering, J. chem.. phys. 111, (1999) 1705-1711.

23. B. V. R. Tata, P. S. Mohanty and M. C. Valsakumar, Phys. Rev. Lett. 88, (2001) 018302.

24. W. van Megen and G. Bryant, Phys. Rev. E 76, (2007) 021402.

CHAPTER 5

DYNAMICS AND YIELDING BEHAVIOR OF DENSE PNIPAM MICROGEL GLASSES

5.1 Introduction

Glass is a disordered solid which is obtained by quenching or compressing the liquid within time smaller than the intrinsic structural relaxation time of the liquid [1-2]. Structural relaxation times in atomic systems are very small (~ 10^{-12} sec), hence these systems need very fast quenching rates and are difficult to probe directly. On the other hand, colloidal systems have slow relaxation times (~ 10^{-6} sec - 10^{3} sec) and hence accessible to dynamic light scattering technique to probe the dynamics in real time [3]. Colloidal suspensions of monodisperse hard sphere particles undergo glass transition at $\phi = 0.57$ [4-5]. Upon glass transition, structure of liquid remains almost same, whereas dynamics at longer time slows down drastically [5-6]. Slowing down of the particle dynamics at long times in hard sphere suspensions, on approaching the glass transition, is understood to occur due to kinetic arrest of the particles within cages formed by neighboring particles [5]. The particles start experiencing the effect of cage in a supercooled liquid state, even before it turns into the glass. The motion of a particle in the supercooled liquid state is diffusive at short times, becomes subdiffusive at intermediate times (due to cage effect) and again diffusive at long times (due to escape of the particle from the cage of neighbouring particles, the behavior of mean square displacement (MSD) of the particle is shown in Fig. 1.6(a)-3). Thus, the structural relaxation in the super cooled liquid occurs in two steps. The first step occur at short times (due to intra-cage dynamics of the particle) which is known as fast or beta relaxation and another at long times (due escape of the particles from the cages) is known as slow or alpha relaxation. On approaching the glass transition (*i.e.* with increase in ϕ), the cages from near neighbour particles becomes more and more rigid resulting into increase in alpha relaxation time (*i.e.* the suppression of long time diffusion of the particles). While alpha relaxation (long time dynamics) of hard sphere colloidal particles in the glassy state is ceased out, beta relaxation (short time dynamics) continues to exist with diffusive particle motion at short times [5].

Unlike hard spheres, PNIPAM microgels are soft particles having a dense core and a thin shell of polymer chains [7-8]. It is shown in Chapter 3 that, PNIPAM microgel particles undergo osmotic deswelling in dense suspensions with crystalline order of particles. Here, we report that the dense suspensions of PNIPAM microgels exhibit a glassy state with a reduction in the particle size upon osmotic compression. We also report here for the first time, subdiffusive dynamics at short times in the glassy state as well in the supercooled liquid state of microgel suspensions. Subdiffusive dynamics in the glasses and the super cooled liquids is argued to arise due to entanglement of dangling polymer chains of neighboring particles, similar to that reported in PNIPAM microgel crystals, discussed in Chapter 4.

Colloidal glasses are viscoelastic in nature and yield under application of the large shear [9]. The yielding behaviour of colloidal glasses has been found to depend on the interparticle interactions [10-11]. While the hard sphere colloidal glass has been found to yield in one step (Fig. 1.7) [10], attractive colloidal glasses have been found to yield in two steps (Fig. 1.9) [11]. In dense PNIPAM microgel glasses, interparticle interactions are soft repulsive [12] and there exists entanglements of dangling polymer chains between neighbouring particles (evidenced by short time subdiffusive dynamics). With an aim to know that how the soft repulsive glass with entangled polymer chains will respond to the applied shear, yielding behavior of dense PNIPAM microgel glasses has been studied by performing non-linear rheological measurements.

Results of non-linear rheological measurements are discussed in this chapter. Rheological measurements have revealed that dense PNIPAM microgel glasses yield in two steps (exhibiting two peaks in G'') in contrast to one step yielding observed in hard sphere glasses. Two step yielding behaviour is explained in terms of breaking of the bonds (entanglements) and breaking of near neighbour cage, similar to that in attractive glasses [11]. We also studied the effect of temperature on yielding behaviour. Two step yielding behaviour (two peaks in G'') of PNIPAM microgel glasses is found to transform into one step (one peak in G'') in supercooled liquid state upon increasing temperature and finally, in the liquid state, no peak in G'' is observed. Two step yielding of PNIPAM microgel glasses is also found to depend on the shear rate / oscillation frequency at which measurements are performed. Results of investigations on the shear rate dependence of yielding behaviour of dense PNIPAM microgel glasses are also discussed in this chapter.

5.2 Experimental details

PNIPAM microgel particles having d_h = 560 nm and SPD = 6% at 25 °C were used to prepare glasses used for this study. Here, particles of larger diameter (560 nm), as compared to previous studies (discussed in Chapter 3 and Chapter 4) were used, in order to tune the first peak of the structure factor within the q range of 0.68×10^5 cm^{-1} to 2.54×10^5 cm^{-1} of our DLS set up. The large sized particles of PNIPAM microgels have been synthesized using the procedure as described in Chapter 2, but without the addition of the surfactant and crosslinker during the synthesis. Dense PNIPAM microgel glasses having particle concentrations of 6.2×10^{12} cm^{-3} and 7.8×10^{12} cm^{-3} (determined using SLS) and labelled as S1 and S2, respectively have been used for the investigations. The ϕ values estimated using d_h (measured using DLS under dilute conditions) are found to be 0.7 and 0.9, respectively for samples S1 and S2. At such a high values of ϕ, particle dynamics is expected to be slow due to kinetic arrest of particle within the cages formed by neighbouring particles, leading to a glassy state [5]. Kinetic arrest of the particles prevents crystallization of these suspensions, despite their SPD is low (6%) [4].

Since PNIPAM microgel particle's size used for the present study is twice than that used for investigating dynamics across melting (Chapter 4), the scattering ability of these particles is quite high even below VPT (moderate turbidity as seen in Fig. 5.1(a)). With increase in temperature, suspensions become much more turbid (Fig. 5.1(b)), due to deswelling of the particles leading to increase in the polymer content within the particle [7].

Fig 5.1 Photographs of dense PNIPAM microgel suspension (Sample S1) showing (a) moderate turbidity at 20 °C and (b) high turbidity at 31 °C.

In turbid suspensions, multiple scattering of light restricts the use of conventional static light scattering (SLS) and Dynamic light scattering (DLS) techniques for characterization of their structure and dynamics [13]. We have employed cross-correlation based light scattering techniques (3D DLS and SLS) for investigating the dynamics and structure in samples S1 and S2. As discussed in section 2.1.5, in 3D DLS experiments, two simultaneous light scattering experiments at identical scattering wave vectors are performed on the same scattering volume, but with detectors at different spatial positions. Under these conditions, when one correlates the intensities, only singly scattered photon contributes to the correlation function. The uncorrelated multiply scattered light reduces the intercept of the correlation function. Thus, 3D DLS helps in probing the structure and dynamics when samples are turbid. 3D DLS and SLS measurements have been carried out on samples S1 and S2 placed in cylindrical glass cells with 8 mm path length. Details of the experimental set up, operation principle and analysis method are given in Chapter 2. Ensemble averaged intensity, $<I(q)>_E$ of the scattered light have been measured by rotating the sample cells about their cylindrical axis, at the speed of 1 rotation/ 90 sec. At each q, $<I(q)>_E$ is collected for 270 sec in a single run. The $<I(q)>_E$ from three such runs are found to be identical. Time averaged intensity cross-correlation, $g_{12}^{(2)}(q,t)$ have been measured at a sample location for 120 minutes in the glassy state of the samples and for 20 minutes in the liquid state of samples. At each temperature, results are obtained by averaging three such measurements. Ensemble averaged $f(q,t)$ has been obtained from the time averaged $g_{12}^{(2)}(q,t)$ by performing the non-ergodic analysis, which is discussed in the section 2.1.6.

Rheological measurements have been carried out using MCR 301 rheometer with a cone and plate geometry. Instrument and measurement details are described in Chapter 2. Upon loading the sample on the rheometer cell, the open area of the cell was sealed with silicon oil (viscosity ~ 99 cp) for preventing the evaporation of water during the measurements. Before performing the experiment, it is necessary to remove the shear history from the loaded sample, which it possesses due to the shear experienced by the sample while loading on the rheometer cell. To remove the shear history, temperature of the sample was raised well above the melting temperature of the glasses and then cooled back to the measurement temperature.

5.3 Static and dynamic light scattering results

5.3.1 Characterization of structural ordering in dense PNIPAM microgel suspensions

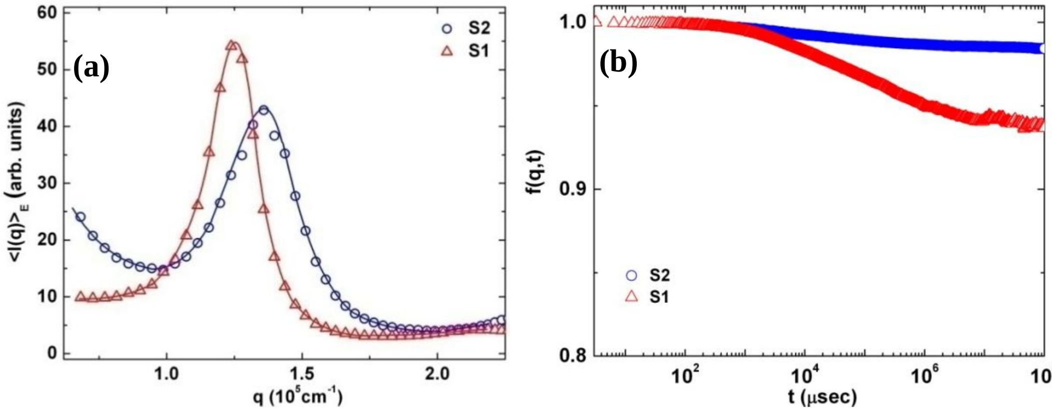

Fig. 5.2. Characterization of structural ordering and dynamics in samples S1 and S2. (a) ensemble averaged scattered intensity, $<I(q)>_E$ versus q, and (b) ensemble averaged $f(q,t)$ versus t, for samples S1 and S2 measured at 20 °C. Lines drawn are guide to the eye.

Samples S1 and S2 did not show iridescence when left undisturbed for several days. Structural ordering and dynamics in the dense samples have been investigated by performing static and dynamic light scattering measurements using 3D DLS setup. For both samples S1 and S2, time averaged and ensemble averaged intensities of the scattered light (measured at a given q) are found to differ from each other, indicating non-ergodic nature of the samples. Figure 5.2(a) shows the ensemble averaged intensity of the scattered light, $<I(q)>_E$ for samples S1 and S2 at 20 °C. For both the samples, $<I(q)>_E$ shows broad peak, suggesting that the samples are disordered. In order to characterize that whether the disorder is liquid-like or glass-like, ensemble averaged dynamic structure factor, $f(q,t)$ have been measured and is shown in Fig. 5.2(b). It can be seen that $f(q,t)$ shows non-decaying behavior, suggesting the dynamical arrest of microgel particles in samples S1 and S2. The non-decaying $f(q,t)$, with broad peak in $<I(q)>_E$, suggest that both the samples are in the glassy state at

20 °C. The volume fraction of samples S1 and S2 in their glassy state has been estimated using relation $\phi = n_p \pi d_h^3/6$ and found to be 0.70 and 0.90, respectively. Here n_p is the particle number density and is related to the position of first peak position, q_m in $<I(q)>_E$ as $n_p = \left(4/3\sqrt{3}\right)(q_m/2\pi)^3$ for fcc-like ordering. These volume fractions are greater than random closed packing fraction of hard spheres (ϕ = 0.64), suggesting that PNIPAM microgel particles have undergone osmotic compression, similar to that observed by us in dense PNIPAM microgel crystals (discussed in Chapter 3).

5.3.2 Identification of the glass transition

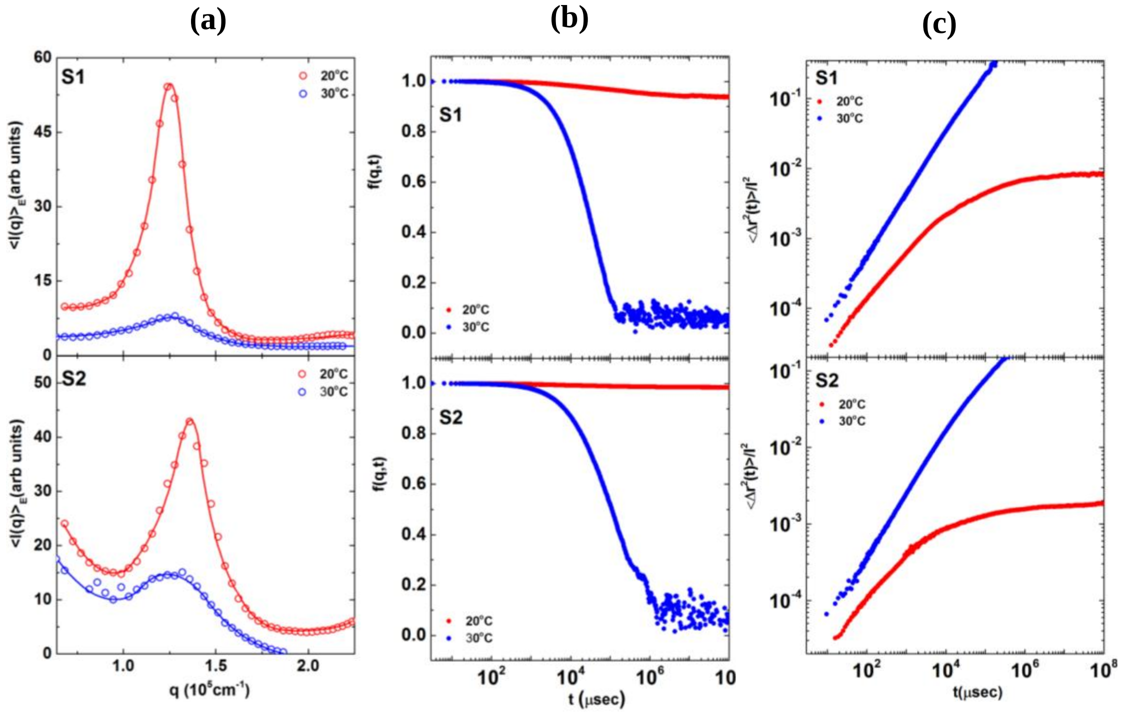

Fig. 5.3 (a) $<I(q)>_E$ vs. q, (b) $f(q,t)$ vs. t and (c) Mean square displacement of PNIPAM microgel particles, in units of average interparticle spacing (l), $<\Delta r^2(t)>/l^2$, measured at 20 °C and 30 °C for samples S1 and S2. Lines drawn are guide to the eye.

Upon increasing the temperature, dense PNIPAM microgel suspensions are expected to transform from the glassy state into a liquid like state, due to decrease in the size of PNIPAM microgel particles and hence, ϕ of the suspension. The $<I(q)>_E$

measured at 20 °C and 30 °C for samples S1 as well as S2 are shown in Fig. 5.3(a). At both the temperatures, samples S1 and S2 show broad peaks indicating the presence of disorder. $f(q,t)$ for the samples, at 20 °C and 30 °C, are shown in Fig. 5.3(b). At 20 °C, $f(q,t)$ for both samples is non-decaying, whereas it decays to zero at 30 °C, indicating the transfer of microgel glass at 20 °C into microgel liquid at 30 °C. Mean square displacement (MSD) in units of the average interparticle separation (l), $<\Delta r^2(t)>/l^2$, (obtained from corresponding $f(q,t)$using Eq. 2.24) at 20 °C and 30 °C for samples S1 and S2 is shown in Fig. 5.3(c). At 20 °C (in the glassy state) MSD shows tendency towards saturation at long times whereas at 30 °C (in the liquid state) it is observed to increase with time, t. Since both the glass and the liquid are disordered structures, while undergoing from the glass to liquid transition, MSD is not expected to show a sharp discontinuity as observed for crystal to liquid transition [14]. MSD (monitored across the glass to liquid transition at a constant time in the long time regime) have been used to identify the glass transition [14], where it shows a change in the slope at the glass transition.

With an aim to identify the glass transition temperature, T_g for samples S1 and S2, detailed 3D DLS and SLS measurements as a function of temperature have been carried out. The MSD at constant delay time of t = 0.15 sec (a time in the long time regime) as a function of temperature for samples S1 and S2 is shown in Fig. 5.4 (upper panel). The MSD increases with increase in temperature exhibiting a change in the slope at ~ 25 °C for sample S1 and at ~ 26 °C for sample S2. The temperature at which change in slope occurs is identified as the glass transition temperature. Identification of the glass transition has also been reported in the literature through the structural studies, where the ratio g_{min}/g_{max} (known as Wendt-Abraham parameter) or its Fourier analogue S_{min}/S_{max} have shown to exhibit a change in the slope at glass transition [15-16]. Here, g_{min} (S_{min}) and g_{max} (S_{max}) represents the minimum in the pair correlation function, *g(r)* (structure factor, *S(q)*) at higher *q* side near the first peak and the maximum value of the first peak in *g(r)*/*S(q)*, respectively. Though we have monitored the $<I(q)>_E$ as a function of temperature across the glass transition (Fig. 5.3(a)), which is related to the *S(q)* via form factor *P(q)* as $\langle I(q)\rangle_E = AP(q)S(q)$ with *A* being a constant (Eq. (2.9)), difficulty in determination of proper *P(q)* of PNIPAM microgel particles in dense suspensions (due to their soft and core-shell nature) restricts the estimation of *S(q)* from $<I(q)>_E$.

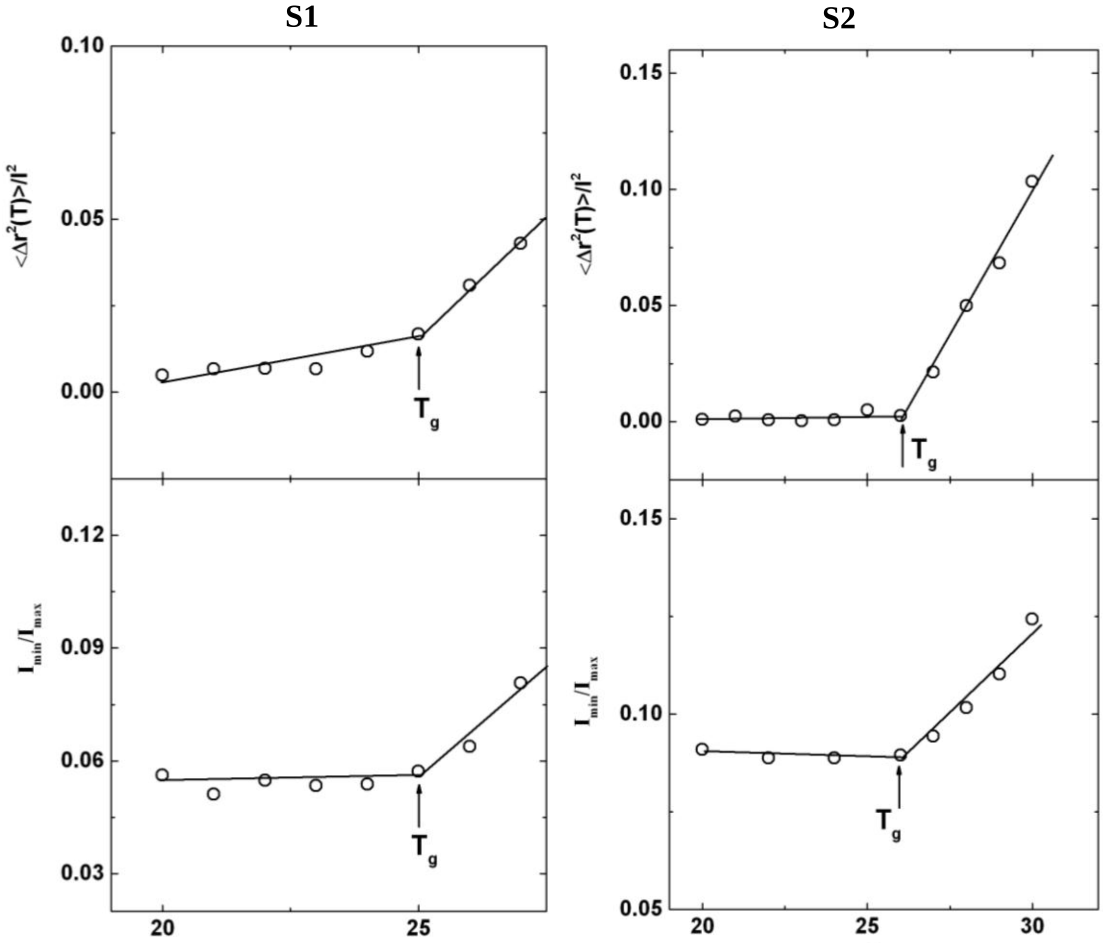

Fig. 5.4 Identification of the glass transition: Upper panel; MSD as a function of temperature, *T* (at the time of 0.15 sec) for samples S1 and S2. Lower panel; The ratio I_{min}/I_{max} as a function of temperature, *T*. Lines drawn are guide to the eye. Arrows indicate the glass transition with corresponding temperature T_g.

The ratio I_{min}/I_{max}, with I_{min} and I_{max} being the minimum in intensity at higher q side near the first peak and the maximum intensity of the first peak in $<I(q)>_E$ respectively, monitored as a function of temperature for samples S1 and S2 is shown in the Fig. 5.4 (lower panel). The ratio I_{min}/I_{max} is also found show a change in the slope at the glass transition, though it is not a proper quantity to be monitored.

5.3.3 Subdiffusive dynamics at short times in dense PNIPAM microgel glasses

Upon identification of the glass transition, we have performed the analysis of MSD at the short time and the long time regime with the power law behavior ($<\Delta r^2(t)> \propto t^\alpha$). The short time ($t << \tau_R$) and the long time ($t >> \tau_R$) regimes are identified with the reference to $\tau_R = d_h^2/4D_0$. τ_R has been estimated by using d_h and D_0 of PNIPAM microgel particles at the corresponding temperatures. MSD shows saturation tendency in the glassy state and increases with time for temperatures higher than glass transition temperature (as shown in Fig. 5.5). Analysis of the MSD at long times, for temperatures above the glass transition, suggested that it exhibits diffusive behavior (α =1), similar to that observed in hard sphere colloidal glasses [5].

At short times, MSD above as well as below T_g is observed to increase with increase in time (Fig. 5.5). Interestingly, the value of α in the glassy state of samples, determined from the short time MSD, is found to be lesser than the unity (α = 0.67 for sample S1 and α = 0.62 for sample S2), indicating the subdiffusive dynamics of PNIPAM microgel glasses at short times. In the case of hard sphere glasses, short time dynamics is observed to be diffusive (α = 1) [5], whereas we observe it to be subdiffusive for dense PNIPAM microgel glasses. Similar kind of subdiffusive dynamics at short time have been observed in dense PNIPAM microgel liquids close to their crystallization (as discussed in Chapter 4) and is understood to occur due to the overlap / entanglement of dangling polymer chains of neighboring microgel particles. The subdiffusive dynamics of PNIPAM microgel particles indicate that entanglements of dangling polymer chains also exist in the glassy state of the dense suspensions. The smaller value of α (= 0.62) for sample S2 than that for sample S1 (α = 0.67) is as expected, since sample S2 (ϕ = 0.90) is expected to have more number of entanglements than sample S1 (ϕ = 0.70) due to its high volume fraction.

With increase in temperature, PNIPAM microgel particles shrink in size and their kinetic energy also increases, which could result into decrease in the overlap/entanglement of the dangling polymer chains between neighbouring particles. Thus, one expects a change of subdiffusive behavior ($\alpha < 1$) of short time MSD at 20 °C (glassy state) to diffusive type ($\alpha = 1$) at temperatures above glass transition. Variation of α, from short time MSD of samples S1 and S2, as a function of temperature is shown in Fig. 5.6(a). Upon increasing the temperature, value of α (from the short time MSD) is indeed observed to rise gradually and tend towards the unity at temperatures close to VPT, suggesting the decrease in overlap/entanglement of dangling polymer chains between neighbouring particles with increase in temperature. The value $\alpha < 1$ for temperatures above the glass transition, suggests the presence of entanglement of dangling polymer chains between neighbouring particles even in the liquid state. $\alpha \sim 1$ at temperatures close to VPT indicates complete disentanglement of dangling polymer chains. At the glass transition, α is found exhibit a change in the slope (Fig. 5.6(a)), suggesting that α can also be used as a parameter to identify the glass transition. Schematics depicting the strong entanglements of dangling polymer chains at temperature well below glass transition (*i.e.* indicated by I in Fig. 5.6(a)) and disentanglement of dangling polymer chains at temperature close to VPT (indicated by II in Fig. 5.6(a)) are shown in Fig. 5.6(b) and (c), respectively.

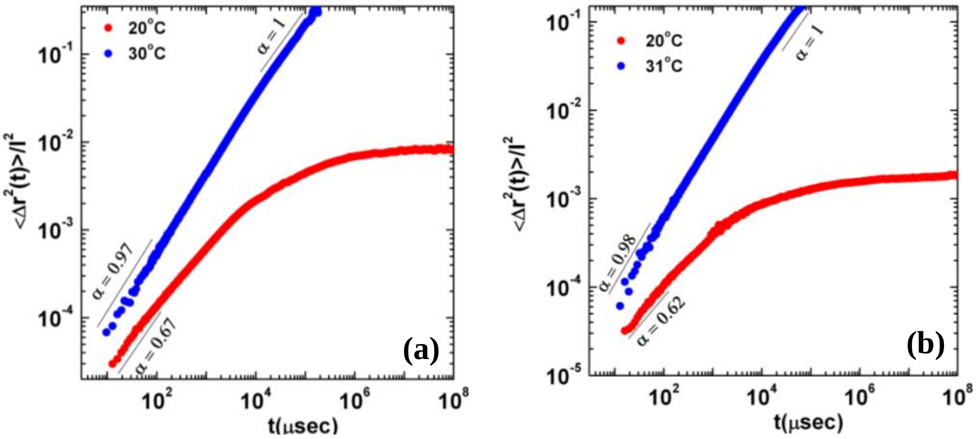

Fig. 5.5 Mean square displacement ($<\Delta r^2(t)>$) expressed in units of average interparticle spacing (l), $<\Delta r^2(t)>/l^2$, for (a) sample S1 and (b) sample S2 in their glassy and liquid states. Values of α, indicated on the MSD curves, are determined from the power law fit of the MSD data ($<\Delta r^2(t)> \propto t^{\alpha}$) over a time range indicated by continuous lines.

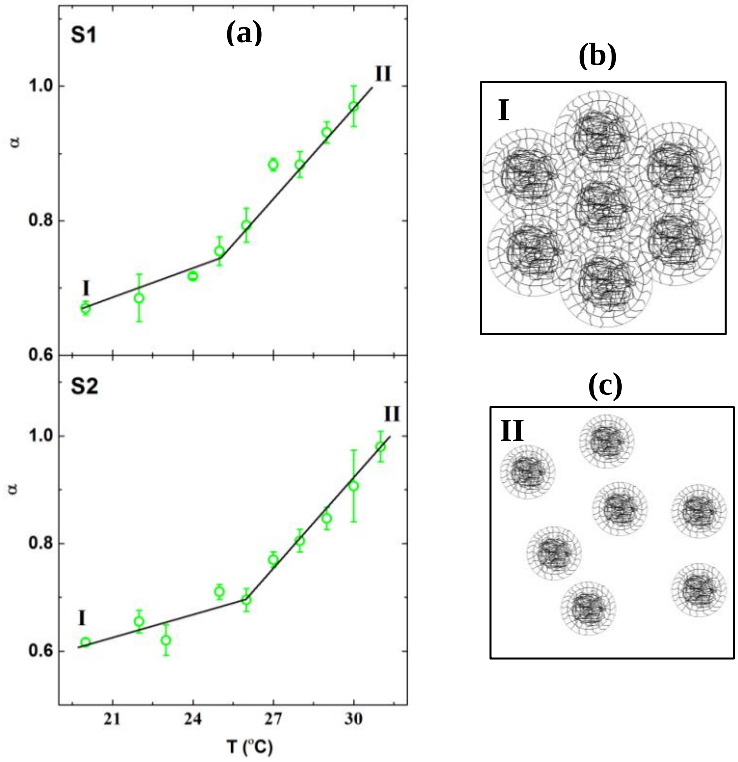

Fig. 5.6 (a) variation of α (obtained from short time MSD) as a function of temperature, T for samples S1 and S2, (b) Schematic depicting the strong entanglements of dangling polymer chains at temperature well below glass transition (*i.e.* deep inside the glassy state indicated by I in (a)) and (c) Schematic depicting the disentanglement of dangling polymer chains at temperature close to the VPT (indicated by II in Fig. 5.6(a)). Lines drawn are guide to the eye.

5.4 Yielding behaviour of PNIPAM microgel glasses

As discussed in Chapter 1, hard sphere colloidal glasses are known to yield in one step, whereas attractive glasses show two step yielding under the application of shear, thus yielding behaviour of colloidal glasses depends on the nature of interparticle interactions. In PNIPAM microgel glasses, interparticle interactions are soft repulsive [12] and also there exists entanglement of dangling polymer chains of neighbouring microgel particles under dense conditions. With an aim to know, how dense PNIPAM microgel glasses with soft repulsive interactions responds to the applied shear, yielding behaviour of samples S1 and S2 have been studied by subjecting them to oscillatory rheological measurements. To remove shear history, loaded samples are melted by heating beyond the glass transition temperature and cooled back to the measurement temperature. Immediately after cooling, G' and G'' have been measured as function of time under the application of small γ_o = 3%, at ω = 10 rad/sec, are shown in Fig. 5.7. Both samples (S1 and S2) have been found to recover rapidly after cooling. It can be seen from Fig. 5.7 that a waiting time of 900 sec is sufficient for performing each measurement to ensure complete recovery of the sample for obtaining reproducible results.

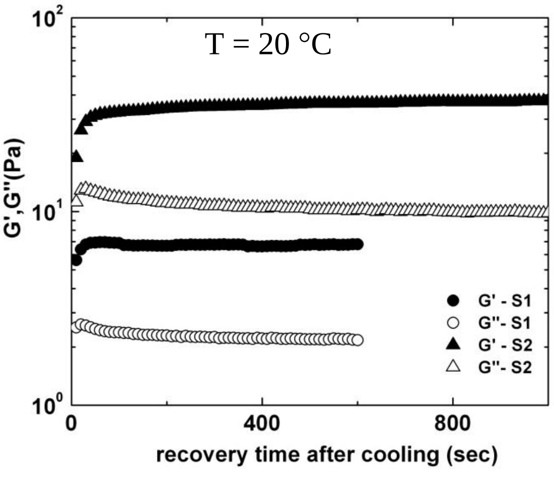

Fig. 5.7 Recovery of G' (solid symbols) and G'' (open symbols) measured at constant ω (10 rad/sec) and γ_o (3%), immediately after cooling the sample.

Dense colloidal suspensions can experience wall-slip due to particle-wall interactions [17-18]. Presence of the wall-slip can affect the flow behavior of dense microgel suspensions considerably [18]. In order to verify, whether the wall-slip is present or not in samples S1 and S2, measurements have been performed with and without attaching a sand paper (grit size 1000) to the measuring tool and to the measuring plate. Figure 5.8 shows dependence of shear stress, σ on shear rate, $\dot{\gamma}$ for measurements with and without the sand paper attached to the measuring tool and the measuring plate. The good overlap between the data obtained with and without sand paper suggests the absence of the wall slip in our samples (*i.e.* particle-wall interactions are negligible).

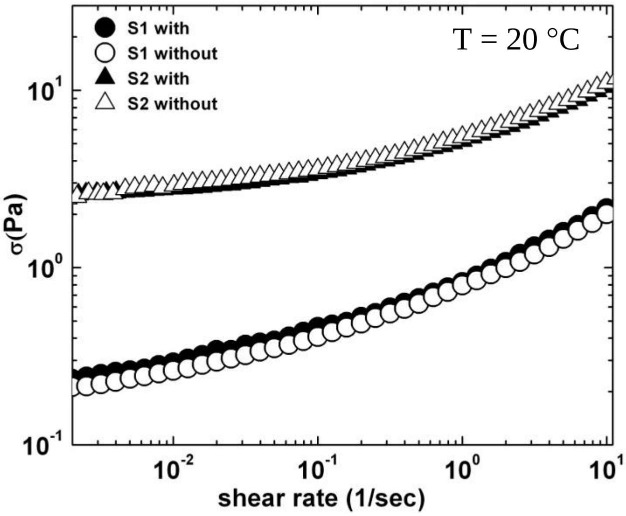

Fig. 5.8 Shear stress, σ versus applied shear rate, $\dot{\gamma}$ for samples S1 and S2 measured with and without the sand paper attached to the measuring tool and the measuring plate.

5.4.1 Linear viscoelasticity of dense PNIPAM microgel glasses

In the previous section on dynamics, it has been shown that the dynamics in dense PNIPAM microgel glasses at short times (*i.e.* intra-cage dynamics or beta relaxation behaviour) is subdiffusive. This observation constitutes evidence for the entanglement of dangling polymer chains between neighbouring particles.

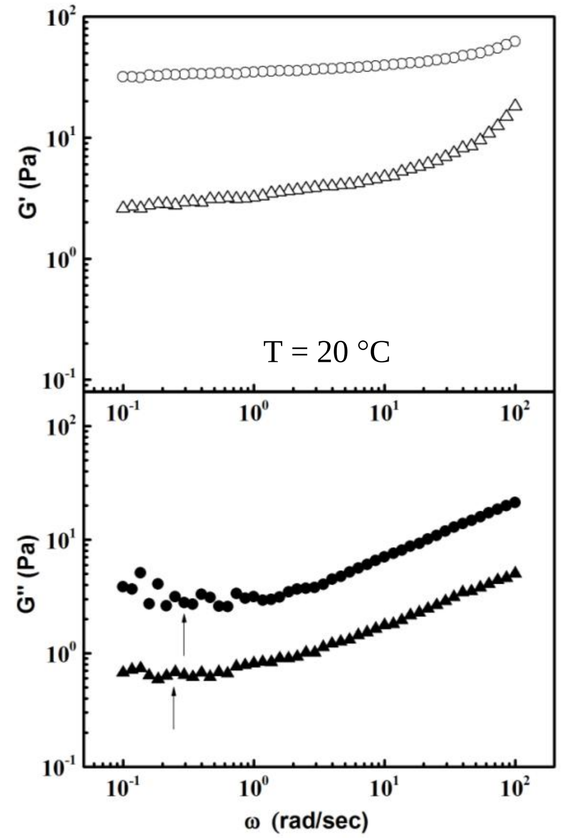

Fig. 5.9 Linear Viscoelastic behavior of samples S1 (triangles) and S2 (circles) in their glassy state (at 20 °C). Arrows indicate the approximate position of minimum in G'' and the corresponding ω represents ω_β.

As expected, the long time dynamics (alpha relaxation behavior) is diffusive and is unaffected by entanglements of dangling polymer chains between neighbouring particles. Once entanglements exist between neighboring particles in dense PNIPAM microgel glasses, their yielding behavior is expected to have the signature. Hence we subject samples S1 and S2 to non-linear rheological studies and results are discussed in sections below. As discussed in section 1.5, relaxation frequencies corresponding to the alpha and beta relaxations of colloidal glasses can be measured by performing the linear viscoelastic measurements. Alpha relaxation frequency, ω_α is identified with the peak in G'' on the lower frequency side and beta relaxation frequency, ω_β with the minimum in the G'' on the higher frequency side. For determining ω_β, linear viscoelastic response of PNIPAM microgel glasses of samples S1 and S2 have been studied. Towards this, G' and G'' have been measured by varying the ω between 0.1 to 100 rad/sec and applying small constant strain of amplitude γ_o = 2% (shown in Fig. 5.9). Notice in Fig. 5.9 that $G' > G''$, within the frequency range of 0.1 to 100 rad/sec, suggesting the solid-like nature of samples S1 and S2 at 20 °C. The minimum observed in G'' (shown with arrows) indicates ω_β for the samples [19]. The peak in G'', corresponding to alpha relaxation, falls out of the measurement window (0.1 to 100 rad/sec) due to very slow alpha relaxation process and hence is not visible. We have chosen ω = 10 rad/sec to study yielding behaviour of samples S1 and S2, which is well above their ω_β.

5.4.2 Non-linear rheological behaviour of dense PNIPAM microgel glasses

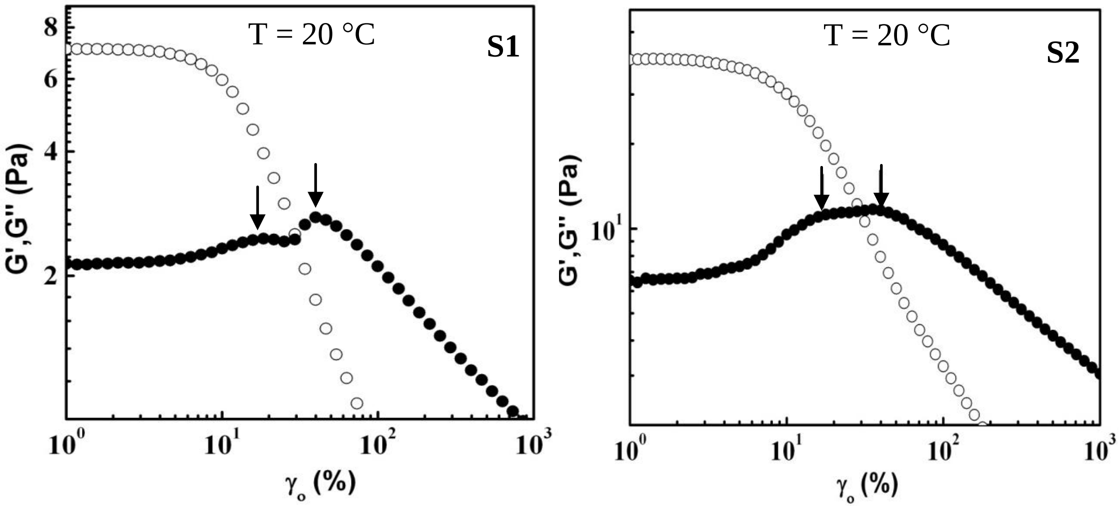

Fig. 5.10 Yielding behavior of samples S1 and S2 in their glassy state showing two step yielding. Measurements have been carried out with ω fixed at 10 rad/sec. Arrows indicate the peak positions. G' (open symbols) and G'' (solid symbols).

Samples S1 and S2, in their glassy state, have been subjected to the non-linear rheological measurements by performing dynamic strain sweep (DSS) measurements, where γ_o has been varied over a wide range (1-1000%) by keeping ω constant at 10 rad/sec. Figure 5.10 shows the variation of G' and G'' as a function of γ_o for samples S1 and S2. In order to probe the intra-cage dynamics and hence the effect of entanglement of dangling polymer chains on the yielding behavior, ω is fixed at 10 rad/sec, which is higher than ω_β ~ 0.25 rad/sec (Fig. 5.9). For lower values of γ_o, both G' and G'' exhibit a plateau indicating the region of γ_o over which PNIPAM microgel glasses show linear response to the applied γ_o. Notice that, in the plateau region, $G' > G''$, which suggests that the glasses behave as viscoelastic solid for low γ_o. For larger γ_o, G' comes down indicating the yielding of glasses under the applied shear. With increase in γ_o, G' further comes down and cross G''. The point at which G' cross G'' is defined as the yield point and the corresponding value of strain, γ_y and stress, σ_y is defined as yield strain and yield stress, respectively. Beyond the yield point, Samples S1 and S2 behaves like a viscoelastic liquid (*i.e.* $G' < G''$) due to the applied shear (shear melting) of the glasses. In the non-linear response regime, G' shows monotonic decrease with increase in γ_o. This behavior is similar to that of hard sphere glasses reported in the literature [10-11]. In contrast to hard sphere glasses [10-11], G'' shows two peaks (indicated by arrows in the Fig. 5.10) in dense PNIPAM microgel glasses. G'' exhibit two peaks at two values of γ_o, imply that two mechanisms are operational during the yielding of PNIPAM microgel glasses. This is the first observation of two step yielding in a dense PNIPAM microgel glass, where interactions are known to be soft repulsive [12].

Since PNIPAM microgel particles shrink in the size with increase in temperature, entanglements of dangling polymer chains between neighbouring particles are expected to come down. This is expected to reflect in the yielding behavior of samples S1 and

S2. We have investigated the effect of temperature on the yielding behavior of samples S1 and S2 by performing DSS measurements at various temperatures and results are shown in Fig. 5.11. For the sake of clarity, only *G″* behavior as a function of γ_o at different temperatures are shown in Fig. 5.11. Notice in sample S1, two step yielding at 20 °C (two peaks in *G″*) changes to one step yielding (single peak in *G″*) at 24 °C and no peak upon further heating to 29 °C. In the case of sample S2, single peak in *G″* is observed at higher temperature (27 °C) than that for S1 (24 °C) and no peak at 30 °C. These observations imply that upon shearing at elevated temperature, the entanglements between neighbours goes off leading to the appearance of single peak in *G″*, which is characteristic of most of the soft colloidal glasses. Upon further heating, the glass melt into a liquid which is evidenced by absence of peak in *G″*. For sample S2, single peak in *G″* appearing at higher temperature than that in sample S1 is also understandable as, S2 is more dense and hence disentanglements are expected to occur at higher temperature.

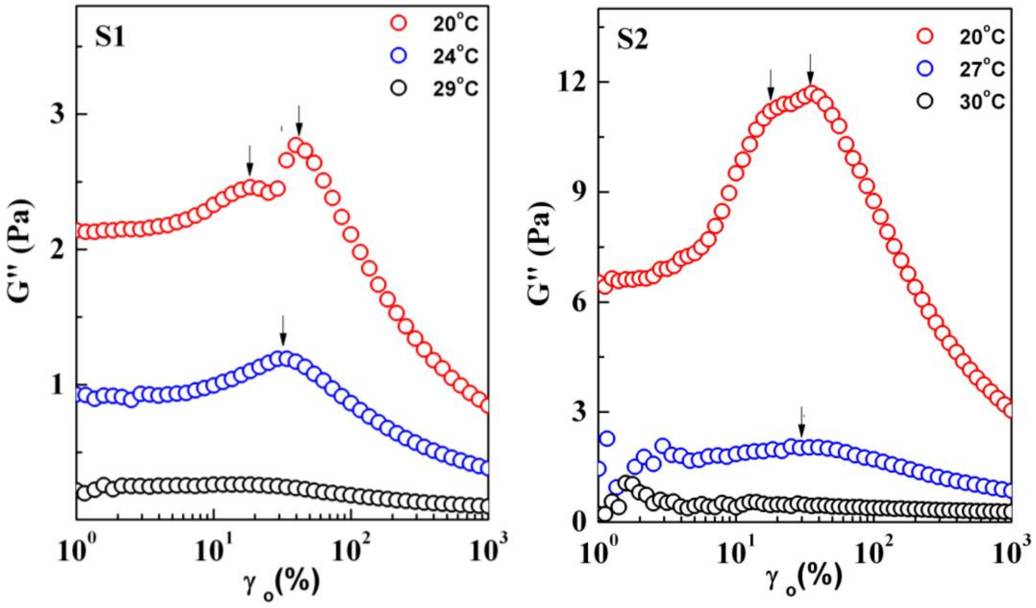

Fig.5.11. *G″* measured using DSS measurements at various *T* for samples S1 and S2. Arrows indicate the peak positions.

5.4.3 Understanding of two step yielding in dense PNIPAM microgel glasses

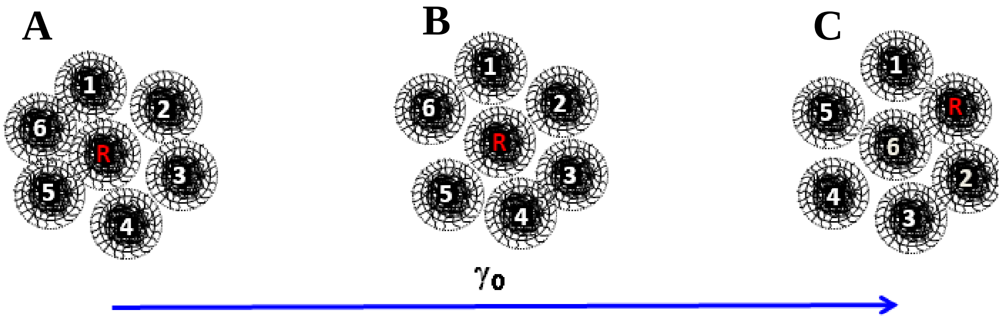

Fig.5.12 Schematic representation of the two step yielding process in dense PNIPAM microgel glasses. State A represents the undeformed state configuration of PNIPAM microgel glass with *R* as reference particle having entangled neighbors as 1,4,6,5 and topological neighbors 1-6. State B shows that, upon application of lower yield strain (γ_1), entanglements with 1,4,6,5 are broken leading to peak in G'' at γ_1. State C shows that, upon application of higher yield strain (γ_2), topological neighbors of *R* changes due to cage breaking, which leads to second peak in G'' at γ_2.

Two step yielding in the form of two peaks in G'' as a function of γ_o is reported by Pham *et al.* [11] in attractive glasses, prepared by introducing depletion attraction between hard spheres by the addition of a non-adsorbing polymer in dense hard sphere suspension. Pham *et al.* [11] have interpreted their observation of two step yielding (two peaks in G'') due to occurrence of two processes, i) breaking of the near-neighbor bonds arising from attractive interactions leading to the first peak in G'' to occur at low γ_o and ii) breaking of the cages (topological constraints arising from neighbouring particles) leading to the second peak in G'' to occur at larger γ_o. The two step yielding reported in our dense PNIPAM microgel glasses is explained by drawing an analogy with attractive glass [11]. With this analogy, the observed two step yielding (two peaks in G'' in Fig. 5.10) in PNIPAM microgel glasses is interpreted through two processes: i) breaking of entanglements of dangling polymer chains between neighbouring

PNIPAM microgel particles giving a peak in G'' at lower strain (γ_1) and ii) breaking of the near neighbor cages giving a peak in G'' at higher strain (γ_2). These two processes are schematically shown in Fig. 5.12. Configurations A, B and C describe changes in the environment of a reference particle *R*, with respect to its entangled neighbors and topological neighbors under the application of shear. In unsheared state (A), the reference particle *R* has topological neighbors (1 - 6) and entanglements neighbors (1, 4-6). When strain of increasing amplitude is applied, particles start moving in the direction of strain. At lower yield strain (γ_1), entanglements with its neighbours (1, 4-6) are broken (configuration B). This process of breaking of entanglements, while keeping the same topological neighbors, gives rise to first peak in G''. As γ_o is increased further to higher yield strain (γ_2), cages break with changes in topological neighbors (configuration C). This breaking of cages results in the second peak in G''.

5.4.4 Yield strains of dense PNIPAM microgel glasses and their frequency dependence

The yield strain values γ_1 and γ_2 for sample S1 at 20 °C are found to be 18% and 40% (Fig. 5.10), whereas those for sample S2 at 20 °C are found to be 20% and 35% (Fig. 5.10), respectively. The yield stress values σ_1 and σ_2 corresponding to γ_1 and γ_2 for sample S1 are found to be 1.1 and 2 Pa, whereas those for sample S2 are found to be 4.6 Pa and 6.2 Pa, respectively. With increase in ϕ, number of entanglements of dangling polymer chains are expected to increase due to increase in the overlap of dangling polymer chains, hence more energy is required to break entanglements in sample S2 than sample S1. The higher values of σ_1/σ_2 and $G''_{\gamma 1}/G''_{\gamma 2}$ for sample S2 than for sample S1 indicates that sample S2 has more number of entanglements than sample S1. Here $G''_{\gamma 1}$ and $G''_{\gamma 2}$ represent the peak amplitudes at γ_1 and γ_2, respectively.

Small increase in γ_1 and decrease in γ_2 for glassy state of sample S2 than that for sample S1 is understandable, because near neighbor separation in sample S2 is smaller than S1 due to its higher volume fraction. Due to decrease in γ_2 and increase in γ_1, peaks in G'' for sample S2 (Fig. 5.10) appear smeared as compared to that of sample S1.

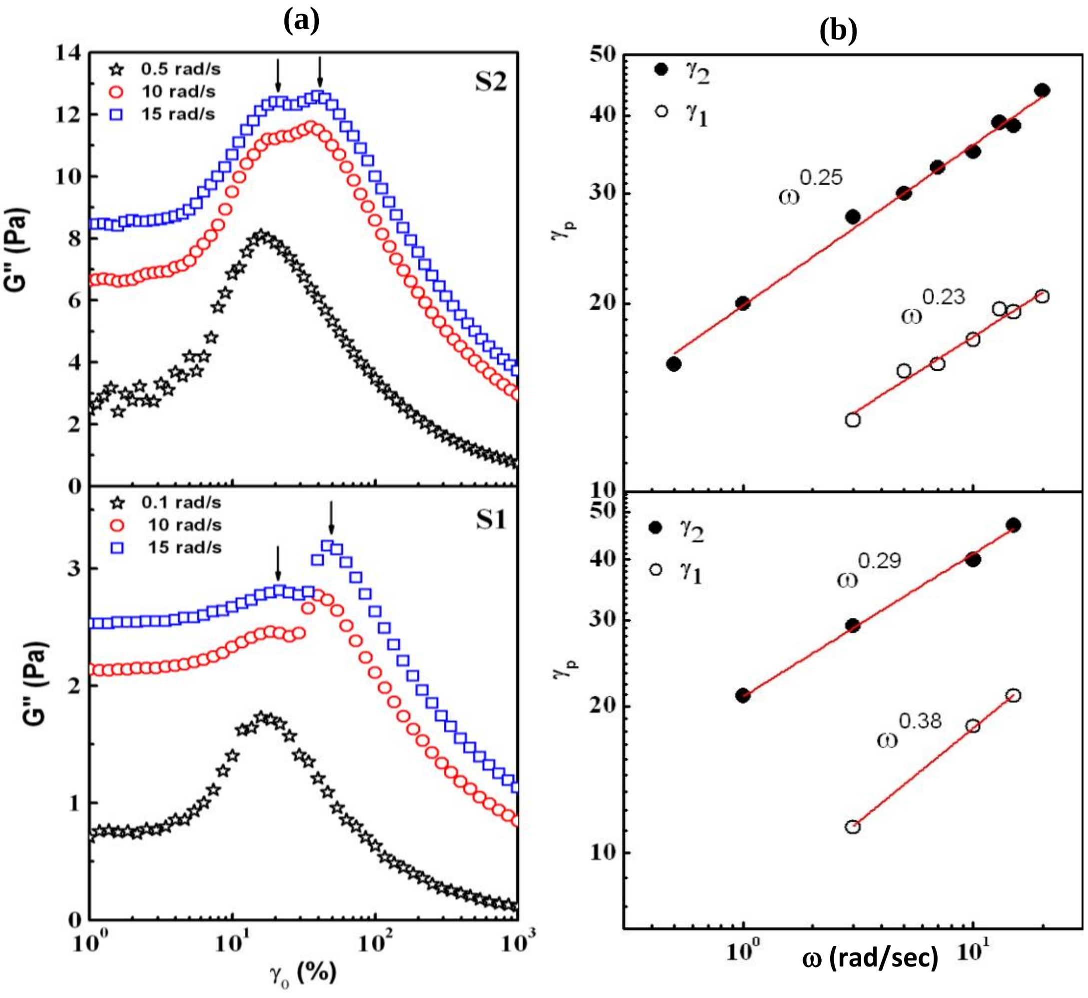

Fig. 5.13 (a) G'' for samples S1 and S2 in their glassy state (at 20 °C) measured using DSS measurements for various ω values, (b) Variation of peak strain, γ_p *(i.e* γ_1, γ_2) with ω for samples S1 and S2 at 20 °C. Continuous lines are the power law fits ($\propto \omega^m$) giving ω dependence of γ_1 and γ_2, with values of m written over the corresponding curve. Arrows indicate the peak positions.

In the case of hard sphere glasses, the yield strain is known to depend on the value of ω at which measurements are performed [20]. In order to know the ω dependence of γ_1 and γ_2 in dense PNIPAM glasses, DSS measurements have been performed at various values of ω and the results are shown in Fig. 5.13(a). For sake of clarity of the peaks, only G'' at different ω values are shown. Upon approaching ω_β (from higher frequency side), peak due to disentanglement is found to disappear, which is expected, since for $\omega \leq \omega_\beta$ intra-cage dynamics becomes insignificant. Variation of γ_1 and γ_2 with ω, for sample S1 is plotted in Fig. 5.13(b). Both γ_1 and γ_2 are found to show the power law dependence on ω (*i.e.* $\propto \omega^m$) with values of exponent m for samples S1 and S2 given in Fig. 5.13(b). As ω increases, γ_1 and γ_2 are found to shift to higher strain values. This is understandable from the increase in G' with increase in ω as shown in Fig. 5.9.

5.5 Summary

We have prepared dense suspensions of thermo-responsive poly(N-isopropylacrylamide) (PNIPAM) microgel particles with different volume fractions by subjecting them to the different osmotic compressions. Structural investigations, carried out using 3D DLS and SLS measurements, have suggested that at low temperatures dense suspensions of PNIPAM microgels exists in glassy state. PNIPAM microgel glasses have been found to transform into the liquid like order upon increasing the temperature. The glass transition temperatures of dense PNIPAM microgel suspensions have been identified by observing the change in the slope of the long time value of mean square displacement (MSD) plotted as a function of temperature. The ratio of the minimum in intensity at higher q side near the first peak and the maximum intensity of the first peak in $<I(q)>_E$, also showed a change in the slope at the same temperature exhibited by long time value of MSD. For the first time the MSD behavior at short times is found to be subdiffusive (*i.e.* $<\Delta r^2(t)> \propto t^{\alpha}$, with $\alpha < 1$) in dense PNIPAM microgel glasses. Subdiffusive behavior at short times is due to the overlap/entanglement of dangling polymer chains from shells of neighbouring particles. Subdiffusive behaviour observed at short times is found to change gradually into diffusive ($\alpha = 1$) upon increasing the temperature, suggesting disentanglement of dangling polymer chains at higher temperature. Non-linear rheological measurements showed that dense PNIPAM microgel glasses, yield in two steps (exhibits two peaks in G'' as a function γ_0) in contrast to the one step yielding observed in hard sphere glasses. The two step yielding in PNIPAM microgel glasses is interpreted due to occurrence of two processes: i) due to the breaking of entanglements of dangling polymer chains, giving rise to the first peak at lower strain and ii) due to the breaking of the near neighbour cages giving rise to the second peak at larger strain. At higher temperature, due to disentanglement, yielding behavior is observed to be single step (one peak in G''). Two step yielding behaviour of the dense PNIPAM microgel glasses is also found to depend on the oscillation frequency/shear rate at which measurements have been performed. Two peaks in G'' are apparent only for $\omega > \omega_\beta$. For $\omega \leq \omega_\beta$ only single peak in G'' is observed, since at these frequencies intra-cage dynamics becomes insignificant. Our measurements suggest that the inhomogeneous structure of PNIPAM microgel particles play an important role in governing the dynamics and shear flow behavior in dense PNIPAM microgel suspensions.

References

1. G. H. Fredrickson, Annu. Rev. Phys. Chem. 39, (1988) 149-180.
2. M. D. Ediger, C.A. Angell and S. R. Nagel, J. Phys. Chem.100, (1996) 13200 - 13212.

3. B.V.R. Tata, in Statistical physics of complex fluids, edt. S. Maruyama and M. Tokuyama, Tohoku University Press, Sendai, Japan.

4. P.N. Pusey and W. van Megen, Nature 320, (1986) 340-342.

5. W. van Megen and S. M. Underwood , Phys. Rev. E 49, (1994) 4206-4220.

6. J. Mattsson, H. M. Wyss, A. Fernandez-Nieves, K. Miyazaki, Z. Hu, D. R. Reichman and D. A. Weitz, Nature 462, (2009) 83-86.

7. B. R. Saunders, Langmuir 20, (2004) 3925-3932.

8. M. Stieger, W. Richtering, J. S. Pedersen and P. Lindner, J. Chem. Phys. 120, (2004) 6197 - 6206.

9. T. A. Mazder, Rheology Handbook, Vincentz Network GmbH & Co, K.G.

10. K. Miyazaki, H. M. Wyss, D. A. Weitz and D. R. Reichman, Europhys. Lett. 75, (2006) 915 - 921.

11. K. N. Pham, G. Petekidis, D. Vlassopoulos, S. U. Egelhaaf, P. N. Pusey and W. C. K. Poon Europhys. Lett. 75, (2006) 624 - 630.

12. J. Wu, B. Zhou and Z. Hu, Phys. Rev. Lett. 90, (2003) 048304.

13. F Grüner and W Lehmann, J. Phys. A: Math. Gen. 13, (1980) 2155-2170.

14. B.V.R. Tata and A. K. Arora, J. Phys. Condens. Matter 4, (1992) 7699; 7, (1995) 3817.

15. H. H. Wendt and F. F. Abraham, Phys. Rev. Lett. 41, (1978) 1244-1246.

16. R. Kesavamoorthy, A. K. Sood, B.V.R. Tata and A. K. Arora, J. Phys. C: Solid State Phys. 21, (1988) 4737.

17. P. Ballesta, R. Besseling, L. Isa, G. Petekidis and W. C. K. Poon, Phys. Rev. Lett. 101, (2008) 258301.

18. S. P. Meeker, R.T. Bonnecaze and Michel Cloitre, Phys. Rev. Lett. 92, (2004) 198302.

19. T. G. Mason and D. A. Weitz, Phys. Rev. Lett. 75, (1995) 2770-2773.

20. G. Petekidis. D. Vlassopoulos and P. N. Pusey, Faraday Discuss. 123, (2003) 287-302.

CHAPTER 6

6.1 Summary and conclusions

This chapter summarizes the investigations carried out on dense aqueous suspensions of thermo-responsive PNIPAM microgel particles using static/dynamic light scattering, cross-correlation static/dynamic light scattering, UV-Vis spectroscopy and Rheology techniques. As mentioned in Chapter 1, PNIPAM microgel particles are temperature sensitive, inhomogeneous density particles with core-shell structure having densely crosslinked core and thin shell (~ 30 nm) of dangling polymer chains. Earlier reports showed that in addition to the temperature, PNIPAM microgels also respond to osmotic pressure, where osmotic pressure on PNIPAM microgel was applied by addition of external polymer to the dilute suspension. In this thesis it is shown that PNIPAM microgels undergo compression in dense suspensions due to osmotic pressure from the surrounding particles of its own kind. In dense suspensions, where interparticle separations are of the order of particle diameter, the core-shell structure of the PNIPAM microgel particles is expected to influence their dynamics and shear deformation. Earlier reports have shown that PNIPAM microgel particle dynamics in liquid like ordered suspensions is affected by their core shell structure. In this thesis, it has been shown that, the dynamics and yielding behavior in the dense suspensions are affected by core-shell structure of PNIPAM microgels.

Towards the above studies, monodisperse PNIPAM microgel suspensions of various particle sizes have been synthesized using free radical polymerization by varying the surfactant and crosslinker concentration. Temperature response of the synthesized PNIPAM microgel particles have been characterized by measuring the diameter of the particle as a function of temperature. Diameter of the PNIPAM microgel is found to decrease with increase in temperature, with sudden collapse at 34°C, which is identified as volume phase transition (VPT). Synthesized suspensions are purified and concentrated. PNIPAM microgel crystals have been prepared by heating the concentrated suspensions to temperatures above VPT followed by its slow cooling (0.5°C/hr). Upon repeated heating and slow cooling suspensions with $\phi < 1.0$ showed iridescence under visible light illumination indicating the crystallization of PNIPAM microgel suspensions. When cooled at faster rate, suspensions are found to exhibit glassy state. Details of the synthesis and sample preparation method have been presented in Chapter 2 of this thesis.

In order to study the osmotic compression of PNIPAM microgel particles in dense suspensions, PNIPAM microgel crystals with different volume fractions have been prepared by compressing the suspensions osmotically. Bragg diffraction of these crystals has been recorded using a UV-Vis spectrometer. Upon increasing the osmotic pressure, the Bragg peak is found to exhibit a blue shift. The Bragg peak has been used to determine the interparticle separation. Beyond a certain osmotic pressure, interparticle separation is found to be smaller than the size of PNIPAM microgel particle under swollen state (measured using DLS on dilute suspension). In dense PNIPAM microgel crystals, the observation of interparticle separation being lesser than the particle size measured under dilute conditions, provides direct evidence for shrinking (deswelling) of PNIPAM microgel particles under osmotic compression in the crystalline state. The experimentally observed swelling/ deswelling behavior of the PNIPAM microgel particles with temperature and pressure is understood using Flory-Rehner (FR) theory. Only qualitative agreement has been observed between theory and experiments. Results reported here suggest the need for improvement of the FR theory for obtaining quantitative agreement with the experiments. These results are reported in the Chapter 3 of the thesis.

In Chapter 4 of the thesis, results on the dynamics studied across the melting of dense PNIPAM microgel crystals using DLS technique are presented. Melting of the PNIPAM microgel crystals have been achieved by raising the temperature. At higher temperature, microgel particle size hence ϕ decreases, causing the melting. In order to identify the melting transition, Bragg peaks from PNIPAM microgel crystals were captured using SLS and the Bragg peak intensity was monitored as a function of temperature. The temperature at which the Bragg peak intensity showed sudden fall, which happen due to loss of the long range order, has been identified as melting transition. The study of dynamics across the melting of PNIPAM microgel crystals revealed the deviation of dynamical criterion at the melting of the PNIPAM microgel crystals (*i.e.* $D_L/D_S < 0.1$). The deviation from 0.1 is found to be larger in the case of suspensions with higher ϕ. Careful studies on the behavior of mean square displacement close to the melting transition showed that the particle motion to be subdiffusive at short times. The subdiffusive behavior observed at short times, is understood to arise from the entanglement of the dangling polymer chains between the shells of the neighboring PNIPAM microgel particles and argued to be the reason for the observed deviation (i.e. $D_L/D_S < 0.1$). Hard sphere or charged colloidal systems undergoing freezing have showed the diffusive dynamics at short times. However, we have observed for the first time, the subdiffusive dynamics at short times in PNIPAM microgel liquids undergoing freezing. Since the dynamics at short times is subdiffusive, there exists no proper scale for long time diffusion, hence the inapplicability of dynamical criterion for the melting of PNIPAM microgel crystals (liquids) undergoing melting (freezing).

Chapter 5 report the results on light scattering and rheological behavior of dense PNIPAM microgel glasses carried out using 3D DLS and a rheometer, respectively. At elevated temperature (~ 30°C), PNIPAM microgel glasses have been found to transform into liquids. Upon rapid cooling of the microgel liquids to room temperature, they are found to freeze back into a glassy state. The glass transition temperature of dense PNIPAM microgel suspensions has been identified using 3D DLS. Non-ergodicity parameter, $f(q,\infty)$ obtained from DLS studies showed a change from finite value to zero across the glass transition. Careful analysis of the mean square displacement of PNIPAM microgel particles at short times revealed subdiffusive behavior, similar to that observed in PNIPAM microgel liquids close to freezing. The observation of subdiffusive dynamics at short times in PNIPAM microgel glasses and in liquids before the glass transition is unique as, there are no reports of the subdiffusive dynamics at short times in hard sphere or charged colloidal glasses. Subdiffusive dynamics observed at short times in PNIPAM microgel glasses is interpreted as due to the overlap / entanglement of dangling polymer chains from shells of neighbouring microgel particles. Upon increasing the temperature, the glass turns into liquid and the subdiffusive behaviour (α < 1) is found to turn into diffusive behavior (α = 1), indicating the disentanglement of the dangling polymer chains at higher temperature. Non-linear rheological measurements on dense PNIPAM microgel glasses showed two step yielding by exhibiting two peaks in loss modulus, G'', in contrast to the one step yielding observed in hard sphere glasses. The two step yielding in PNIPAM microgel glasses is interpreted as : i) due to disentanglement of the dangling polymer chains giving a first peak at lower strain (first peak in G'') and ii) breaking of near neighbour cages giving a second peak in G'' at large stain. Upon increasing the temperature, when the glass showed melting into super cooled liquid state, yielding is observed to be single step (single peak in G''). The change of yielding from two step at low temperature to single step at higher temperature is understood to be due to the disentanglement of the dangling polymer chains existing between the shells of neighbouring PNIPAM microgel particles. Though two step yielding have been observed in attractive glasses, our experiments constitute first evidence for the observation of two step yielding in soft repulsive glasses.

The major findings of the thesis are as follows,

1. PNIPAM microgel crystals of different volume fractions have been prepared and Bragg diffraction from these crystals has been recorded using UV-Vis spectrometer. The interparticle separation in PNIPAM microgel crystals with $\phi >$ 0.74, determined from the Bragg peak position, is found to be smaller than the diameter (d_h) of the PNIPAM microgel particles measured under dilute condition.
2. The observation of interparticle separation being lesser than the particle diameter (d_h), in dense ($\phi > 0.74$) PNIPAM microgel crystals, constitutes first evidence for deswelling of PNIPAM microgel particles under osmotic compression. PNIPAM microgel particles undergo osmotic compression as osmotic pressure on microgel particles exceeds their Bulk modulus (~ kPa).
3. Flory-Rehner (FR) theory is shown to provide the qualitative understanding for osmotic compression of PNIPAM microgel particles beyond a certain volume fraction.
4. DLS has been employed to study the dynamics across the melting of dense PNIPAM microgel crystals. Careful analysis of mean square displacement showed for the first time that dynamics of PNIPAM microgel particles, close to melting of the crystals, is subdiffusive at short times. The subdiffusive dynamics

at short times is argued to arise due to the entanglements of dangling polymer chains of neighbouring PNIPAM microgel particles. Observation of subdiffusive dynamics at short times implies the deviation of the dynamical criterion for melting of PNIPAM microgel crystals.

5. Upon sudden cooling, dense PNIPAM microgel liquids are shown to freeze into a glassy state. The glass transition temperatures of dense PNIPAM microgel liquids have been identified using 3D DLS technique. Non-ergodicity parameter, $f(q,\infty)$ is shown to show discontinuity across glass transition.
6. The dynamics in dense PNIPAM microgel glasses is shown to be subdiffusive at short times, suggesting the existence of the entanglements of the dangling polymer chains between neighbouring PNIPAM microgel particles in the glassy state as well as in the super cooled liquid state (*i.e.* above the glass transition temperature).
7. Non-linear rheological measurements on dense PNIPAM microgel glasses have shown that these glasses yield in two steps by exhibiting two peaks in $G''(\omega, \gamma_0)$. It is the first report of two step yielding in a soft repulsive glass. Earlier reports of the two step yielding are in attractive colloidal glasses.
8. Two step yielding observed in dense PNIPAM microgel glasses is argued to arise i) due to breaking of the entanglements of dangling polymer chains between neighbouring particles and ii) due to breaking of topological cages formed by neighbouring particles.

6.2 OUTLOOK FOR THE FUTURE WORK

Present studies have shown that dense PNIPAM microgel suspensions exhibit distinct dynamics and yielding behavior as compared to that of hard sphere or charged colloidal suspensions, which is attributed to the overlap / entanglement of dangling polymer chains from the shells of neighbouring PNIPAM microgel particles. The presence of entanglements has been evidenced by observation of subdiffusive dynamics at short times. In order to support the idea of entanglement of dangling polymer chains and to provide more evidences about the entanglements, following studies will be carried out.

a) **Dynamics in dense suspensions of charged PNIPAM microgels:** PNIPAM microgel particles are as such a neutral and can be made charged by copolymerization of NIPAM with ionic monomers like acrylic acid, 2-acrylamido-2-methyl-1-propanesulfonic acid. Dynamics in dense suspensions of charged PNIPAM microgels will be studied. Addition of the electric charges is expected to prevent the entanglements of dangling polymer chains due to electrostatic repulsion and hence short time dynamics is expected to be diffusive rather than subdiffusive.

b) **Structural investigations in dense PNIPAM microgel suspensions using SLS:** In dense suspensions overlap / entanglement of dangling polymer chains may result into the local clustering of PNIPAM microgel particles and the formation of networks, which can affect their structure. The structure of dense PNIPAM microgel suspensions will be investigated (from analysis of scattering profiles measured using SLS by assuming PNIPAM microgel as fuzzy spheres), to look at the presence of local clustering and hence the entanglement of dangling polymer chains.

c) **Direct imaging of the dense PNIPAM microgel suspensions using atomic force microscope:** Density of polymer within the core of PNIPAM microgel particles is very high as compared to that of the shell. Therefore, in imaging of microgel particles in dilute suspensions (where there is no overlap of the shells), only core of the microgel becomes apparent and shell stays invisible. On the other hand, overlap of the shells should lead to increase in polymer density within shells and make them visible. Typical thickness of the shells is ~ 20-30 nm, which can be resolved using atomic force microscope (AFM). Dense suspensions of PNIPAM microgel particles will be imaged using AFM with liquid cell to look at the overlap of the polymer chains via rise in the polymer density of the shells.

d) **Immobilization of the PNIPAM microgel crystals in a gel matrix:** Ordered crystalline arrays of PNIPAM microgel particles serve as sensors for temperature, pH, various chemicals etc. But the PNIPAM microgel crystals are fragile and lose their ordering against even smaller mechanical shocks, hence non portable. PNIPAM microgel crystals will be immobilized within a gel matrix, in order to make them portable.